

The Mine Sequence of the  
Central Noranda Volcanic Complex: Geology, Alteration  
Massive Sulphide Deposits and Volcanological Reconstruction

by

Harold L. Gibson, B.Sc., M.Sc.

Thesis submitted to the  
Faculty of Graduate Studies and Research  
in partial fulfillment  
of the requirements for the degree  
Doctor of Philosophy

Department of Geology  
Carleton University  
Ottawa, Ontario, Canada

© October 1989

# APPENDIX A. A PONDED MASSIVE FLOW AND PILLOW VOLCANO AT ANSIL HILL

## A.1 LOCATION AND SIGNIFICANCE

Ansil Hill, located 750m north of Minnova's Ansil Mine, is situated near the stratigraphic centre of the Rusty Ridge formation in the Ansil Sector (Map 1). A rhyolite dome of the Northwest formation directly underlies the Rusty Ridge formation at Ansil Hill and contributes there to the marked decrease in thickness of this formation.

Ansil Hill is not only one of the best exposures to illustrate subaqueous andesitic flow morphology in the Noranda area, but is also the most accessible. Andesitic flows display textures and structures which typify subaqueous andesitic sheet flows and tube-fed pillowed flows. Ansil Hill also provides a unique exposure of a ponded massive flow and pillow volcano complete with underlying feeder dike.

## **A.2 STRATIGRAPHY AND UNIT DESCRIPTIONS**

### **A.2.1 STRATIGRAPHY**

Ansil Hill is underlain by four andesitic flows (Map Units 1, 2, 3, and 4) that strike north  $45^{\circ}$  east and dip gently ( $15\text{-}25^{\circ}$ ) to the southeast, and a disconformable north  $50^{\circ}$  west striking, steeply ( $85^{\circ}$ ) east dipping fault breccia. The contacts and stratigraphic position of the flows are illustrated in the stratigraphic column of Figure A.1. Map unit 1, a massive andesitic flow, underlies strata at Ansil Hill and is conformably overlain by two tube-fed pillowed flows (units 2 and 3) and by a massive andesitic flow (unit 4). A synvolcanic fault offsets flows of units 1, 2 and 3 and influences the disposition of unit 4, but does not offset this younger flow.

The distribution of flows is illustrated in the geological map (Figure A.3). Idealized east-west (A-A') and north-south (B-B') idealized cross-sections through the Ansil Hill flows are shown in Figure A.4.

### **A.2.2 LITHOLOGY and FIELD CHARACTERISTICS**

#### **Unit 1, Massive Andesitic Sheet Flow**

The massive flow provides an excellent cross-section through a  $>40\text{m}$  thick subaqueous andesitic sheet flow. Vertical variations in both texture and structure of the flow are illustrated in Figure A.2, and are discussed in detail in Chapter 5,

and briefly described below.

Massive, brown-weathering, fine-grained, aphyric andesite containing <1% amygdules (up to 2cm) and 5%, <1mm-3mm mafic "spots" characterizes the bulk of the flow. Within 3-4m of the flow top the flow is aphanitic and contains 5-6% amygdules (up to 3cm) which increase in abundance to 12% within 1.5m of the flow contact and thereafter decrease to <6% (Figure 2). Amygdules within the flow interior are typically spherical and near the flow top, where the andesite is laminar jointed, are elongate parallel to the flow contact and laminar joints. Amygdules aligned along laminar joints have flat bottoms and arched tops and are elongate north-south presumably parallel to the flow direction. Large mega amygdules, up to 20cm in diameter, are restricted to a 2-3m wide zone approximately 4-5m from the flow top; these large amygdules are filled by quartz and epidote.

Planar laminar joints are conspicuous within 5-6m of the flow top and upward, within the flow, the number of joints increases and spacing between joints decreases (Figure A.2). Laminar joints within 2m of the flow top are contorted and conform to the shape of lobes (Figure A.2). The lobes are ribbon-like fingers of massive andesite that project upward into the hyaloclastite-rich breccia flow top. Many of the lobes resemble elongate, amoeboid-shaped pillows with distinct chilled margins that are outlined by a rusty sideromelane selvage that continues into and terminates within underlying massive andesite.

The flow top breccia contains intact, isolated, amoeboid "pillows" that are interpreted to have "budded" from lobes, angular blocky fragments of broken lobes, and plate-like, laminar jointed fragments derived from lobe margins complete with sideromelane selvedge within a microlitic and sideromelane shard hyaloclastite matrix. The breccias are poorly sorted and range in thickness from <0.5m to 2m.

### **Unit 2, Tube-Fed Pillowed Flow**

Tube-fed pillowed flows of unit 2 consist of aphyric, aphanitic, rusty weathering amygdaloidal andesite. In cross-section pillows have variable forms and range from <1m to >5m in size whereas in plan, pillows occur as intertwined elongate tubes with individual tubes traceable for 2m. Pillow interiors contain <6% amygdules whereas pillow margins and tops of pillows contain from 15-20% amygdules (up to 3cm). Radially oriented pipe amygdules (3cm long X 0.5cm wide), although not common, occur along pillow margins. A thin (<1cm), resistant, rusty, chloritized sideromelane selvedge mantles pillows. The pillows are densely packed and contain only minor hyaloclastite.

### **Unit 3, Tube-Fed Pillowed Flow**

Tube-fed andesite of unit 3 is distinct from unit 2 in that it weathers to a deep tan, contains <8% amygdules (<1cm-3cm) that are distributed evenly

throughout pillows, and is characterized by well developed concentric joints filled with epidote, actinolite, chlorite and quartz. Unit 3 is well exposed along the top of Ansil Hill where outcrop slopes reveal the elongate, intertwined tube-like form of the pillows. Tube-elongation and branching of tubes indicate a northwest to southeast paleoflow direction. Thin, chloritized, rusty, sideromelane selvages (<1cm wide) rim densely packed pillows that have little interpillow hyalocastite.

#### **Unit 4, Massive Andesite; "Ponded" Flow**

Massive andesite of Unit 4 is aphanitic, aphyric and weathers a light rusty brown. The massive flow is homogeneous, contains <1% amygdules (<1cm) and is speckled with <1mm mafic spots (5%). Where in contact with other flows or with fault breccia the flow is marked by an amygdaloidal (up to 20%), and chilled border with a 1cm wide dark grey to rusty chilled selvedge (Figure A.6). Amygdules not only increase in abundance toward contacts but also upward within the flow (Figure A.4, section A-A).

#### **Fault Breccia**

A breccia zone, <50cm wide, defines a northwest trending synvolcanic fault. The breccia consist of rounded to angular fragments of strongly amygdaloidal (15% amygdules) andesite that is similar to both the amygdaloidal margin of the

massive flow and adjacent pillowed flow of Unit 2. Radial pipe amygdules in some fragments suggest that the breccia is in part derived from brecciation of adjacent pillows. The matrix consists of finer andesitic fragments and rusty, pyritic hyaloclastite.

### A.2.3 PETROGRAPHY

Both massive and pillowed flows have relict hyalopilitic textures with randomly oriented (weakly pilotaxitic in Unit 1) skeletal plagioclase microlites (40-45%) in a fine homogeneous mesostasis of massive chlorite (30-40%), minor actinolite (<5%) and interstitial grains of epidote (5-10%), quartz (<8%) and opaque minerals (10%). Microlites range from <0.5 mm to 1.0mm in length with subhedral plagioclase phenocrysts (<1%) up to 1.2mm.

Amygdules with "concentric infilling" are common and from margin to interior the typical succession is granular to massive quartz, epidote and opaque minerals, followed by chlorite and then epidote. Fine "dusty" opaque minerals define coliform banding within massive, fine-grained quartz, lining some amygdules. The groundmass is dotted with 5 to 10% irregular clots of massive chlorite up to 1.0mm in diameter; these clots grade into the chlorite mesostasis and are interpreted as chloritized glass.

A fine-grained (<1.5mm) andesitic xenolith found near the flow top of Unit 1 massive andesite (Reference point X, Figure A.3) has a relict sub-ophitic texture. Stubby albite crystals (<.8mm) constitute up to 35% of the groundmass and are

partially surrounded by granular quartz (15% - up to 1.5mm) and massive chlorite (30%) with interstitial granular epidote (10%), opaque minerals (6%) and trace apatite.

#### **A.2.4 ALTERATION**

The principal alteration type is epidote-quartz alteration as described in Chapter 12. This alteration, common in andesitic and basaltic flows, is typified by total destruction of primary textures and mineralogy leaving an assemblage of granular epidote and quartz with minor actinolite, carbonate and opaque minerals. The alteration is characterized by an increase in Ca, a decrease or increase in Si, and a marked decrease in Al, Fe, Na and Ti. (Gibson, 1979; Chapter 12) compared to least altered andesite.

Epidote-quartz alteration occurs as discrete, round to irregular patches from <2cm to >1m in size within both massive and pillowed flows. The alteration preferentially developed around amygdules and displays a marked increase in intensity toward flowtops and the vent area to the unit 2 pillowed flow. Interpillow hyaloclastite is often totally replaced by epidote and quartz.

#### **A.2.5 CHEMICAL COMPOSITION**

Five representative samples of least altered andesite from the four flow units at Ansil Hill were analyzed for 11 major elements and selected trace elements



(Table A.1). The samples show no textural or mineralogical evidence of alteration and the analytical totals (>98%), lack of normative corundum and nepheline (indicative of Ca depletion, Na enrichment) are compatible with only weak epidote-quartz alteration and spilitization (Chapter 12). The data projected onto an AFM diagram straddle the tholeiitic and calc-alkaline field boundary (Figure 5). Normative mineralogy (Table A.2) indicate that they are tholeiitic andesite or basalt (Irvine and Baragar, 1971) . The Fe-enrichment or tholeiitic character of the Ansil Hill flows is typical of the Rusty Ridge formation.

### **A.3 DISTRIBUTION OF UNITS, FIELD RELATIONS AND RECONSTRUCTION**

The distribution of flows and their field relations allow recognition of a fault-bounded, ponded flow and a small "pillow volcano".

Most of Ansil Hill is underlain by a massive flow of unit 1 which strikes northeast and dips shallowly to the southeast. The flow is thought to have issued from a vent located within the Old Waite Dike Swarm 3 km the south.

Pillowed andesite of unit 2 issued from a feeder dike shown by F in Figure A.3, and covered parts of unit 1. The feeder dike consists of aphanitic, aphyric, weakly amygdaloidal andesite with narrow chilled margins; it intrudes underlying massive andesite and flow top breccia (unit 1) and grades into pillows of Unit 2. This gradation is marked by an increase in amygdules within the dike, and by the development of crude pillow-like forms that merge into large mega-pillows (>5m)

which spread laterally and symmetrically away from the dike (Figure A.3). The mega-pillows branch out and feed smaller tubes leaving a "spine" of large mega-pillows which extends north to south across the outcrop. The spine is interpreted to represent the core of a pillow "mound" or "volcano" built by continued eruptions along its feeding fissure. The rapid thinning and pinchout of the unit 2 pillowed flow 80m southwest of its fissure (Figure A.4, section A-A") supports the presence of a localized pillow mound or volcano. Pillow volcanoes with similar morphology have been identified within the Troodos Pillow lavas of Cyprus (H. Schmincke, personal communication, 1983).

Discontinuous lenses of breccia intercalated with pillows in the vent area are composed of angular pillow fragments in a fine-grained microlitic and sideromelane shard hyaloclastite matrix. The breccias are interpreted to result from collapse of partially drained tubes and may be similar to collapsed, hollow pillows described by Ballard and Moore (1977) from subaqueous pillow volcanoes along mid-ocean ridges.

The tube-fed pillowed flow of unit 3 issued from a vent located to the northwest, and conformably covered pillows of unit 2. Angular fragments within intact tubes are interpreted to have been derived from collapsed pillow shelves within a partially drained tube that was subsequently re-inflated with new lava that rafted fragments along the tube.

The distribution and contact relations of unit 4 massive andesite, interpreted as a ponded flow, are best described with respect to reference points on the geological map of Figure A.3, and cross-sections of Figure A.4. The massive flow is conformable along its lower contact with underlying, unit 3 pillowed flow at point B. At point A the massive flow rests directly and conformably on massive andesite of Unit 1 where pillowed flows of Unit 2 and 3 have pinched out (section A-A' and B-B', Figure A.4).

At point C, the massive flow has a sharp and disconformable contact with the tube-fed pillowed flow of Unit 3. This contact dips steeply ( $70^{\circ}$ ) to the south whereas strata dip  $15^{\circ}$ - $25^{\circ}$  to the southeast (Figure A.6). The massive flow is chilled against the pillowed flow (Figure A.6) and breccias containing amygdaloidal fragments identical to the massive flow margin, and laminar jointed fragments indistinguishable from adjacent pillow borders occur in pockets along the contact.

Southeast striking breccias between points D and E mark a fault contact between massive andesite and adjacent, older pillowed flows (Units 2 and 3). The breccia contact is interpreted to be a primary synvolcanic fault similar to those described by Ballard and Moore (1977) from mid-ocean ridges. The fault does not offset flows north of point E, the interpreted hinge area, whereas strata to the south and on the west side of the fault are down-faulted and tilted to the east (Figure A.4). At point E, breccia located along the fault contact between units 4 and 2 abruptly terminates and Unit 3 pillow flows are covered by massive andesite

(unit 4) with incipient pillows.

In the reconstruction, andesite of Unit 4, entered the fault block from the southwest where it was ponded against a synvolcanic fault scarp of older pillowed flows (Units 2 and 3) until it overrode the fault scarp at E and ramped up against down faulted pillows of Unit 3 at point C. Fragments within the fault breccia are interpreted as debris derived through tectonic brecciation of pillows during faulting and autobrecciation of the massive flow margin as it abutted against, and rose up along the fault scarp.

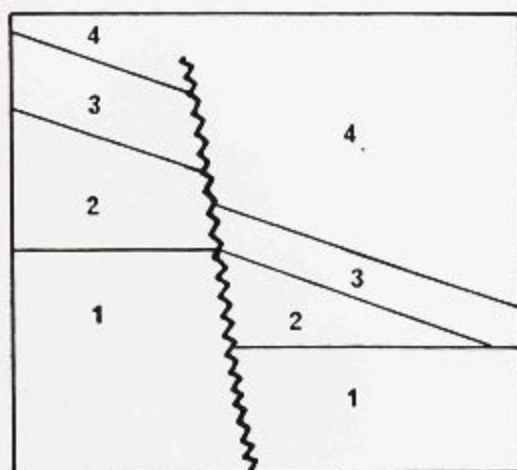


Figure A.1. Stratigraphic column for the Ansil Hill flows. Numbers refer to map units 1 through 4 in Figure A.3.

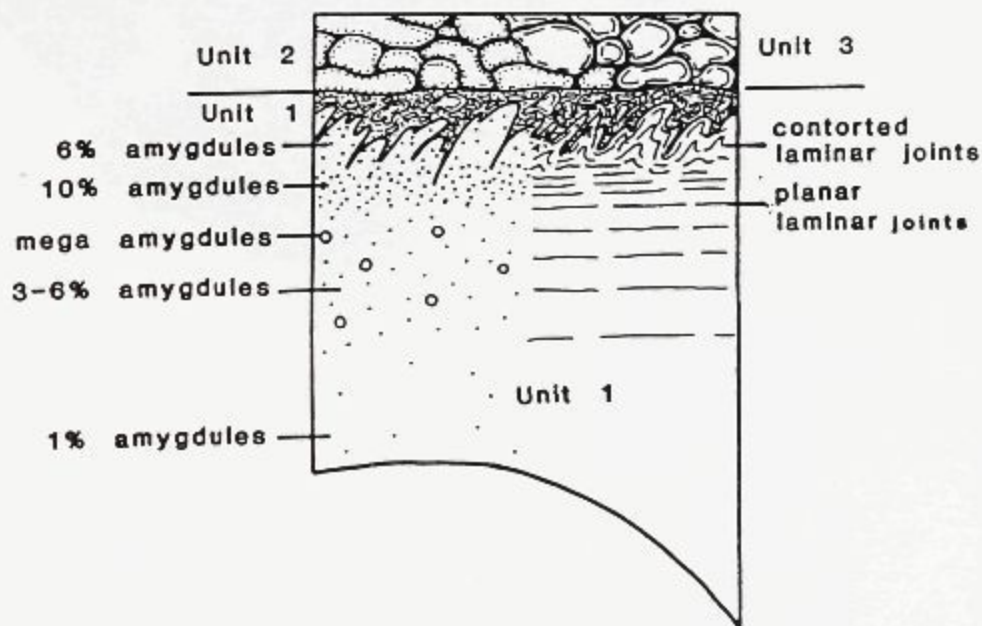


Figure A.2. Vertical variation in textures and structures within a massive andesitic flow of unit 1.



Figure A.3. Geologic map of Ansil Hill showing the distribution and attitude of andesitic flows (units 1-4), fault breccia (closed triangles), flow breccia (open triangles) and epidote-quartz alteration (half-coloured circles).

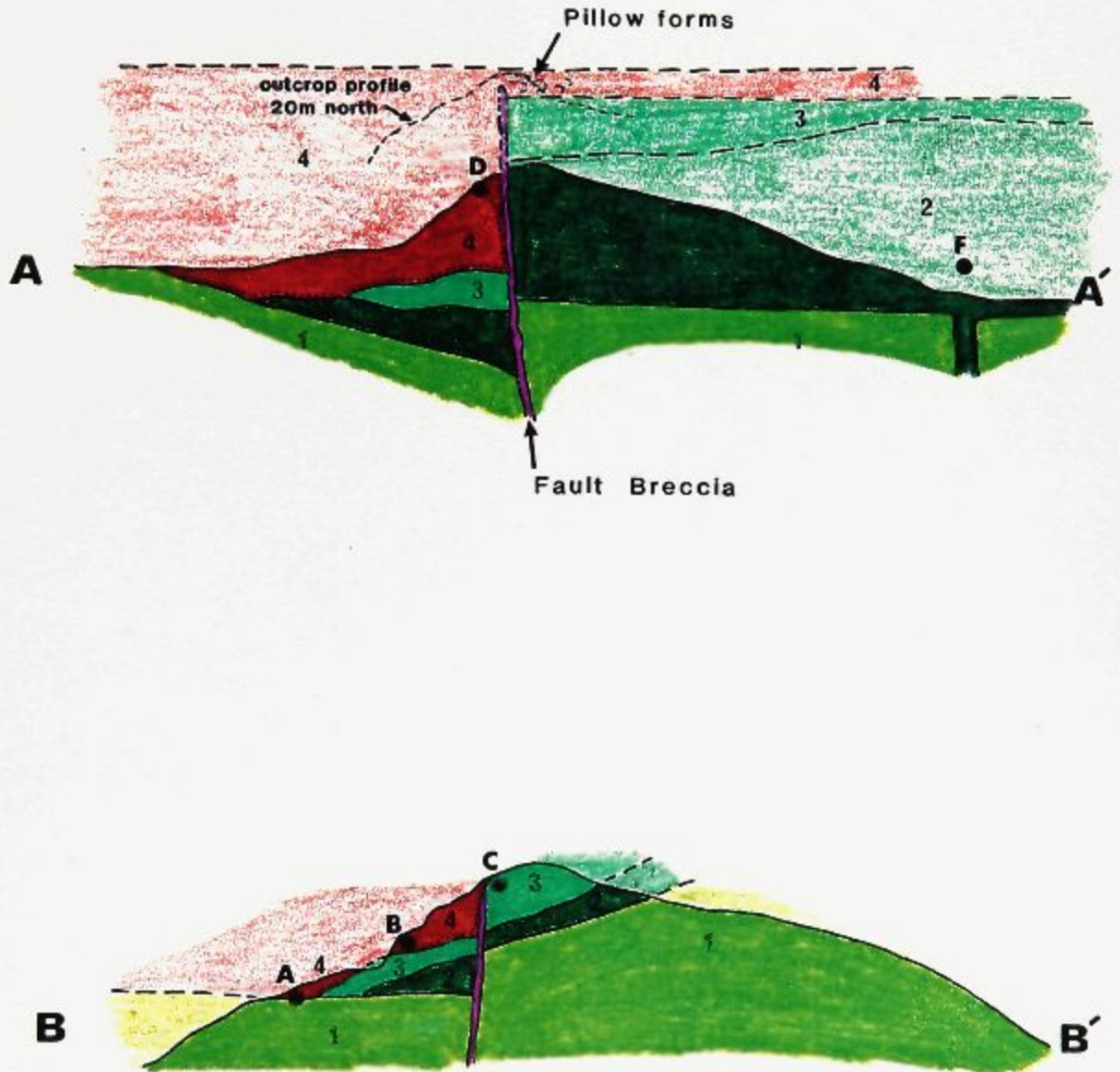


Figure A.4. Idealized cross-sections through Ansil Hill. Reference points A-F correspond with those in Figure A.3.

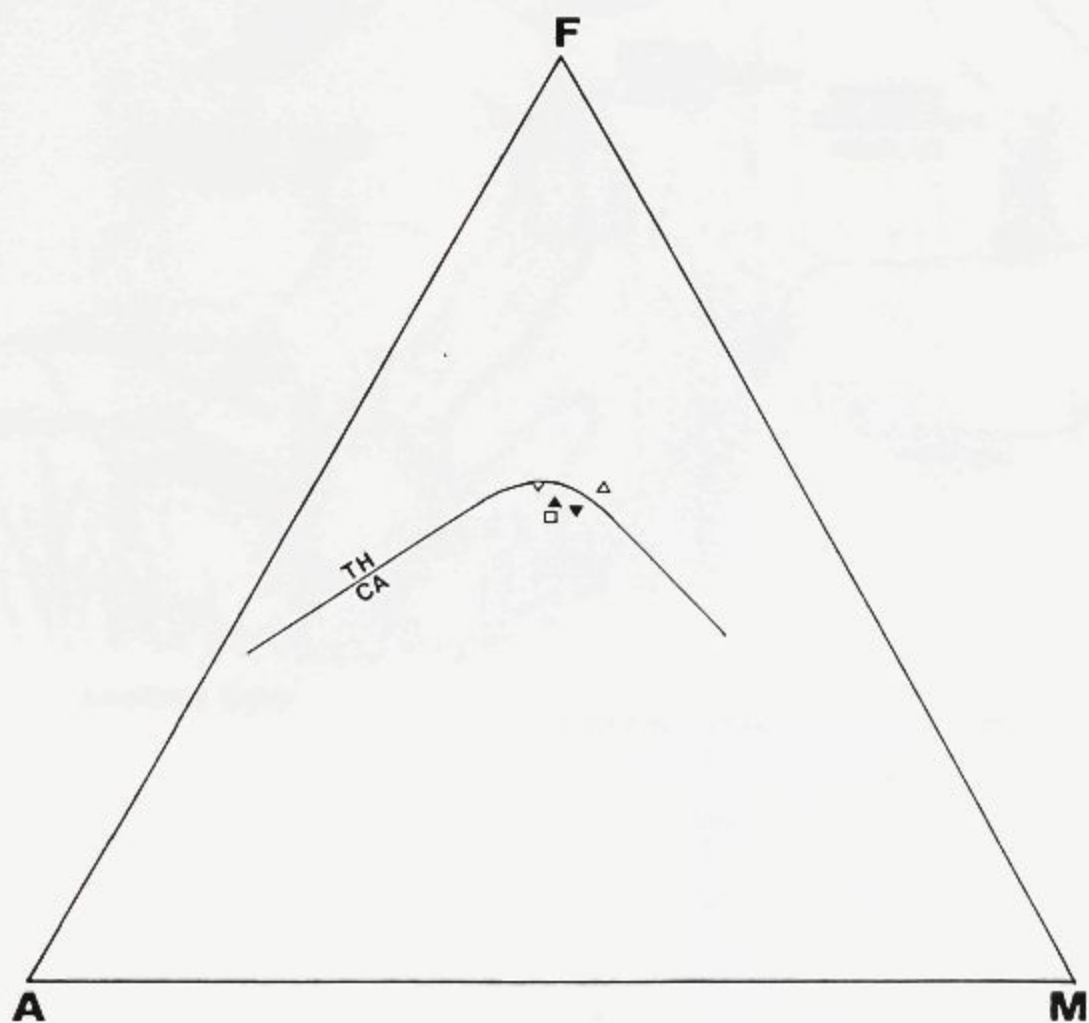


Figure A.5. Representative samples of Ansil Hill flows straddle the tholeiitic - calc-alkaline field boundary on the AFM diagram.



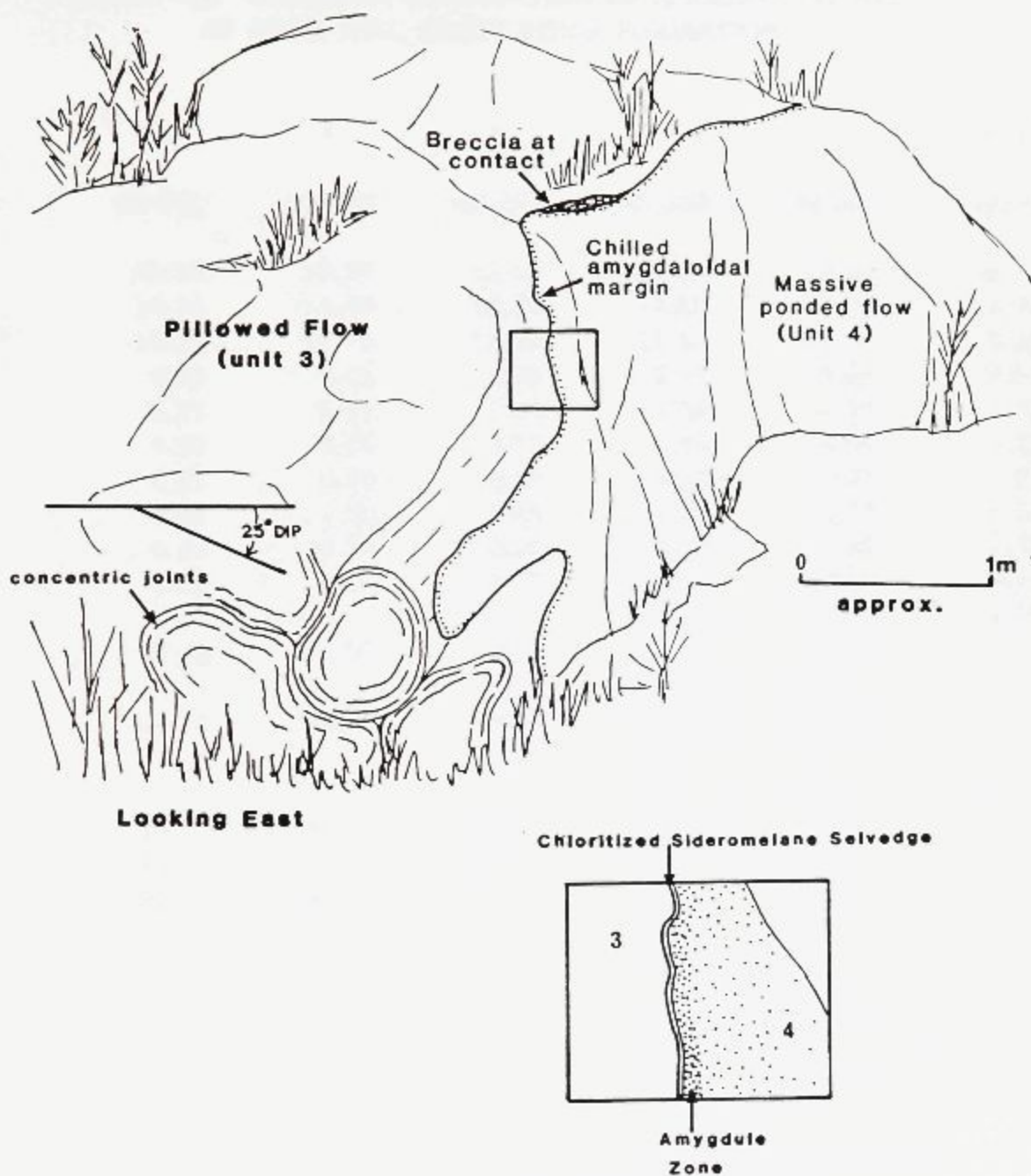


Figure A.6. Sketch illustrating the discordant contact between the tube-fed andesitic flow of unit 3 and the massive, ponded andesitic flow of unit 4 at reference point C. The massive flow is chilled and amygdaloidal adjacent to pillows with local pockets of breccia developed at the contact.

TABLE A.1. CHEMICAL COMPOSITION OF ANDESITIC FLOWS  
AT ANSIL HILL, RUSTY RIDGE FORMATION

Unit:	2	4	4	3	1	Xenolith
	83-261	83-263	83-264	83-265	83-266	I-82-43
SiO <sub>2</sub>	55.90	53.30	52.60	53.60	54.20	58.73
Al <sub>2</sub> O <sub>3</sub>	14.10	14.40	14.30	14.60	14.70	14.96
Fe <sub>2</sub> O <sub>3</sub> *	10.30	11.70	11.20	11.40	11.10	9.39
MgO	4.25	4.16	5.08	5.17	4.63	3.64
CaO	6.21	6.43	7.22	4.98	4.92	1.72
Na <sub>2</sub> O	4.30	4.49	3.57	4.46	4.69	4.25
K <sub>2</sub> O	0.21	0.49	0.16	0.20	0.37	1.55
TiO <sub>2</sub>	1.52	1.60	1.63	1.65	1.58	1.25
P <sub>2</sub> O <sub>5</sub>	0.20	0.20	0.20	0.22	0.20	0.38
MnO	0.15	0.16	0.17	0.14	0.15	0.16
S	-	-	-	-	-	0.00
LoI	2.00	1.93	2.39	2.62	2.23	-
Total	99.14	98.86	98.52	99.04	98.77	96.03
Ba						642
Cr	20	40	40	30	40	31
Zr	110	110	110	150	120	177
Sr	130	120	150	50	150	95
Rb	<10	<10	20	10	10	31
Y						48
Nb						6
Zn						163
Ni						0

XRF Fused Pellet Analyses, X-Ray Assay Laboratories except I-82-43:  
XRF Fused Pellet Analysis, Ottawa University

\* Total Fe as Fe<sub>2</sub>O<sub>3</sub>

TABLE A.2. CIPW NORMATIVE MINERALOGY OF ANDESITIC FLOWS AT ANSIL HILL

Unit:	2	4	4	3	1
	83-261	83-263	83-264	83-265	83-266
Quartz	10.42	4.67	7.91	6.42	6.22
Orthoclase	1.28	3.00	0.99	1.23	2.27
Albite	37.52	39.33	31.48	39.22	41.20
Anorthite	19.13	18.32	23.48	19.99	18.66
Diopside	4.68	5.06	5.37	1.80	2.20
Hedenbergite	4.70	6.11	4.99	1.68	2.23
Enstatite	6.65	6.38	8.39	10.22	8.79
Ferrosilite	7.65	8.84	8.95	10.91	10.20
Magnetite	4.52	4.65	4.73	4.75	4.64
Ilmenite	2.98	3.15	3.23	3.26	3.12
Apatite	0.48	0.48	0.48	0.53	0.48

Irvine and Baragar (1971) - Rock Name

83-261 - Tholeiitic Andesite  
83-263 - Tholeiitic Andesite  
83-264 - Tholeiitic Basalt  
83-265 - Tholeiitic Andesite  
83-266 - Tholeiitic Andesite

**APPENDIX B.**

**SUBAQUEOUS**

**PHREATOMAGMATIC EXPLOSION BRECCIAS**

**AT BUTTERCUP HILL**

**B.1 INTRODUCTION**

White-fragment breccia, so-called because of the striking white colour of the fragments, occurs as dikes and localized deposits conformable to the top of the Amulet formation and within the lowermost andesitic flows of the overlying Millenbach Andesite formation. The Amulet and Millenbach Andesite formations occur within the 3000m thick Mine Sequence, a cauldron-fill succession (Figure 1), of the Archean, Noranda Volcanic Complex of the Abitibi greenstone belt in northwestern Quebec (Gibson et al., 1984; Dimroth et al., 1982; Spence, 1976). Within the Noranda Cauldron, the Buttercup Hill breccias and numerous other breccia dikes (Figure B.1) are clustered within 2 km of the synvolcanic McDougall-Despina fault (Knuckey and Watkins, 1982; Setterfield, 1987).

The breccias are interpreted here to record a period of widespread hydrovolcanic explosions during magma resurgence prior to and during the onset of Millenbach Andesite volcanism. Buttercup Hill provides a unique cross-sectional exposure of a subaqueous, phreatomagmatic, explosion breccia deposit and its underlying feeder dikes. An origin through successive, shallow, phreatomagmatic eruptions and emplacement as fluidized breccias is proposed. The breccia deposit at Buttercup Hill is similar to coarse, blocky "explosion breccia" deposits which typically comprise the basal deposits of subaerial maar volcanoes. Silicification and sericitization, which predate and postdate emplacement of the breccias are described by Gibson and Watkinson (1979) and Leshner *et al.*, (1986), and are not described in detail herein.

## **B.2 STRATIGRAPHY OF BUTTERCUP HILL**

The simplified geologic map and accompanying cross-sections of Buttercup Hill (Figure 2) illustrate the distribution of map units, and the stratigraphic column (Figure 3) summarizes the stratigraphy and contact relations between the units. The Amulet formation, upper member, is the basal stratigraphic unit exposed at Buttercup Hill. The upper member consists of variably silicified, andesitic flows. The Amulet lower member is composed of rhyolitic flows (Chapter 9). The Millenbach Andesite formation conformably overlies the Amulet upper member from which it is separated by the "C" Contact Tuff, a thin, plane-bedded deposit of ash

and chert. The Millenbach Andesite formation consists of massive and pillowed andesitic flows and, near its base, local deposits of breccia as at Buttercup Hill.

### B.2.1 AMULET FORMATION, UPPER MEMBER

A green to white-weathering, plagioclase-porphyritic and amygdaloidal, silicified, andesitic flow of the Amulet upper member forms the base of the Buttercup Hill section. This flow is identical to others of the upper member and consists of massive columnar jointed andesite, overlain by a lobe and chloritized, vitrophyric flow-breccia facies (Figure B.4).

Least altered andesite from the massive and lobe facies has a hyalopilitic texture (Plate B.1A) with fine (<0.2 mm) randomly oriented to flow-aligned skeletal plagioclase microlites (40-45%), now albite, in a groundmass (45%) of "blebby" quartz (<.3 mm) and fine chlorite replacing original glass, with interstitial, accessory epidote (1%) and opaque minerals (5%). Plagioclase phenocrysts up to 1.3 mm (1-2%), and 3-10% amygdules (<3 cm) filled by quartz, epidote and chlorite are typical.

Thick, massive and compound flows of the upper member are interpreted to be products of a brief, voluminous eruption (approximately 40 km<sup>3</sup>) that inundated underlying rhyolite (lower member) and resulted in a relatively flat and horizontal paleosurface (Chapter 9).

### B.2.2 "C" CONTACT TUFF

Extrusion of the Amulet upper member was followed by a period of quiescence characterized by deposition of fine, waterlain ash and widespread hot-spring activity to form the "C" Contact Tuff (Chapter 11). The "C" Contact Tuff is a thin (<20cm thick) deposit of laminated andesitic ash, grey chert, and pyrite. The tuff is plane bedded and dips shallowly (<10°) to the southeast.

### B.2.3 MILLENBACH ANDESITE FORMATION

A rusty, brown-weathering, quartz-amygdaloidal and plagioclase-porphyritic, pillowed, andesitic flow marks the base of the Millenbach Andesite formation and conformably overlies the Amulet upper member and intervening "C" Contact Tuff. The flow is aphanitic with a felted microlitic to pilotaxitic intersertal texture with 45% plagioclase microlites (<0.4 mm), variably pseudomorphed by sericite and quartz, in a fine-grained mesostasis (40%) of chlorite and quartz (replacing original glass) with interstitial accessory epidote (1%) and opaque minerals (6%). Plagioclase phenocrysts (<1%) are typically <1 mm in size and amygdules (8%) are filled with quartz, epidote, and chlorite.

The andesitic flow is exposed immediately south of, and in windows through the overlying Buttercup Hill breccia. Contacts between the pillowed flow and overlying breccia are conformable and indicate a dip of <15° to the southeast (Plate B.1B).

#### B.2.4 BRECCIA DIKES

Breccia dikes at Buttercup Hill are identical to other breccia dikes which occur at the top of the Amulet upper member within 2 km of the McDougall-Despina Fault (Gibson, 1979). The Buttercup Hill breccia dikes contain angular, equant, white fragments of silicified andesite (up to 0.35 m) in a fine-grained (<3 cm), green, andesitic breccia matrix. The breccia dikes cross-cut all map units at Buttercup Hill except for the overlying, conformable breccia into which they merge (Figures 2 and 5). Analogous and contemporaneous breccia dikes elsewhere in the upper member are shallow intrusions extending <200 m from its top.

The main breccia dike strikes N20°E, dips 75° - 80° to the west, has a width of 2m and a strike length of 80 m. At its south end, a thin (<1 m wide) finger-like offshoot extends from the breccia dike and invades adjacent wall rock for 10 m (Figure 2). The main dike bifurcates vertically and laterally into two branches (Figures 2 and 5) that effectively isolate a wedge of silicified andesite (Amulet formation) approximately 3 m wide X 25 m long. Immediately above this wedge of andesite the dikes bifurcate and merge into an overlying, conformable breccia deposit (Figures 2 and 5 and Plate B.1C). Offshoots of the main dike dip inward toward this structure.

A second, parallel, 1 m wide X 12 m long breccia dike occurs 35 m southwest of the main dike. A third 2 m wide X 10 m long breccia dike occurs



26 m south of the main dike and strikes N45°W parallel to a mapped fault (Figure 2).

The breccia dikes pinch and swell along strike and display both sharp and gradational contacts with adjacent wall rocks. Where gradational, the wall rock is intensely fractured and veined by the dike matrix imparting an "in situ" breccia texture with wall rock fragments displaying all stages of detachment and incorporation into the breccia dike (Plates B.1C and D). Spring (1976), Comba (1977), Gibson (1979) and Gibson and Watkinson (1979) have demonstrated that white silicified fragments of the breccia dike and breccia deposit are derived from silicified andesite of the Amulet upper member to which they are identical in texture, mineralogy and composition.

Breccia dikes are chaotic, framework-supported intrusive breccias that contain fragments showing a complete size gradation from <0.1 mm to 0.35 m.

### Framework Fragments

1. White-weathering, angular, equant fragments of silicified andesite ranging from 0.35 m to <5 mm (typically 5-20 cm) are the dominant framework fragments (80%). Fragments display all variations in grain size and alteration that are common to adjacent flows of the Amulet formation and have a relict hyalopilitic texture (Plate B.2A) with 25-40% plagioclase microlites (<0.2 mm) and 1-2% plagioclase phenocrysts (<1.2 mm) in a fine mesostasis of granular and blebby

quartz, chlorite (after original glass) and accessory epidote and opaques. Amygdules are filled by quartz and epidote and constitute up to 10% of some fragments. Variable silicification of these megascopic fragments imparts a distinctive and striking "heterolithologic" appearance to the breccia.

2. Equant, angular fragments of fine-grained, intersertal textured Millenbach andesite constitute <5% of the breccia and range in size from 5 cm to <1 cm. Fragments contain up to 2% plagioclase phenocrysts (<1 mm), 5% quartz-epidote filled amygdules and 40% randomly oriented plagioclase microlites (<0.4 mm) with interstitial chlorite, sericite, quartz, epidote and opaques. Plagioclase phenocrysts and microlites are commonly pseudomorphed by sericite and quartz.

### **Matrix Fragments**

Chloritized shards of sideromelane (3 mm - <0.2 mm) constitute 10% of the breccia. The shards typically have angular, equant shapes and less commonly plate-like forms with delicate tails (Plates B.2B,C,D and F). Fragment boundaries are smooth, curved (concave-convex forms) and commonly meet in knife-like points (Plate B.2B). The shards are composed of massive chlorite, are aphyric (1% plagioclase microphenocrysts, <1 mm) to feldspar porphyritic and contain up to 10% fine (<0.1 mm) skeletal plagioclase microlites (Plate B.2D). Clots of granular epidote replace chlorite of the shards (Plate B.2B). Chloritized shards have a morphology and mineralogy identical to andesite sideromelane shard hyaloclastite

and the presence of perlitic cracks (Plate B.2D) attests to the original glassy nature of the fragments. Chloritized sideromelane shards are foreign fragments that were not derived from adjacent wall rocks. Chloritized vitrophyre of the Amulet upper member although similar, is silicified, spherulitic and is not microlitic.

Angular, equant, quartz-rich fragments (<5 mm) comprise <1% of the breccia. The fragments contain up to 35% elongate and round quartz amygdules (<0.2 mm) in a massive, granular, recrystallized quartz groundmass. Fine (<0.01 mm) granular epidote and opaque minerals (15%) define internal structures such as flow banding and amygdules (Plate B.2E). These fragments form a minor accessory component of the breccia matrix and may represent fragments derived from underlying rhyolite flows. Fragment boundaries cross-cut amygdules and fragment shape is not governed by morphology of contained amygdules.

Aphyric, subrounded fragments (0.1 mm) of silicified, perlitic-textured, chloritized vitrophyre and totally devitrified quartz-rich fragments (Figure 6f) form a minor (<1%), accessory constituent of the breccia. These fragments are identical mineralogically and texturally to vitrophyric, flow-top breccia of the Amulet upper member.

Fine-grained (<0.3 mm), granular-textured andesitic tuff constitutes <5% of the breccia matrix. The tuff consists of chloritized sideromelane and minor microlitic shards, <0.2 mm in size, and fine (<0.01 mm) granular quartz, chlorite, epidote and opaque minerals. Intact and broken plagioclase crystals are common

(Plate B.2B and C).

The morphology of chloritized sideromelane shards, both as matrix fragments and within the andesitic tuff matrix, the absence of vesiculated shards and the occurrence of broken plagioclase crystals within matrix ash suggests explosive fragmentation resulting from fluid-magma interaction. The sideromelane shards are interpreted as juvenile, andesitic glass fragments derived from the explosive interaction of rising andesitic magma, contained within dikes, and an external, near-surface fluid.

#### **B.2.5 "IN SITU" BRECCIA ZONE**

A discordant, narrow (7 mm wide X 22 m long), N40°W striking zone of "in situ" breccia cross-cuts silicified andesite northwest of the breccia dikes (Figure 2). "In situ" brecciation affects both lobes within the flow top breccia and underlying massive andesite; features which characterize and are significant to its origin are described below:

1. Intense, polygonal fracturing characterizes "in situ" brecciation and results in formation of equant fragments ranging from <1 cm to 15 cm separated by a thin chloritic vein-like breccia matrix (Plate B.3A). Fragment margins are sharp but are locally chloritized. The veins range from 0.1 mm - 0.5 cm in width and are composed of massive chlorite, chloritized fragments, sulphides and sphene. Chloritic envelopes up to 1cm wide mantle veins within adjacent silicified andesite;

alteration is weak, as albite microlites are largely intact (Riverin and Hodgson, 1980).

2. The "in situ" breccia zone has a core area of intense brecciation and fragment development with a transitional margin of polygonally veined, "in situ" brecciated andesite that grades through a decrease in fractures into massive andesite.

3. "In situ" brecciation is confined to massive andesite and is best developed in strongly silicified andesite, whereas adjacent autobrecciated vitrophyre and hyaloclastite are not brecciated. The restriction of "in situ" brecciation to areas of competent "lithified" and, in this case, silicified andesite indicates that brecciation was early, before the hyaloclastite/vitrophyre flow breccia was cemented and competent.

4. The "in situ" breccia zone lies on the strike continuation of a northwest-trending fault (Figure 2) and parallels the third breccia dike. The N40°W direction, common to the above structures, is approximately perpendicular to the main breccia dike and defines a second, primary fault direction parallel to the adjacent, synvolcanic McDougall-Despina fault (Knuckey *et al.*, 1982; Knuckey and Watkins, 1982; Setterfield, 1987).

Fragments produced by "in situ" brecciation are identical to fragments within the breccia dikes, overlying breccia and to underlying brecciated, silicified Amulet andesite exposed in "windows" within the breccia. The "in situ" breccia zone is interpreted as the roots of a northwest-trending breccia dike that contributed

fragments to the overlying breccia which has subsequently been eroded (Figure 2). This zone of brecciation was also a locus of continued hydrothermal activity as indicated by chlorite alteration and sulphide deposition within the vein network matrix and adjacent fragment margins.

#### **B.2.6. BUTTERCUP HILL BRECCIA**

The Buttercup Hill breccia is a localized (60m x 35m), <1m to 10m thick deposit which rests conformably on a pillowed flow of the Millenbach Andesite formation and, where the latter is absent, directly on silicified andesite of the Amulet upper member. Although exposures of the breccia are now restricted to areas east of the breccia dikes, the original deposit was likely larger and thicker. The occurrence of an "in situ" breccia zone northwest of the main breccia dike and smaller northeast- and northwest-trending dikes to the southwest suggest that the original deposit may have extended 35m northwest and 60m southwest of its present distribution. The original deposit may have had a crudely oval shape and approximate dimensions of 130m x 90m. The present distribution of the breccia, and underlying Millenbach Andesite, in an area southeast of the main breccia dike and northeast of the mapped fault (Figure 2) is interpreted to represent its preservation within a subsided or down-faulted block. The surrounding breccia was eroded leaving only the breccia "feeder dikes" and areas of "in situ" breccia to define its original limits.

The breccia is poorly sorted and consists of angular, lapilli to block sized fragments (40 cm maximum, average 10-20 cm) of silicified, white to brown weathering, amygdaloidal andesite of the Amulet upper member (Plate B.3B). Angular, equant fragments (2 cm-1 m) of rusty weathering, Millenbach andesite occur as exotic fragments within the breccia (<1%) and locally are prominent enough (15-60%) to define a distinct bed (Plate B.3C). The breccia is typically massive but variations in the amount of matrix define two crude, non-graded to reverse-graded depositional units (1.5 m to 1 m thick), that dip shallowly (<10°) to the east (Figure 5 and Plate B.3D). Thin, discontinuous lapilli tuff beds separate virtually identical beds of coarse, blocky breccia. In total, the breccia contains five discontinuous depositional units.

Fragments within the breccia matrix are identical to those within the breccia dikes. Angular to subangular, equant fragments of densely packed, hyalopilitic, silicified andesite (Plate B.4A) predominate (3 cm to <0.2 mm). Chloritized sideromelane shards have angular, equant and plate-like shapes and where squeezed between silicified andesite fragments are aligned and define a "flow foliation" parallel to fragment boundaries (Plates B.4A and B).

Fragments of hyalopilitic andesite and chloritized sideromelane grade into a fine (<0.01 mm) tuff matrix of quartz, chlorite, minor epidote and opaque minerals with 2% intact and broken plagioclase crystals (<0.2 mm). This fine tuff constitutes <10% of the matrix but where associated with laminated andesitic

tuff at the eastern limit of the breccia may account for up to 20% of the matrix.

Isolated "windows" reveal underlying intact and "in situ" brecciated silicified Amulet andesite and Millenbach andesite principally along the eastern edge of the outcrop where the breccia is thinnest (Figure 2). Where andesite within the "windows" is intact, sharp contacts with the breccia are common and often marked by thin beds of laminated ash. Where andesite exposed within the "windows" is brecciated, fragments of silicified andesite or Millenbach andesite show every stage of separation and incorporation into the adjacent breccia. This gradational relationship between the breccia and "in situ" brecciated, shattered, underlying units indicates that fragments were not all emplaced via breccia dikes but that underlying units contributed directly to the overlying breccia.

Although the contact is not preserved, the Buttercup Hill breccia is interpreted to be conformably overlain by andesitic flows of the Millenbach Andesite formation. This relationship has been observed in drill core where an identical breccia deposit intersected in hole D-416, located 2 km to the south, is conformably overlain by Millenbach Andesite flows.

#### **B.2.7 ANDESITIC TUFF**

Discontinuous, irregular deposits of bedded andesitic tuff occur within the breccia. The tuff is a thin bedded (1-3 cm) to laminated (<1 cm), plane bedded sediment with light grey, quartz-rich laminae interlayered with thin beds of green andesitic ash. The irregular and discontinuous character of the tuff, illustrated in



Figure 2, reflects the irregular, blocky, topography upon which it was deposited; tuff often occurs in isolated pockets that have slumped between large fragments (Plate B.4C). Thick sections of tuff (>10 cm) are conspicuously absent adjacent to breccia dikes but increase in abundance along the east side of the outcrop where they separate and define at least two discontinuous depositional units within the coarse breccia.

Andesitic tuff has a granular texture and consists of fine-grained quartz (<0.01 mm), chlorite and epidote. Fragments include round to subround lithic clasts of quartz-rich silicified microlitic andesite (<3%, <0.7 mm), 10% chloritized sideromelane shards (<0.1 mm), <2% skeletal plagioclase microlites (<0.2 mm), 3-4% broken and intact plagioclase crystals (<0.4 mm), 10% quartz grains (<0.2 mm), and 10% sulphides, chiefly pyrite with minor chalcopyrite and trace sphalerite (Plate B.4D). Bedding is defined by alternating laminae that are dominated by quartz, sulphides (20%) and chloritized sideromelane shards (+15%).

Andesitic tuff, a plane-bedded, waterlain ash, is identical to the tuff matrix of both the breccia dikes and breccia deposit. Andesitic tuff is interpreted to have been derived by explosions during dike emplacement and was deposited with the breccia during pauses between phreatomagmatic explosions.

### **B.3 ALTERATION**

The dominant alteration recognized at Buttercup Hill is silicification (Comba, 1977; Gibson, 1979; Gibson and Watkinson, 1979; Leshner *et al.*, 1986).

Several characteristics of silicification that are pertinent to unravelling the paleovolcanology of Buttercup Hill are outlined below:

1. Silicification, as illustrated in Figure 2, is most pervasive in lobes and massive andesite immediately adjacent to flow breccia which is also intensely altered.
2. Silicification is localized by vesicles; as the number of amygdules increases toward the flow top so does the degree of silicification. Silicified halos mantling quartz amygdules often merge and overlap forming large mottled silicification patches and irregular ribbon forms (Gibson *et al.*, 1983).
3. The geologic map (Figure 2) illustrates a marked increase in silicification immediately adjacent to and along the north-east trending main breccia dike and north-west trending zone of "in situ" brecciation. Both breccia zones are interpreted to be localized along synvolcanic faults.
4. The pillowed andesitic flow of the Millenbach Andesite formation is not silicified.

Points 1 and 2 indicate that silicification is controlled by the primary permeability of the flows and is most intense and pervasive along flow contacts indicating a primary lateral component to fluid movement (Gibson 1979; Gibson *et al.*, 1983). The marked increase in intensity of silicification toward the two synvolcanic faults suggests that these structures were operative before brecciation and dike emplacement and focused both lateral and vertical hydrothermal fluid movement. The latter possibly resulted in the discharge of SiO<sub>2</sub>-rich fluids at the

seafloor (Chapter 12).

Other alteration types recognized are chloritization and sericitization. Chloritization, primarily located within the vein-network matrix of the "in situ" breccia zone and locally within the matrix of the main breccia dike, indicates continued hydrothermal alteration and fluid movement after silicification and breccia dike emplacement.

Sericitization, unlike silicification is a discordant alteration that affected all stratigraphic units at Buttercup Hill. Areas of sericite alteration (Figure 2) are subparallel to northwest- and northeast-trending breccia dikes. Sericite alteration is texturally, mineralogically and compositionally identical to that which characterizes the periphery of discordant alteration pipes associated with volcanogenic massive sulphide deposits in the Noranda Camp (Riverin and Hodgson, 1980; Knuckey *et al.*, 1982; Lesher *et al.*, 1986).

In summary, silicification is an early, primarily stratabound, conformable alteration that was operative prior to extrusion of the Millenbach Andesite formation and emplacement of breccia dikes. Sericitization and chloritization post date silicification and initial Millenbach Andesite volcanism. Northeast- and northwest-trending synvolcanic structures controlled early silicification, breccia dike emplacement and discordant sericite and chlorite alteration.

#### B.4 ORIGIN AND EMPLACEMENT OF THE BUTTERCUP HILL BRECCIAS

Breccia dikes at Buttercup Hill are interpreted as the principal conduits of shallow subsurface explosions that erupted on the seafloor forming a localized deposit of chaotic blocky breccia. Fragments within dikes and conformable breccia are overwhelmingly lithic and of local provenance, derived from immediately underlying and adjacent Amulet and Millenbach Andesite flows. Chloritized sideromelane shards, a minor and foreign constituent, are interpreted as primary, juvenile, andesitic glass fragments. Morphology of the sideromelane shards indicates fragmentation by thermal strain during fluid-magma interaction which, in this case, involved hydrovolcanic explosions (Heiken, 1972; 1974). The absence of vesiculated sideromelane and "Y-shaped" shards suggests that fragmentation and quenching preceded volatile escape and that rapid exsolution of juvenile volatiles did not play a major role in fragmentation.

The explosive effect of rapid steam generation accompanying magma/fluid interaction (Fisher and Schminke, 1984; Wohletz, 1983; Wohletz and Sheridan, 1983; Wohletz and McQueen, 1984) is interpreted as the driving mechanism for generation and emplacement of breccia dikes. It is suggested that interaction of downward migrating seawater or shallow circulating hydrothermal fluid (evolved seawater) with rising andesitic magma (eruptions contemporaneous with Millenbach Andesite volcanism) resulted in shallow, subsurface phreatomagmatic explosions. The restriction of breccia dikes to <100m from the Amulet formation paleosurface

and the shattering interpreted from the "in situ" brecciation of units adjacent to dikes and below the breccia are consistent with violent, near-surface explosions.

Explosively generated, rapidly expanding and ascending turbulent steam is capable of mobilizing, suspending and transporting a chaotic mixture of wall rock and juvenile fragments to surface as fluidized breccia (Reynolds, 1954; Lambert, 1974). Lateral and vertical breccia dike bifurcation and injection into adjacent shattered and brecciated wall rocks was also accompanied by localized subsidence that resulted in the isolation of large blocks of spalled and slumped wall rock within the vent area. Localized, near-surface, shattering and brecciation of wall rocks, as well as isolated, slumped, wall-rock blocks, and emplacement of inward converging breccia dikes (Figure 2) are consistent with development of a funnel-like orifice that may have been expressed by a surface crater. The areally restricted character of the breccia deposit and underlying Millenbach Andesite pillowed flow, as compared to breccia dikes and "in situ" breccia, is interpreted to reflect the latter's preservation within the subsided vent area or crater.

The breccia dikes were emplaced by successive, shallow phreatomagmatic explosions that deposited at least five crude beds of a coarse, unsorted, breccia both within the vent or "crater" and along its margins. Fine, waterlain andesitic ash was deposited with and on the irregular surface of the blocky breccia during brief pauses that separated eruptions.

Conformable breccias at Buttercup Hill are probably only a remnant of a once larger deposit whose exact morphology is unclear. Subaerial hydrovolcanic eruptions are characterized by particular volcanic landforms (Fisher and Schmincke, 1984; Wohletz and Sheridan, 1983; Lorenz, 1970; Lorenz *et al.*, 1973) such as, tuff cones, tuff rings, maars and littoral cones. Littoral cones are not considered analogous to breccias at Buttercup Hill as they lack a feeding fissure and are essentially "rootless deposits" produced where lava or pyroclastic flows move over or enter water (Fisher and Schmincke, 1984). Tuff rings, tuff cones and maars are possible analogs and are collectively grouped as maar volcanoes (Fisher and Schmincke, 1984). Tuff rings have large craters at or above ground surface and are surrounded by a low (<100 m) rim composed of coarse to fine tephra, whereas tuff cones possess rim deposits up to 300 m high (Wohletz and Sheridan, 1983; Fisher and Schmincke, 1984). Maars are similar to tuff rings except in the former the crater cuts below the ground surface (Lorenz, 1973).

Although only a part of the coarse, blocky, unsorted and crudely layered, breccia deposit at Buttercup Hill remains, it is similar to coarse breccias which form the basal units to maar volcanoes (Figure 6). These coarse deposits are termed "explosion breccias" by Wohletz and Sheridan (1983), who attribute them to initial, phreatomagmatic explosions responsible for cratering during tuff ring and tuff cone formation. In subaerial analogs the primary mechanism of emplacement for "explosion breccia" is ballistic fall (Fisher and Schmincke, 1984; Wohletz and

Sheridan; 1983). The same may be true for the subaqueous Buttercup Hill breccias but the overlying water column might have more effectively sorted fragments, elutriated and suspended fine ash and restricted the trajectory of fragments resulting in a more localized deposit. In subaerial maar volcanoes, the coarse "explosion breccias" are interlayered with airfall ash and base-surge deposits, whereas subaqueous explosion breccias at Buttercup Hill are interlayered with thin discontinuous deposits of bedded, waterlain ash (Figure 6).

In comparing the stratigraphy of tuff rings and cones to the Buttercup Hill breccias (Figure 6) there is the noticeable absence, at Buttercup Hill, of thick and thin bedded surge and airfall tephra deposits which overly "explosion breccia" deposits and are characteristic of subaerial maar volcanoes. Their absence is not an artifact of erosion as an identical and "complete" breccia deposit, intersected in drill hole (D-416), lacks surge deposits and thick units of plane-bedded tuff. However, some maar volcanoes consist almost entirely of coarse, blocky "explosion breccia" deposits (Self *et al.*, 1980) and do not possess the typical stratigraphy shown in Figure 6. The absence of strata containing interlayered base surge and bedded tuff deposits above the coarse "explosion breccia" deposit at Buttercup Hill may be a), characteristic of relatively deep (>200 m to <500 m,) subaqueous phreatomagmatic eruptions, b), a product of weak phreatomagmatic eruptions (Wohletz and Sheridan, 1983), and/or c), a result of rapid burial by penecontemporaneous andesite flows that arrested explosive activity.

## B.5 SUMMARY

Breccia dikes at Buttercup Hill are interpreted to have been emplaced as a fluidized breccia, products of successive, shallow phreatomagmatic explosions. Lateral and vertical bifurcation of breccia dikes, their injection into adjacent wall rocks and intense shattering and brecciation of near-surface rocks accommodated slumping of wall-rock blocks within the vent area that may have resulted in the development of a topographic crater on the seafloor. "Explosion breccia" deposits interlayered with waterlain ash were deposited at the seafloor within the vent or crater and probably along its rim forming a small breccia deposit that may be analogous to "explosion breccias" associated with subaerial maar volcanoes. The clustering of breccia dikes and breccias deposits, including those at Buttercup Hill, to within 2 km of the synvolcanic McDougall-Despina Fault is also typical of recent subaerial maar volcanoes which often occur in "groups" or "fields" (Lorenz, 1973). The original size of the Buttercup Hill breccia deposit can only be estimated; the present distribution of breccia dikes and "in situ" breccia suggest a crudely oval form with approximate dimensions of 130m x 90m.

Buttercup Hill breccias and other identical deposits are located at the top of the Amulet upper member and C "Contact" Tuff or above the basal flow of the Millenbach Andesite formation. These breccias are interpreted to have formed during a "brief" time interval that marked the end of a hiatus in volcanic activity, which was characterized by vigorous hot-spring activity, and the onset of renewed



volcanism during a second period of magma resurgence (Chapters 11, 12 and 13). Interaction of downward migrating seawater or convecting hydrothermal fluids with rising andesite magma during the onset of Millenbach Andesite volcanism is interpreted to have triggered shallow phreatomagmatic explosions responsible for the generation of breccia dikes and localized "explosion breccia" deposits. Penecontemporaneous andesitic flows quickly buried the breccia deposits and arrested further phreatomagmatic eruptions. Continued eruption of andesitic and rhyolitic flows infilled the Noranda Cauldron (Chapter 11).

The sequence of events at Buttercup Hill is illustrated in Figure 7, and briefly outlined below:

A. 1. Extrusion of the uppermost andesitic flow of the Amulet formation, upper member.

2. Silicification, preferentially along permeable flow contacts and synvolcanic northwest- and northeast- trending faults that intersect at Buttercup Hill.

3. Ascent and discharge of silica-saturated hydrothermal fluid along synvolcanic faults coincident with deposition of fine ash and chert that comprise the "C" Contact Tuff during a hiatus in volcanic activity.

B. 1. Onset of widespread andesitic volcanism (Millenbach Andesite formation) and emplacement of high-level feeder dikes. The pillowed flow at Buttercup Hill may have issued from a fissure now occupied by breccia dikes.

2. Shallow, subsurface phreatomagmatic explosions within intersecting northeast- and northwest-trending synvolcanic faults, a result of explosive interaction between ascending andesitic magma and downward migrating seawater or convecting hydrothermal fluid.

C. 1. Emplacement of fluidized breccia dikes and eruption of coarse breccia and ash at the seafloor.

2. Intense shattering, brecciation at surface and slumping of wall-rock blocks producing a small vent and possibly an overlying crater.

3. Successive phreatomagmatic eruptions depositing coarse "explosion breccias" interlayered with waterlain andesitic ash to form a small, localized breccia deposit that may be similar to "explosion breccias" associated with subaerial maar volcanoes.

4. Rapid burial of the Buttercup Hill breccias by penecontemporaneous andesitic flows (Millenbach Andesite formation).

5. Contemporaneous and continued hydrothermal activity producing chloritization and sericitization within and adjacent to breccia dikes. This alteration may be coincident with formation of stratigraphically higher volcanogenic massive sulphide deposits and their proximal, discordant alteration assemblages.

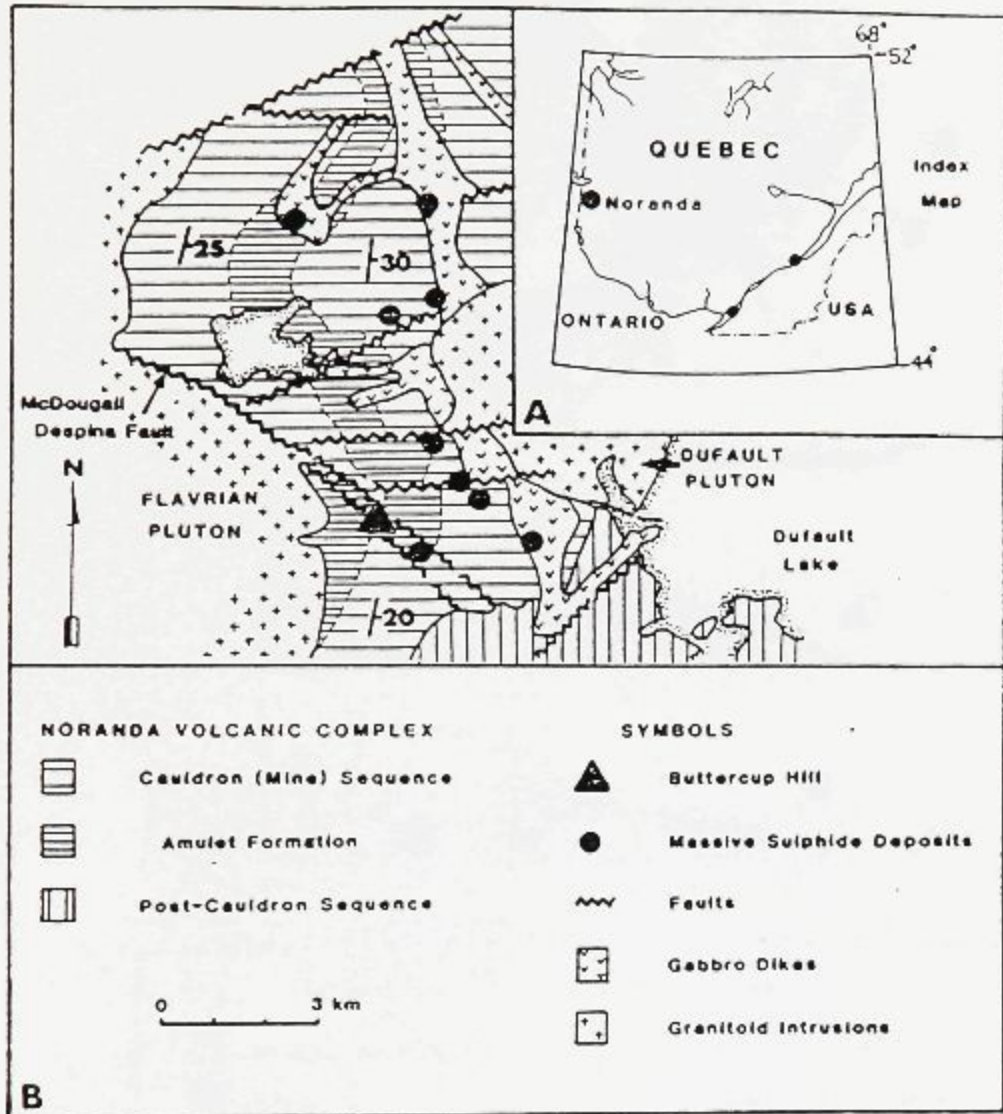


Figure B1. General geology of the central part of the Noranda Volcanic complex, illustrating the cauldron sequence and location of Buttercup Hill. Modified after Dimroth *et al.* (1982) and de Rosen-Spence (1976).

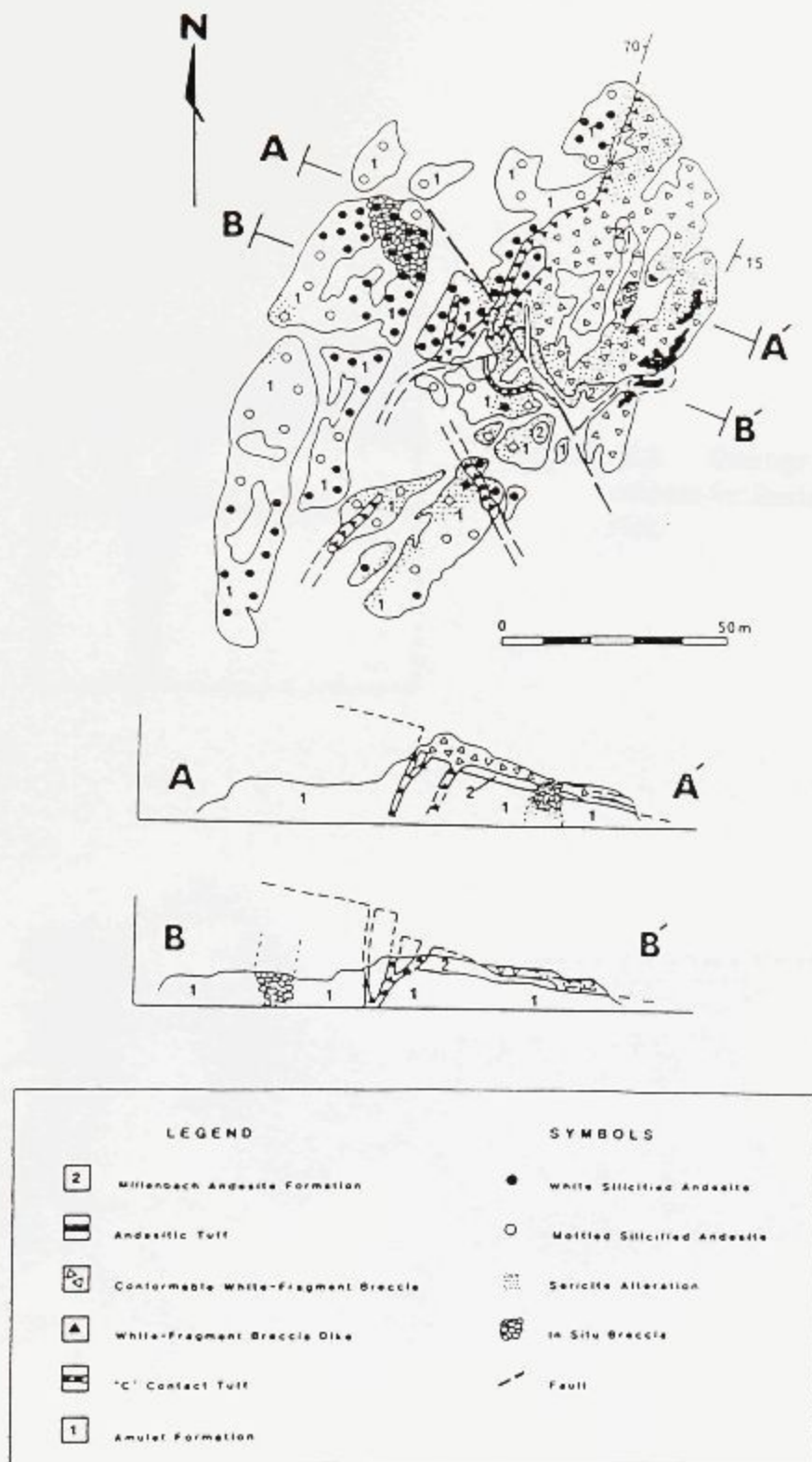


Figure B2. Simplified geologic map and cross section of Buttercup Hill. Breccia dikes trend northeast and northwest and bifurcate along strike and upward, where they are continuous with an identical, overlying conformable breccia. Deposits of andesitic tuff occur along the southeast margin of the outcrop, where they separate thick, massive beds within the breccia. The dashed line shows the *inferred* original extent of the breccia.

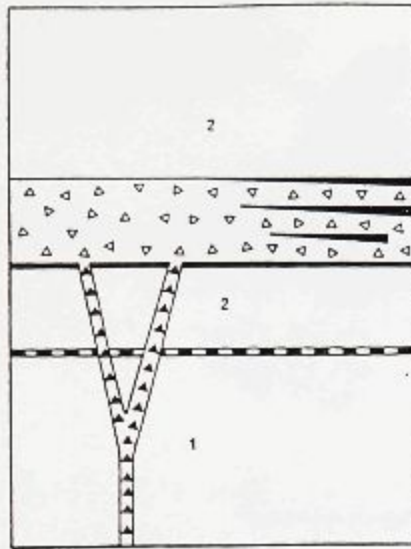


Figure B.3. Stratigraphic column for Buttercup Hill.

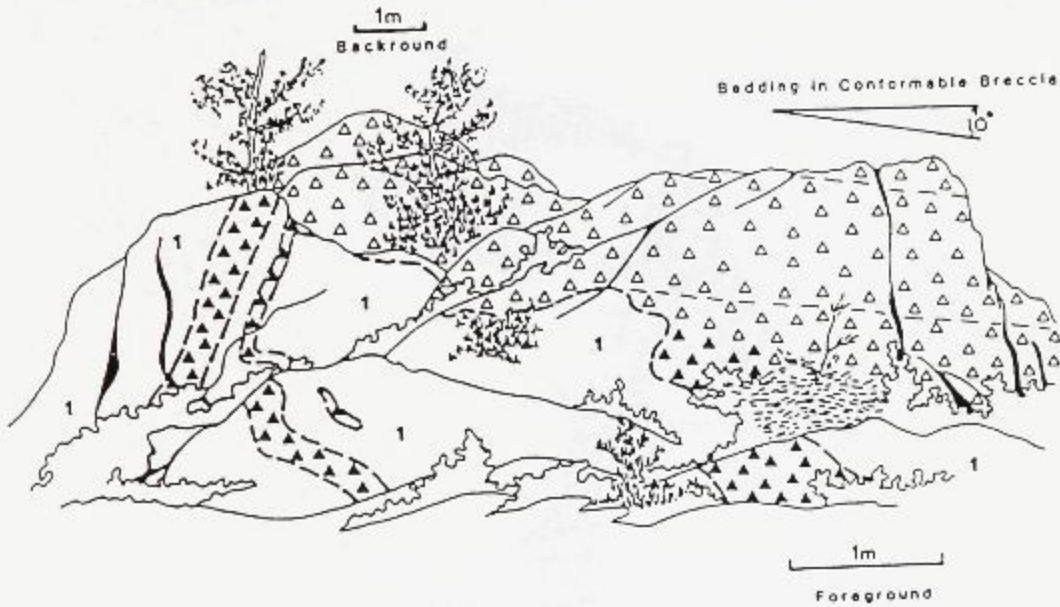


Figure B.5. Sketch of Buttercup Hill looking northeast and along strike of the breccia dikes. Note the steep north dip of the breccia dikes and their gradation into overlying, gently south-east dipping ( $<10^\circ$ ) conformable breccia. Crude thick beds are defined by a decrease in fragment size and increase in proportion of matrix ash (see Plate B.3d). Dike at left divides into two separate dikes that merge with overlying breccia (see Plate B.1c). Legend as in Figure B.2.

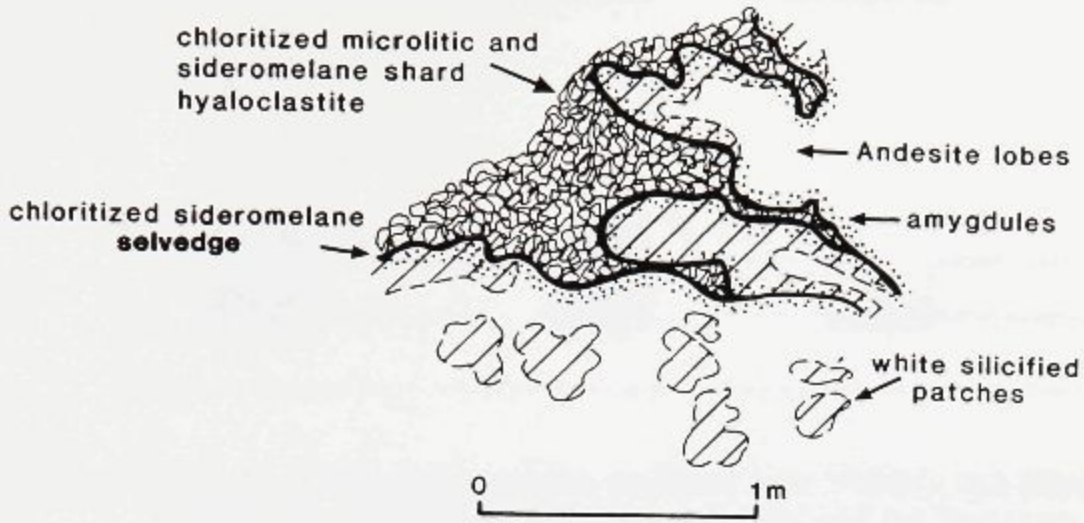


Figure B.4a. Silicified lobes of andesite mantled by a chloritized sideromelane selvage in contact with chloritized microlitic and sideromelane shard hyaloclastite. Note silicification in massive andesite (Amulet upper member).



Figure B.4b. Plan view of autobrecciated, silicified lobes in flow breccia.

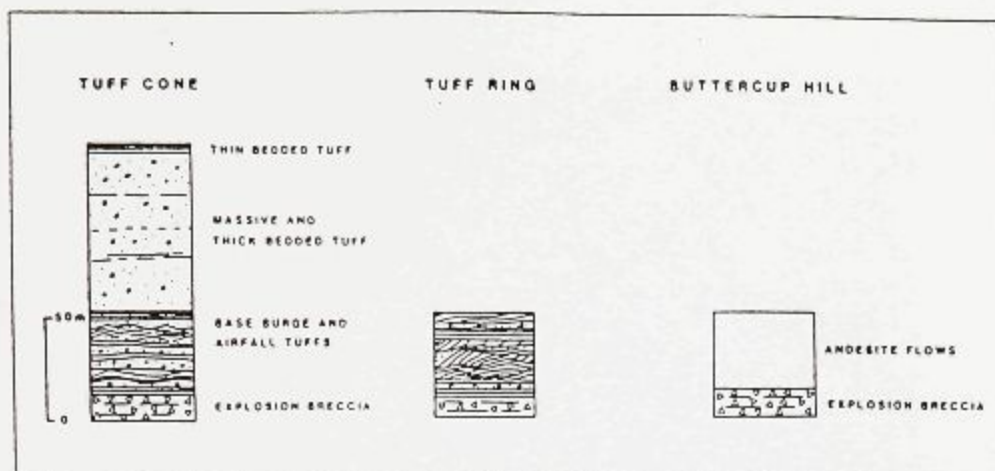


Figure B.6. Schematic stratigraphic sections modified from Wohletz and Sheridan (1983) for an idealized tuff cone and ring and for Buttercup Hill breccias. Explosion breccia in tuff cones and rings consists of chaotic, blocky breccia (open triangles) interlayered with minor air-fall and surge deposits (lines). Buttercup Hill breccias (open triangles) are interlayered with waterlain tuff (lines).

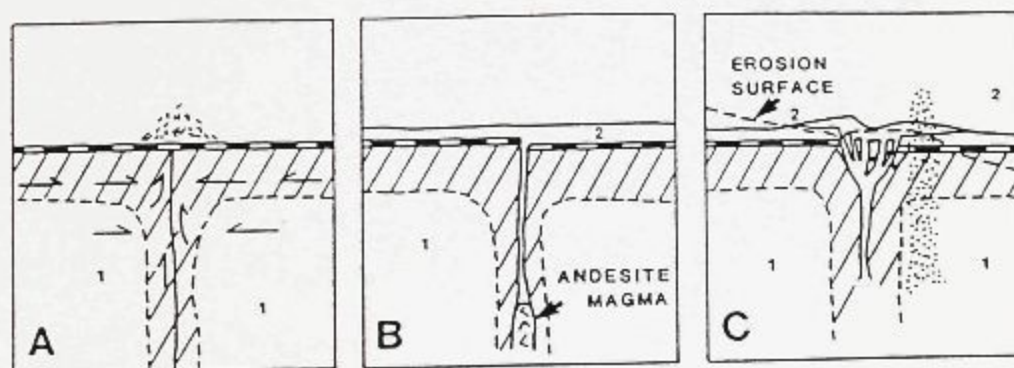


Figure B.7. Diagrammatic reconstruction portraying the sequence of events leading to the formation of the Buttercup Hill breccia (legend as in Figure B.2). **A.** Amulet formation paleosurface following deposition of the C Contact Tuff; hot-spring discharge occurred along faults that will later host the main breccia dike (arrows show intrastatal fluid flow; diagonal lines areas of silicification). **B.** Emplacement of andesitic magma (cones) and extrusion of andesitic flow (Millenbach Andesite formation). **C.** Emplacement of the Buttercup Hill breccia dikes and surface deposit, which is buried by penecontemporaneous andesite flows; dashed lines show present erosion surface.

**PLATE B1**

**A.** Hyalopilitic texture of silicified Amulet andesite. Albite microlites and phenocrysts in a groundmass of chlorite and blebby quartz. Amygdules filled with quartz and chlorite. Bar scale is 1mm long.

**B.** Conformable, shallow, southeast-dipping contact between the breccia deposit and Millenbach andesite flow. Tape measure is 4cm wide.

**C.** White-fragment breccia dikes merging with conformable breccia (see Figure 5).

**D.** Gradational, brecciated margins of dikes.



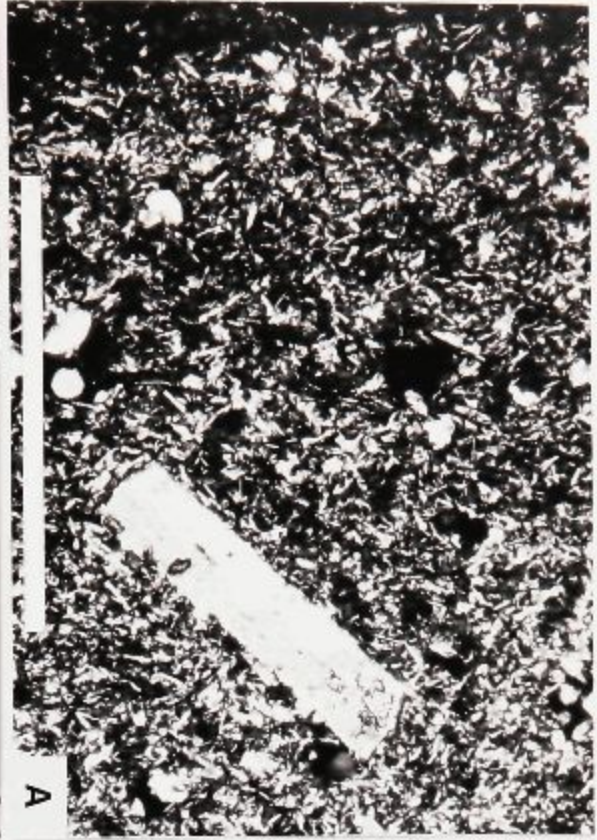


## PLATE B2

- A. Hyalopilitic texture of a silicified Amulet andesite fragment. Albite microlites and phenocrysts in a fine groundmass of chlorite and blebby quartz.
- B. Angular chloritized sideromelane shards (S) with curved smooth boundaries replaced by epidote, from main breccia dike.
- C. Microlitic, chloritized sideromelane shards (M) from main breccia dike; note variable size of fragments and broken plagioclase crystals in matrix.
- D. Arcuate fractures, "perlitic cracks," in a chloritized sideromelane shard (S) from breccia dike.
- E. Quartz amygdaloidal, opaque-rich rhyolite fragment (R) and silicified andesite fragment (A) from breccia dike.
- F. Silicified fragment identical to Amulet vitrohyre (V) from breccia dike.

Bar scale is 1mm long.

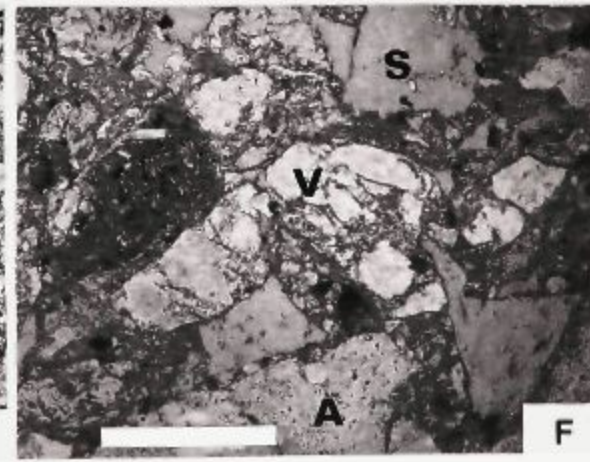
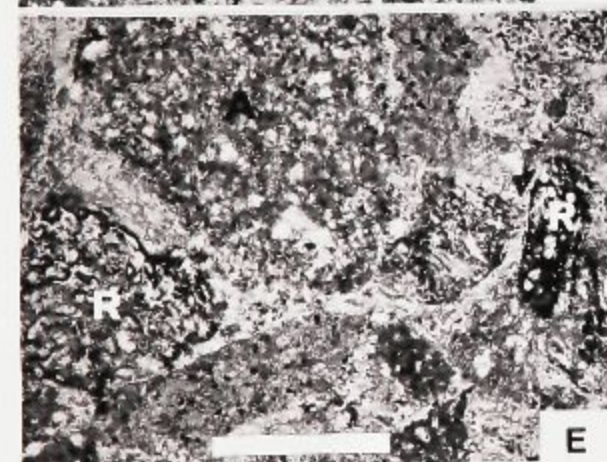
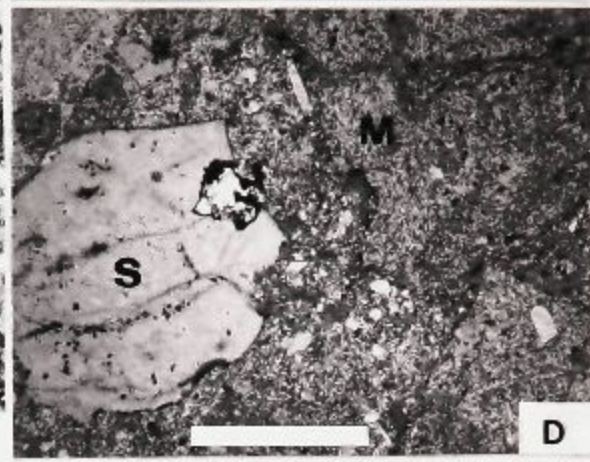
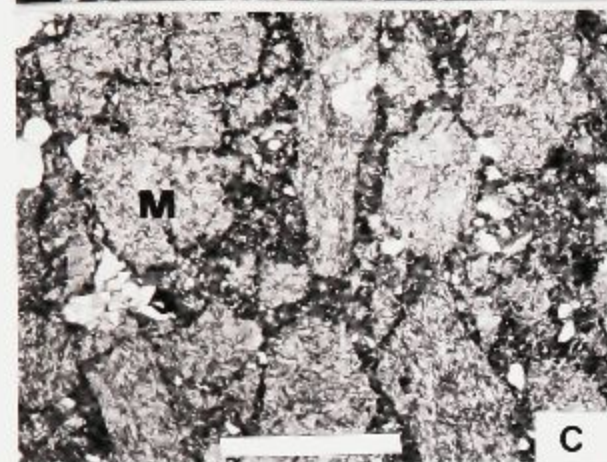
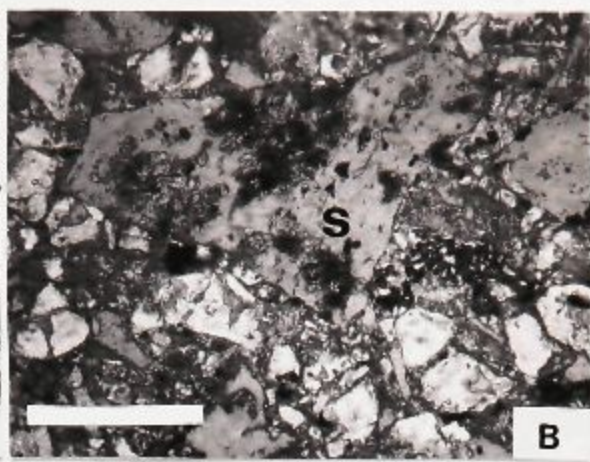
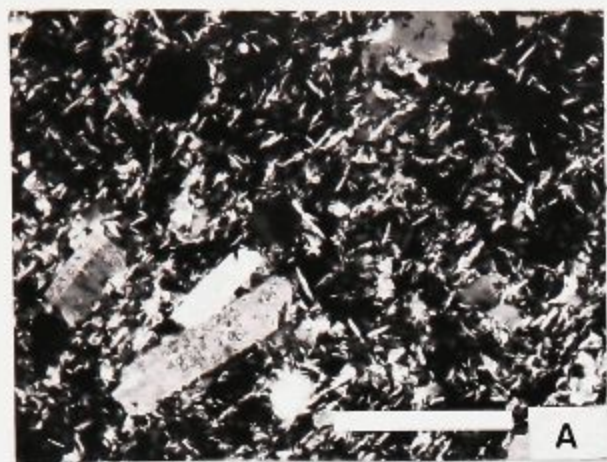


**PLATE B3**

**A.** In situ brecciated, silicified Amulet andesite. Fragments separated by veins of fine, chloritized breccia. Tape measure is 4cm long.

**B.** Poorly sorted, angular, variably silicified Amulet andesite fragments that constitute the conformable breccia deposit.

**C.** Bed characterized by numerous fragments of Millenbach andesite.

**D.** Crude bedding within the conformable breccia deposit. Hammer rests on top of bed; overlying bed is reversely graded (see Figure B5).

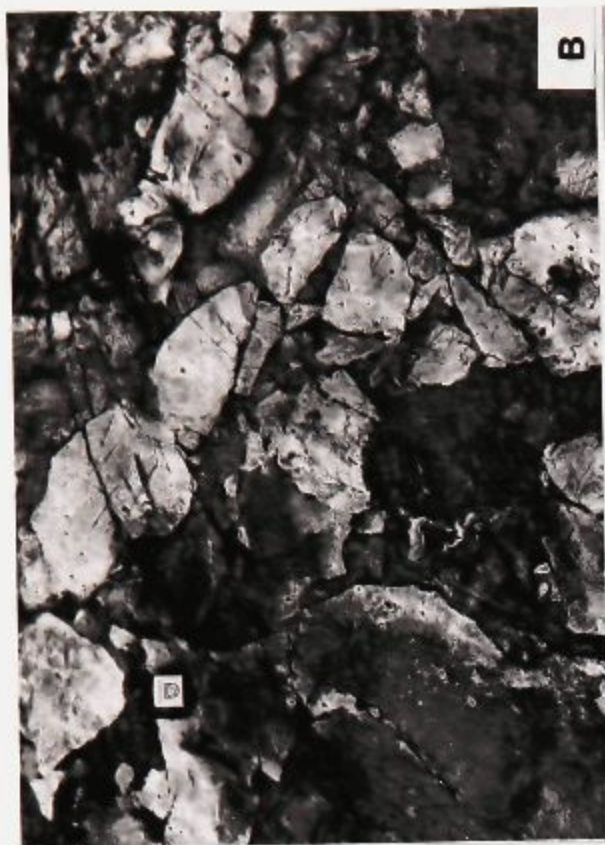


**PLATE B4**

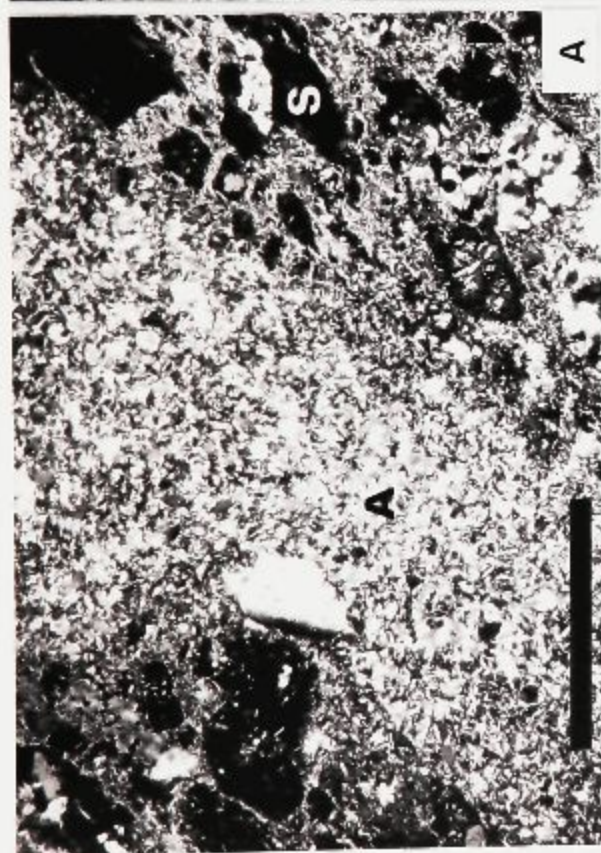
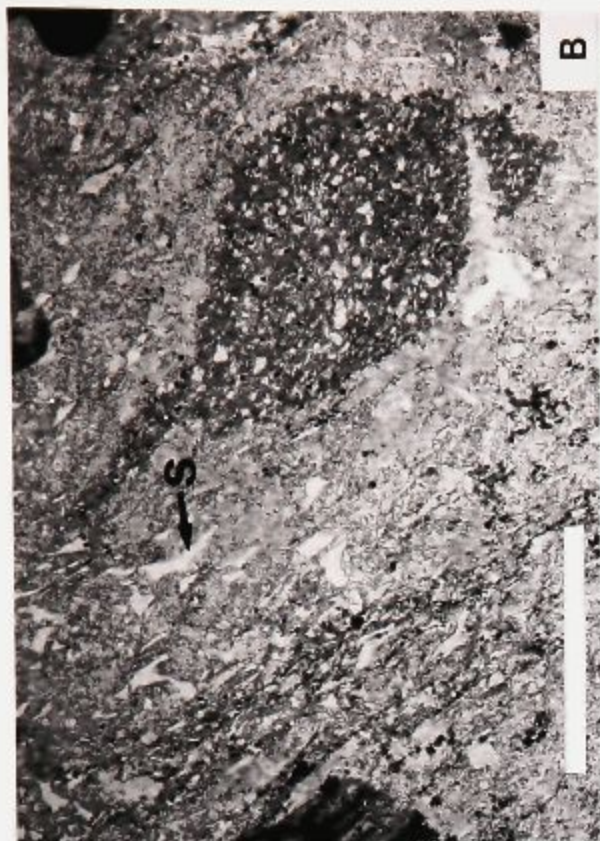
**A.** Chloritized sideromelane shards (S) and silicified andesite fragment (A) in matrix of breccia deposit.

**B.** Aligned sideromelane shards in a tuff matrix to breccia.

**C.** "Sagged bedding" in andesitic tuff (T) that slumped between fragments of silicified Amulet andesite within the breccia deposit.

**D.** Quartz-, chlorite- and opaque-rich laminae define bedding within andesitic tuff. Note angular, chloritized sideromelane shards (S) within ash laminae.

**Bar scale is 1mm long.**



APPENDIX C.

RECONSTRUCTION OF THE CORBET  
BRECCIA PILE AND  
VOLCANOGENIC MASSIVE SULPHIDE DEPOSIT

C.1 INTRODUCTION

The Corbet Mine produced 3.06 M tons of ore grading 3.0% Cu, 0.96% Zn, 0.06 oz Ag/t and 0.03 oz Au/t until it closed in September 1986. The deposit was discovered in 1974, at a vertical depth of 750m, during a drill program designed to test mineralized and altered volcanic strata within fault blocks adjacent to the synvolcanic McDougall-Despina Fault. Previous exploration for VMS in the Noranda camp was based on a single time-stratigraphic hypothesis and favourable tuff units were essentially grid drilled. The conception of stratigraphically stacked Cu-Zn deposits localized along synvolcanic northeast and northwest trending faults proposed by M.J.Knuckey in 1974, prompted a deep drilling program in an area



that had been previously "written off"; this led directly to the Corbet Mine discovery.

The Corbet discovery was particularly significant in modifying hypotheses of ore-localization within the Noranda camp. Not only is the Corbet deposit situated 1000m deeper stratigraphically than any previously mined deposits but it is located within an andesitic vent and overlain by rhyolite. The purpose of this chapter is amplify descriptions of the Corbet deposit by Watkins (1980) and Knuckey and Watkins (1982). New data presented are based on detailed underground mapping and drill programs. The setting of the Corbet deposit is described first, followed by a description of a quartz diorite intrusion which underlies the Corbet area and breccias which host the deposit and comprise the upper part of the Flavrian formation in the Corbet area. A reconstruction of the volcanic and hydrothermal history is discussed last.

## C.2 GENERAL GEOLOGY AND SETTING

The Corbet deposit is located at the top of the andesitic Flavrian formation, the lowest formation within the Mine Sequence (Figure C.1). Corbet is a proximal, copper-zinc, VMS deposit that consists of 7 lenses located within an andesitic vent area. Lenses 1, 2, and 3 comprise the main lens which forms the bulk of the Corbet deposit that, at the time of deposition, formed a continuous sulphide body that was subsequently separated into 3 lenses by faulting (Figure

C.2). Lenses 4, 5 and 7 are small zinc-rich satellite massive sulphide deposits located stratigraphically higher than the main lens (lenses 4 and 5 are located at the contact with overlying Northwest formation) whereas 6 lens is a copper-rich stringer zone situated 150m stratigraphically below the main lens.

The main lens is 400m long by 150m wide in plan, has an maximum thickness of 70m and is elongate parallel to the McDougall-Despina Fault (Knuckey and Watkins, 1982). The main lens is composed of stacked stratiform lenses (Figures C.4 and C.5) separated by semi-massive stringer and disseminated mineralization in altered volcanoclastic breccias. The deposit is underlain by a discordant stringer zone surrounded by an irregular envelope of chlorite and fringing sericite alteration that plunges  $70^{\circ}$  to the northwest, parallel to the McDougall-Despina Fault (Gibson, 1982).

Watkins (1980) and Knuckey and Watkins (1982) interpreted the main lens to have been deposited within a topographic depression or crater and the northeast trending "tongue of ore" to be massive sulphide that decanted over the rim of the crater and followed an irregular channel down the slope of the andesitic edifice. There is no doubt that part of #3 lens was localized within a crater. Evidence for this interpretation is illustrated in Figure C.5, where massive sulphide and an overlying massive flow have a flat or shallow west dip that contrasts with enclosing southeast-dipping breccias which comprise the edifice. This angular discordance defines a crater that has an approximate diameter of 250m (Figure

C.3).

Underground mapping and diamond drilling indicate that the tongue of ore is not massive sulphide, but a mixed, crudely bedded melange of massive sulphide blocks exceeding 10m in size incorporated within volcanoclastic debris (Figures C.6).

Of fundamental importance in volcanic reconstruction is the location of the Corbet deposit within an aerially restricted, topographically positive, volcanic edifice whose upper part (100m) is composed predominantly of breccia. This breccia edifice is separate but coeval with a larger on-lapping andesitic edifice immediately to the north. Volcanoclastic debris and flows from this larger edifice eventually covered the Corbet deposit. Features which are consistent with this interpretation include:

1. A 1200m X 300m, ridge-like paleotopographic high lies immediately adjacent and parallel to the McDougall-Despina Fault (Figure C.3). The high point of this edifice lies immediately northwest of the Corbet deposit.

2. East-west cross-sections through the Corbet deposit at 600 and 800 north (Figures C.4 and C.5) although slightly oblique to strike indicate a steepening of dip immediate to the deposit. This steepening reflects the east slope of the ridge which, after allowing for a regional dip of approximately  $30^{\circ}$ , indicates a primary slope of  $<15^{\circ}$ .

3. The tongue of breccia ore (Figure C.6) clearly separates volcanoclastic breccias and flows of the Corbet edifice from an adjacent larger edifice. The attitude of this tongue of transported ore also indicates a primary slope of  $<20^{\circ}$  for the northeast flank of the Corbet breccia pile.

A schematic north-south section through the Corbet area in Figure C.7, within the plane of the McDougall-Despina Fault, illustrates the small, separate breccia edifice hosting the Corbet deposit main lens and underlying stringer zone. Two massive sulphide lenses (#4, #5), each with their own stringer zone, occur stratigraphically above the Corbet main lens on the south flank of the larger andesitic edifice to the northwest. Volcanoclastic breccia covering the Corbet main lens contains strongly altered lithic and sulphide fragments which are interpreted to be debris shed from altered volcanoclastics and the small massive sulphide deposits located up-slope, along the south flank of the larger edifice.

### C.3 CORBET QUARTZ DIORITE

The Corbet quartz diorite is texturally, mineralogically and chemically similar (Watkins, 1980) to the Meritens phase of the synvolcanic Flavrian Pluton whose annular distribution is thought to be controlled by an early ring-fracture system (Goldie, 1976). The Corbet quartz diorite has a subophitic to ophitic texture with 45%, inclusion-rich, subhedral albite crystals ( $<3\text{mm}$ ) partially surrounded by 15-20% anhedral quartz ( $<1.3\text{mm}$ ) and 30% massive to prismatic

actinolite (replaced by chlorite) with 5-10% interstitial opaque minerals, epidote, myrmekite and trace sphene. Where altered, feldspars are replaced by fine quartz, chlorite and/or sericite. Contacts with adjacent flows are sharp, and the quartz diorite is typically fine-grained and chilled. Adjacent flows show no evidence of contact metamorphism and in some instances the distinction between flows and fine-grained border phase of the quartz diorite is based solely on the occurrence of quartz phenocrysts in the latter.

### **C.3.1 SIZE AND SHAPE**

The quartz diorite is a plug-like intrusion emplaced within 500m from the top of the Flavrian formation. Its location and approximate dimensions are illustrated in Figure C.3. Underground drilling indicates that the footwall contact (west) is straight and defines the McDougall-Despina Fault (Section P-P, Figure 9.6) whereas the hangingwall contact is hummocky and roughly conformable to the Flavrian-Northwest contact but locally disconformable to andesitic flow contacts. The Corbet quartz diorite occupies a position immediately underlying volcanic edifices and massive sulphide lenses at the Corbet Mine.

### **C.3.2 TIMING**

The Corbet quartz diorite is an early synvolcanic intrusion emplaced along the McDougall-Despina Fault during extrusion of the Flavrian formation. Where

the diorite is cut by the Na depleted, chloritic alteration pipe of the Corbet deposit, it is similarly altered and mineralized with disseminated and stringer sulphide (Figure 9.6 P-P; Gibson, 1982).

### C.3.3 SIGNIFICANCE

The coincidence of location of surface volcanic edifices, general "doming" of the Flavrian formation and the underlying and contemporaneous quartz diorite plug suggest that the latter is a subvolcanic intrusion. The intrusion of a hot, high-level (500m from paleosurface) subvolcanic intrusion into its own volcanic pile undoubtedly re-opened or generated new fractures that established cross-stratal permeability and focused ascending hydrothermal solutions to coincident volcanic vents at the sea floor.

The Corbet quartz diorite is part of the Meritens phase of the Flavrian Pluton and, like the latter, was emplaced along a synvolcanic ring fault, the McDougall-Despina Fault (Chapter 9). The earliest recognized phase of cauldron development, namely generation of ring faults and concomitant emplacement of high-level quartz diorite intrusions, coincided with extrusion of the Flavrian formation, the lowest stratigraphic unit within the cauldron-filling Mine Sequence.

## C.4 VOLCANIC BRECCIAS

Volcanic breccias and subordinate massive and pillowed andesitic flows comprise the uppermost 100m of a small volcanic edifice hosting the Corbet main lens (Figures C.4 to C.7). The breccias are not laterally extensive but are confined to the Corbet area. Breccias were subdivided into volcanoclastic, "in situ" breccia, and a third subordinate type termed "spatter breccia". The origin and distribution of these breccias are essential to unravelling the constructional history of the breccia edifice and environment of massive sulphide deposition.

### **C.4.1 VOLCANICLASTIC BRECCIA**

#### **Description and Distribution**

The vertical and lateral distribution of volcanoclastic breccia is illustrated in an idealized stratigraphic column (Figure C.1) and in the schematic north-south cross section of Figure C.7. Volcanoclastic breccia forms the base of the Corbet breccia pile which overlies strongly amygdaloidal (up to 20% amygdules) massive and pillowed flows. Volcanoclastic breccia envelopes the Corbet deposit and constitutes the bulk of the breccia edifice.

Volcanoclastic breccia consists of poorly sorted, thick-bedded deposits of lapilli tuff and subordinate lapillistone, tuff and tuff-breccia. The heterolithologic appearance of the breccia reflects multi-coloured fragments of chloritized, sericitized, silicified and unaltered andesite. Depositional units (10cm-2m) are

defined by variations in fragments size, matrix versus framework supported character, and dominance of lithic versus scoriaceous fragments (Figures C.8 and C.9). The breccias are poorly sorted and display crude normal grading and occasionally, reverse grading. Framework fragments (>1cm in size) are described below.

#### **Lithic Andesitic Fragments**

Lithic andesitic fragments are accessory pyroclasts that constitute the dominant framework of volcanoclastic breccia overlying the Corbet main lens and are a common constituent of all volcanic breccias comprising the Corbet edifice. Fragments vary from white to dark green, are angular to subangular, and range in size to 20cm, but are typically <6cm. The well bedded lapilli tuffin Plate C.3, is composed primarily of altered lithic fragments.

Lithic fragments are aphanitic, aphyric and weakly amygdaloidal (<5%) with a hyalopilitic texture composed of 15-40% plagioclase microlites in a fine mesostasis of chlorite with interstitial sulphides (Plate C.1A and C). Amygdules are filled by quartz and chlorite. Where altered, microlites are replaced by quartz, sericite and/or chlorite.



### **Scoriaceous Fragments**

Andesite scoria fragments are juvenile pyroclasts of vesiculated lava. They are a common but typically subordinate constituent of volcanoclastic breccia, but they are the dominant framework fragment within individual beds (Plate C.4) such as those at the base of the breccia edifice. Scoria fragments, commonly sericitized and silicified, are subrounded to rounded, and range to 15cm in diameter but are typically <5cm in size. Fragments consist of hyalopilitic andesite with 5-30% skeletal albite microlites and up to 40% round to elongate quartz- and chlorite-filled amygdules ranging in size from <1mm to 2cm (Plate C.1A and H).

### **Fluidal Andesitic Fragments**

Fluidal andesitic fragments are juvenile pyroclasts that are the least common framework fragments and typically occur with scoria fragments. The fragments have a characteristic elongate, irregular "fluidal form" with delicate tails and edges and range up to 4cm in size. Megascopic amygdules (5-20%) are common. Fluidal fragments are often indented by, or mold around, adjacent lithic fragments indicating hot deposition and incipient welding. The fragments consist of microlitic, chloritized sideromelane containing <15% albite microlites (Plate C.2B).

### **Massive Sulphide Fragments**

Massive sulphide fragments composed of pyrite, chalcopyrite and sphalerite are accidental fragments incorporated within volcanoclastic breccia overlying the

Corbet main lens and characterize debris flow deposits which constitute a "tongue of ore" on the north flank of the Corbet breccia pile. Massive sulphide fragments in volcanoclastic breccia above the main lens are <10cm in size, angular to subangular, and constitute <1% of the breccia. They may be derived from small massive sulphide deposits located up slope along the southern flank of the larger on-lapping andesitic edifice (Figure C.7).

Massive sulphide fragments within debris flow deposits which comprise a "tongue of ore" were subdivided into two types based on their contacts with andesitic fragments. The first type of fragments range in size to 1m, have sharp contacts with surrounding breccia and are fragments of consolidated massive sulphide (Figure C.9, Plate C.9). The second, and dominant fragment type ranges from 30cm to >10m in size, and has irregular contacts with surrounding andesitic fragments which are incorporated within their margins (Figure C.9). These features plus small scale loading structures along their margins suggest that they were incorporated and transported within volcanoclastic debris flows in a semi-consolidated state.

### **Matrix**

The matrix to volcanoclastic breccia consists of fine (<1cm) subangular to subrounded framework fragments, angular chloritized sideromelane fragments and fine (<0.02mm) tuff now composed of quartz, chlorite, sericite and shard-like

fragments of quartz and minor albite crystals with 3 to 30% sulphides. Chloritized sideromelane fragments are either massive or amygdaloidal (Plates C.1A to H and C.2 A to C).

Massive sideromelane fragments consist of fine massive chlorite with skeletal albite microlites (<5%) and opaque minerals (3%). Fragments contain <10% amygdules, are typically equant, and angular with smooth straight or slightly concave or convex boundaries that meet in knife-like points (Plate C.1A and E). Fragment boundaries distinctly cross-cut amygdules and fine arcuate perlitic cracks attest to the original glassy nature of the shards. Fragment morphology is consistent with fragmentation in response to thermal strain, resulting from fluid-magma interaction (Heiken, 1972; 1974; Honnorez and Kirst, 1975). Massive sideromelane shards are interpreted to be fragments of juvenile, quenched andesite magma.

Amygdaloidal sideromelane fragments consist of massive chlorite with <5% skeletal microlites and opaque minerals and from 5-25%, round to elongate quartz- and chlorite-filled amygdules. Fragments range from subrounded to rounded, strongly amygdaloidal "scoria" fragments (Plate C.1G and H) with smooth curved boundaries to subangular, elongate, ragged fragments with delicate tails and irregular boundaries (Plate C.1C, E and F). Thin, curved, plate-like fragments may be remnants of vesicle walls. The morphology of amygdaloidal sideromelane fragments is definitely controlled in part by ruptured amygdules, and is consistent

with fragmentation by rapid exsolution of volatiles and quenching during subaqueous pyroclastic explosions (Heiken 1972; 1974, Honnorez and Kirst, 1975).

### **Interpretation**

Volcaniclastic breccia deposits are interpreted to be products of phreatomagmatic and strombolian eruptions. Volcaniclastic breccia composed principally of accessory lithic fragments and non-vesiculated juvenile sideromelane shards are interpreted as phreatomagmatic deposits produced by explosive steam generation during seawater interaction with near-surface ascending andesitic magma.

Volcaniclastic breccia with numerous scoriaceous fragments, amygdaloidal sideromelane shards and subordinate accessory lithic fragments are interpreted as strombolian deposits produced by rapidly exsolving and expanding volatiles which disrupted near-surface ascending magma producing a lava-fountain of ash, scoriaceous lapilli and block sized fragments. Most volcaniclastic breccia represents transitional deposits as it contains both lithic and scoria fragments with variable proportions of massive and amygdaloidal sideromelane shards. These deposits are interpreted to be products of "mixed" eruptions where intermittent introduction of water to ascending magma results in a shift from strombolian to phreatomagmatic activity during a single eruption. The occurrence of composite lapilli (Plate C.2A and C), where strongly amygdaloidal, subround lapilli are bound by an

amygdaloidal lava matrix within both scoria and lithic dominated beds, is consistent with transitional phreatomagmatic and Strombolian deposits (Fisher and Schmincke, 1984).

In both Strombolian and phreatomagmatic eruptions the primary mechanism for pyroclast emplacement is ballistic fall (Fischer and Schmincke, 1984; Williams and McBirney, 1979). However, in subaqueous eruptions the overlying water column may tend to elutriate and suspend fine ash and restrict the trajectory of fragments resulting in a more localized deposit. Sandwave bed forms (Figure C.8) in ash deposits interbedded with volcanoclastic breccia suggest that phreatomagmatic eruptions may have generated base surges that spread laterally from the vent to deposit both ash and fine lapilli tuff. The constructional edifice produced was a gently sloped ( $<20^\circ$ ) tuff cone with a central crater, marking the primary vent, that was also the locus of vigorous hydrothermal discharge producing the Corbet main lens (Figure C.3 and C.7).

Phreatomagmatic and strombolian eruptions were restricted to the late-stage growth of an underlying broad lava shield and presumably occurred when water depth allowed pyroclastic eruptions. Based on theoretical calculations of Allen (1980) and observations of Moore and Schilling (1973) for vesiculation and explosive activity in subglacial and submarine eruptions in Iceland, water depth is estimated at 100-200m and definitely  $<300\text{m}$ ; this is the greatest depth at which steam generation has been reported (Tanakadati, 1935; in Fisher and

Schmincke, 1984).

Volcaniclastic breccia containing numerous sulphide fragments within the "tongue of ore" along the north slope of the tuff cone are interpreted as submarine debris flow or avalanche deposits (Plate C.9). These volcaniclastic deposits are crudely bedded, both normally and reversely graded, range from matrix- to framework-supported, and occur as "channels" or "lenses" that are often unconformable with each other (Figure C.9).

#### C.4 "IN SITU" BRECCIA

##### Description and Distribution

"In situ" breccia is of limited areal extent and is intimately associated with massive and pillowed flows that underlie the Corbet main lens (Figures C.4 to C.7). "In situ" breccia deposits were derived through fracturing and brecciation of massive and pillowed flows. The massive flow in Plate C.5, is shattered and fractured by a crudely perpendicular vein set that separated individual blocky, angular fragments ranging from 3cm to 0.5m that fit together like pieces of a puzzle. Where veining is most intense, fragments are correspondingly smaller and rotated. Sulphide outlined pillows in Plate C.6, grade upward through an "in situ" shattered and veined breccia into an angular, monolithologic, unsorted, blocky breccia where fragments are separated and rotated with respect to each other. A close up of the chaotic breccia in Plate C.7, illustrates the angular nature of the

fragments, their poor sorting and matrix-supported character.

The andesitic fragments are typically unaltered and consist of weakly amygdaloidal (quartz-sulphide filled), aphyric, aphanitic hyalopilitic andesite. The vein-network matrix in both "in situ" brecciated and chaotic blocky breccia consists of pyrite-sphalerite-galena-quartz. Veins separating fragments are typically zoned with an outer margin of massive or coliform pyrite (with shrinkage cracks), and an inner zone of quartz, sphalerite and trace galena. Coliform textures and zoning within veins suggest open-space deposition within a highly permeable unit.

"In situ" breccia is completely gradational into underlying andesitic flows. Contacts with volcanoclastic breccia are irregular, locally abrupt, where bedded volcanoclastic breccia rests in sharp contact with underlying "in situ" breccia, but more commonly are gradational where the former occurs between fragments of the latter.

### **Interpretation**

Monolithologic "in situ" breccia is interpreted to be a "shock product" of explosive phreatomagmatic eruptions which shattered and brecciated massive and pillowed flows localized within and underlying the tuff breccia pile. Breccias produced were largely subsurface (no bedded ash component) but their gradation into volcanoclastic breccia indicates that fragments were incorporated into overlying

and adjacent breccias.

"In situ" breccia deposits provided an extremely porous and permeable footwall that directed contemporaneous ascending metalliferous hydrothermal solutions both vertically to surface and laterally below the sea floor. Precipitation of sulphides within the matrix of "in situ" brecciated andesite essentially sealed and cemented the breccia footwall producing a semi-conformable zone of stringer mineralization (with or without significant attendant alteration) below the Corbet deposit.

### C.4.3 SPATTER BRECCIA

#### Description and Distribution

Spatter breccia constitutes small (<5m X 2m) localized deposits within volcanoclastic breccia underlying the Corbet main lens. The breccia consists of strongly sericitized, scoriaceous (+ 40% quartz amygdules, <0.5cm in size) ribbon-like to amoeboid fragments with distinctly chilled margins (smaller amygdules) within a chloritized, massive and amygdaloidal sideromelane shard hyaloclastite matrix. The fragments are tightly packed (Plate C.8) and separated by a thin hyaloclastite envelope, or occur as matrix-supported fragments within chloritized hyaloclastite. Spatter breccia forms distinct mounds on and within volcanoclastic breccia; angular fragments produced by autobrecciation of amoeboid fragments are incorporated into adjacent volcanoclastic breccia.



## Interpretation

Spatter breccia deposits, as the name implies, are interpreted to be small subaqueous spatter cones or ramparts that formed within and outside the crater during lava-fountaining that accompanied Strombolian eruptions. Similar breccias within volcanic breccias on emerging seamounts are interpreted to have an analogous origin (H.U.Schmincke, personal communication, 1983).

## C.5 TUFF DEPOSITS

### C.5.1 DESCRIPTION AND DISTRIBUTION

Thin (<1m thick) aerially restricted and discontinuous tuff deposits occur along the base and top of the main lens and within overlying volcanoclastic breccia. Tuff deposits consist of thinbedded to laminated, locally graded, plane parallel and mantle bedded andesitic ash intercalated with chert and sulphide-rich (>40% sulphide) beds. Convolute bedding and undulating laminae with dune-like forms, although not common, characterize some exposures (Figure C.8, Plate 6.).

The ash-sized component is identical to the tuff matrix of volcanoclastic breccia and consists of fine (<0.02mm) quartz and chlorite with minor, <5% angular shard-like fragments of quartz and subordinate feldspar crystals. Crystal rich laminae containing 15-25% quartz crystal fragments are common (Plate C.2D).

### C.5.2 INTERPRETATION

Plane parallel bedding and mantle bedding indicate that most tuffs are waterlain deposits that accumulated during brief hiatuses in volcanic activity. The andesitic component is presumably derived from settling of fine suspended ash generated by explosive volcanic activity. Sulphide-rich and chert laminae represent chemical components presumably derived from contemporaneous discharge of metalliferous and SiO<sub>2</sub>-rich hot springs.

Although not unequivocal the bedforms of some tuff deposits are consistent with their emplacement as base surges. Ash laminae inclined to plane parallel beds (Figure C.8, Plate 6.3) define antidunes that are a characteristic bed form of the sandwave facies in base surge deposits. Similarly, convolute bedding and load casts may be a product of shear-deformation caused by an overriding base-surge deposit (Fisher and Waters, 1970) or simply gravity sliding and slumping of water-saturated ash. However, as pointed out by Cas and Wright (1987) the probability of subaqueous base surges is generally considered low, due mainly to the resistance of the surrounding water which is interpreted to be great enough to inhibit surge propagation.

### C.6 SILICEOUS DEPOSITS

Aerially restricted (<5 X 5m), discontinuous, deposits of non-bedded to laminated massive chert (<0.01mm quartz) cement both volcanoclastic and "in situ" breccia

within the footwall and lateral to the Corbet main lens. The chert is a pure chemical sediment (no ash component), interpreted to be a silica-sinter deposited from localized low-temperature, metal poor,  $\text{SiO}_2$ -rich hotsprings preceding and contemporaneous with discharge of metalliferous fluids forming the Corbet deposit.

### C.7 SUMMARY AND SEQUENCE OF EVENTS

The sequence of events outlined below is summarized, diagrammatically, in Figure C.10.

1. Voluminous eruptions of andesitic flows issued from a fissure within the McDougall-Despina Fault now occupied by rhyolite dikes. Continuous Hawaiian-type eruptions built up a northwest-trending andesitic lava shield composed of two overlapping "vents" along the feeding fissure (Figure C.10A).

2. A shallow subvolcanic intrusion, the Corbet QP diorite, was emplaced into its own volcanic pile, during contemporaneous surface eruptions. Emplacement of the intrusion resulted in a general doming of the vent area (Figure C.10A).

3. During the final phase of lava shield construction, volcanic activity changed from quiet effusion of lava to pyroclastic eruptions, possibly corresponding to a decrease in water depth. Initial eruptions were primarily Strombolian followed by an ever increasing number of phreatomagmatic eruptions as water

increasingly gained access to the vent. The end result was a breccia pile composed of volcanoclastic breccia transitional between Strombolian and phreatomagmatic deposits (Figure C.10A).

4. Massive and pillowed flows, erupted within and proximal to the breccia pile crater, were shattered and brecciated during continued explosive eruptions. Discharge of metalliferous fluids within the crater formed the main lens of the Corbet deposit. Contemporaneous SiO<sub>2</sub>-rich hydrothermal fluids discharged from hot springs both within and outside the crater.

5. Continued pyroclastic and hydrothermal activity resulted in the formation of smaller massive sulphide lenses stacked above the main lens. With continued eruptions the north wall of the crater collapsed and massive sulphide-volcanoclastic breccia debris flows were channelled down the north slope of the Corbet tuff cone (Figure C.10A).

6. Continued pyroclastic eruptions and effusion of lava from the Corbet vent along with volcanoclastic debris shed from the larger edifice to the northwest covered the Corbet deposit and breccia pile. Contemporaneous hydrothermal activity formed 2 small massive sulphide deposits on the south flank of the larger edifice.

7. Andesitic volcanic activity ceased and was immediately followed by extrusion of a thick compound rhyolite flow of the Northwest formation. This flow issued from northwest- and northeast-trending feeder dikes in the Corbet area

(Figure C.10B). Continued hydrothermal activity resulted in alteration of the overlying rhyolite flow for up to 100m above the Corbet deposit .

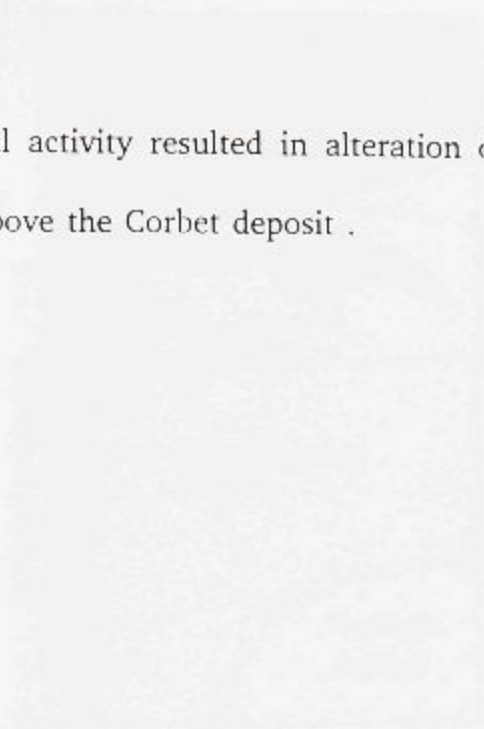


Fig. C.1. Map of the hydrothermal system at the Corbet deposit, showing the location of the hydrothermal system and the alteration zone.

Figure C.1. Simplified stratigraphy of the Corbet Mine.

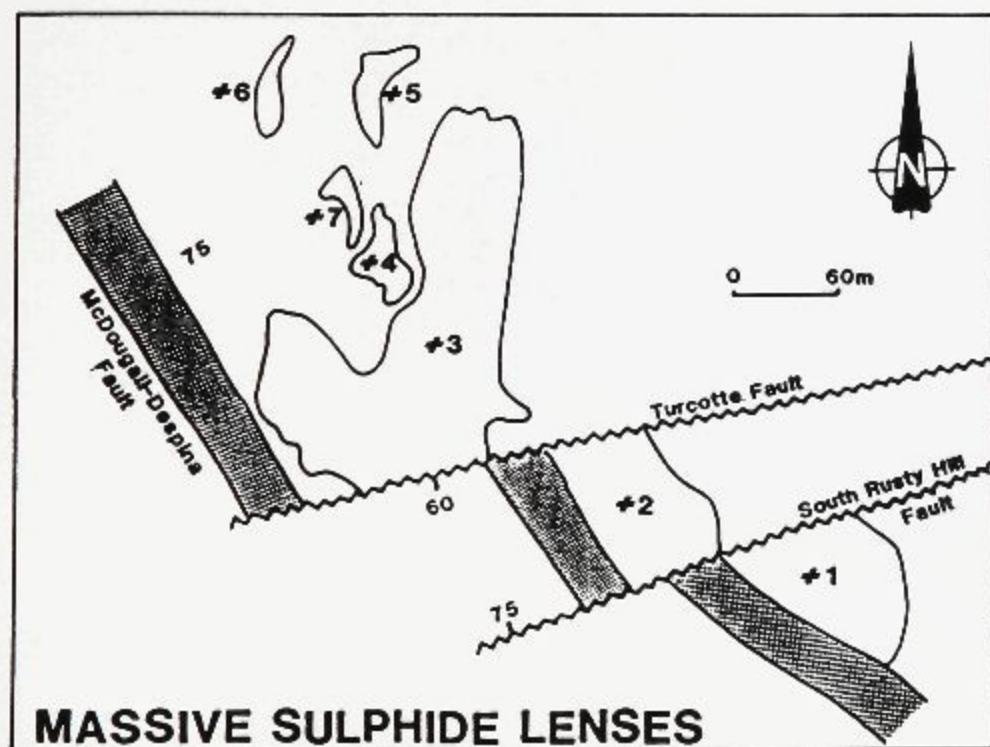
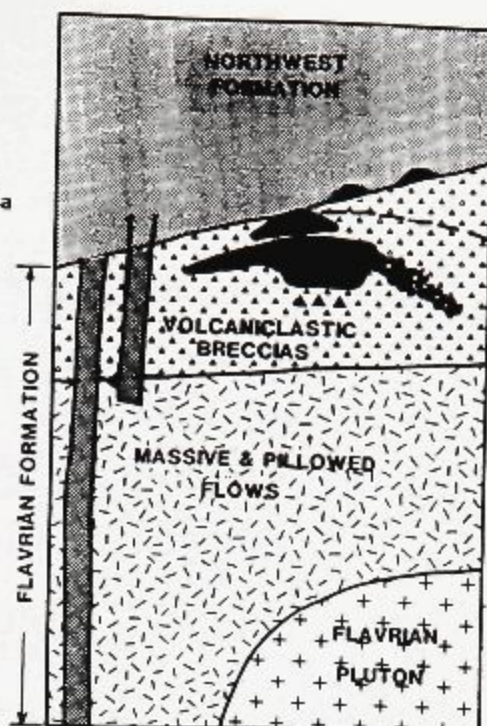
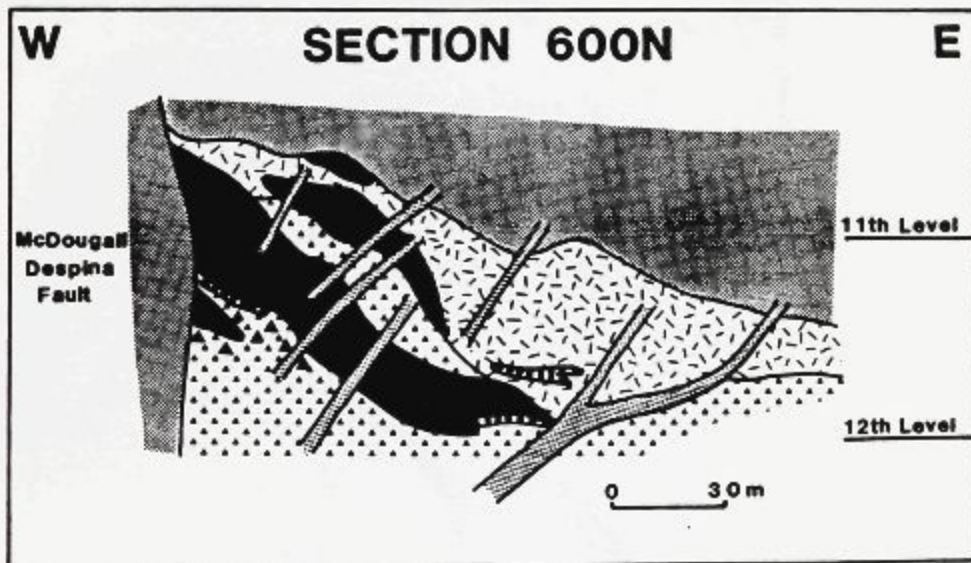
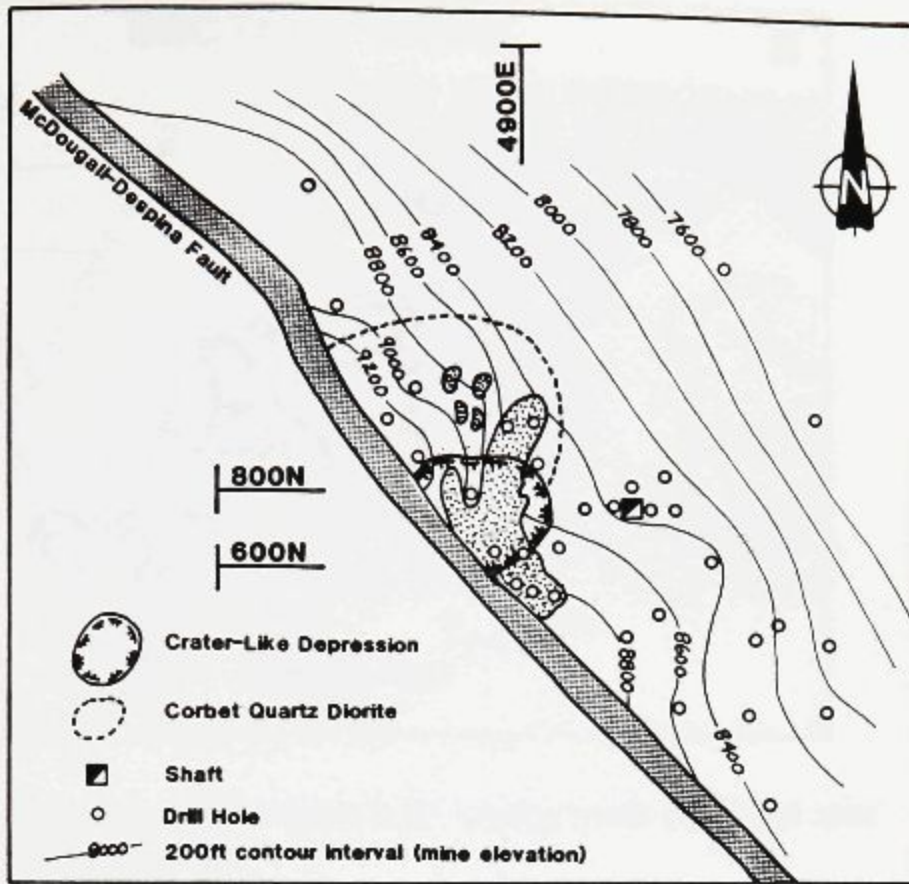


Figure C.2. Massive sulphide lenses at the Corbet Mine. The McDougall-Despina Fault is occupied by rhyolitic dikes.

Figure C.3. Subsurface topography of the Flavrian formation at the Corbet Mine showing the location of the Corbet massive sulphide lenses with respect to a paleotopographic ridge (8800 contour), crater-like depression and underlying Corbet Quartz Diorite intrusion. Diagram was constructed using data from both surface (open circles) and underground drill holes/workings; fault offset was removed for simplification.

Figure C.4. Geology of Section 600N (Figure C.3), looking north (modified from Knuckey and Watkins, 1982).





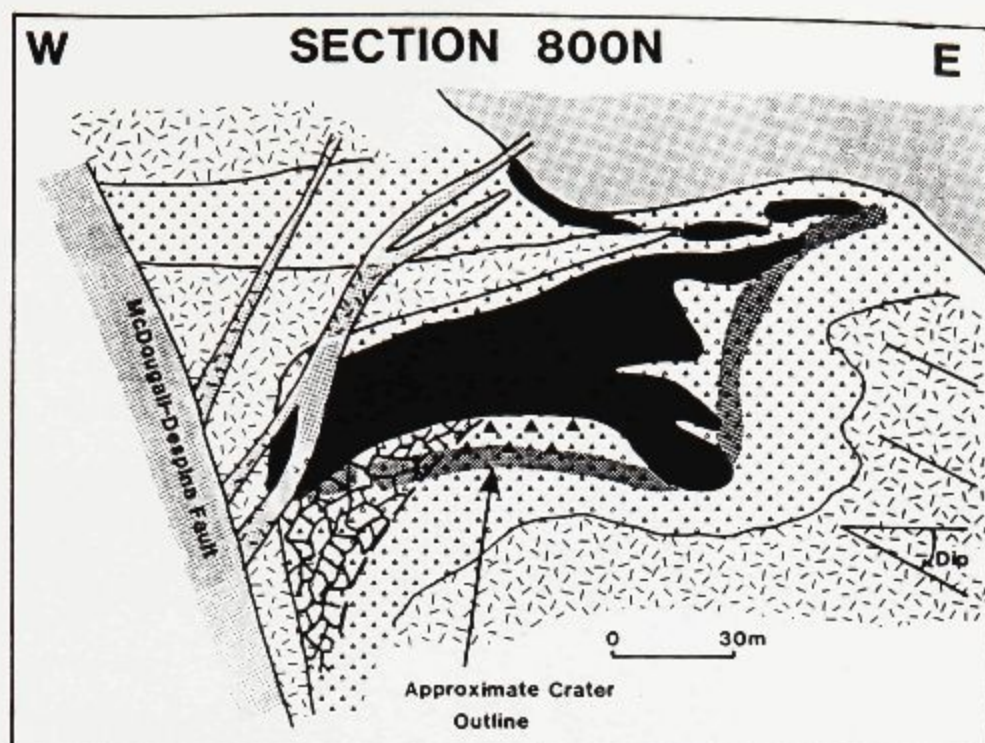


Figure C.5. Geology of Section 800N (Figure C.3), looking north (modified after Knuckey and Watkins, 1982).

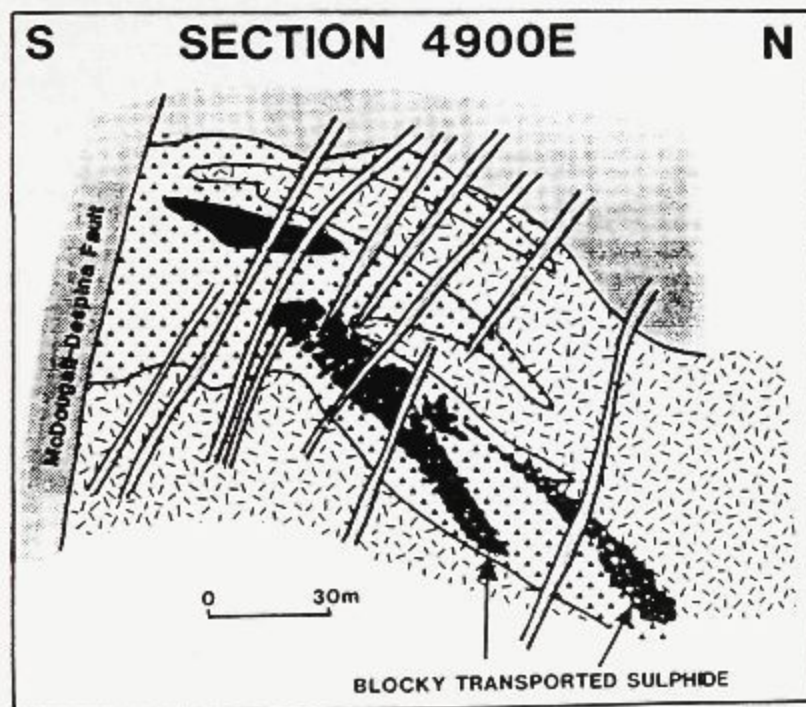
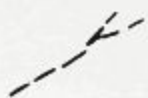


Figure C.6. Geology of section 4900E (Figure C.3), looking west (modified after Knuckey and Watkins, 1982).

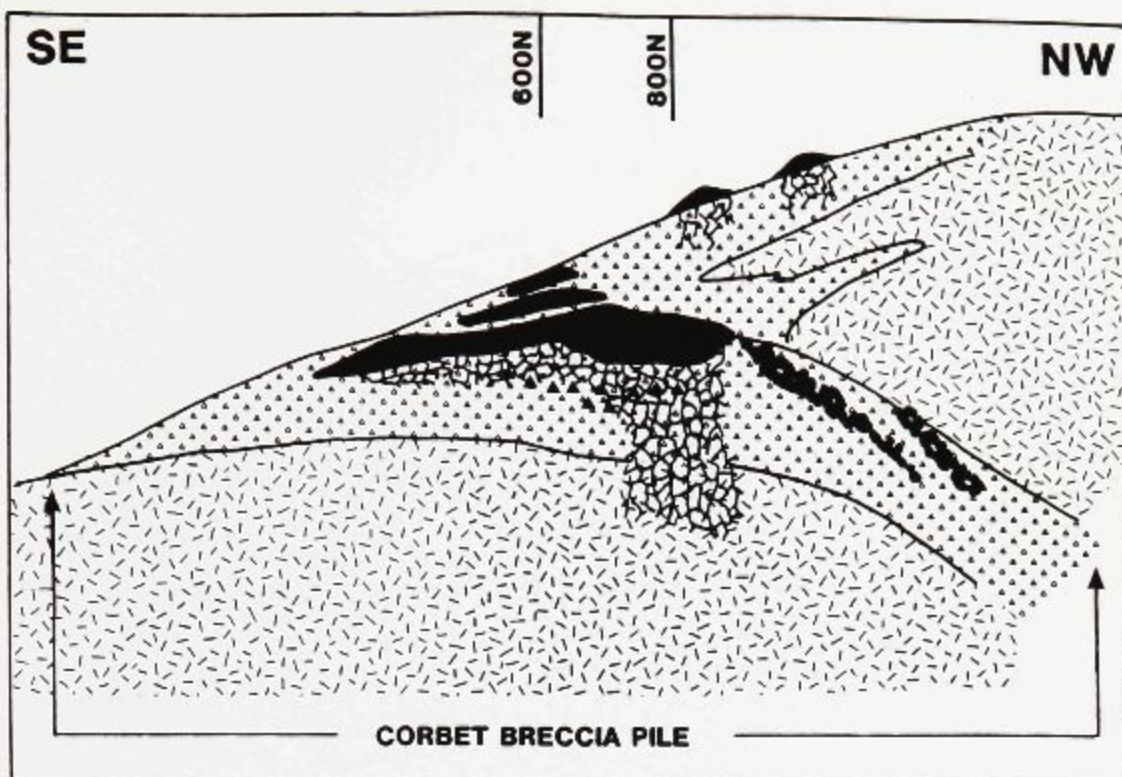
Figure C.7. Schematic north-south cross-section through the Corbet breccia pile and an on-lapping larger edifice to the north (looking west).

Figure C.8. Wall map detailing geology of the #1 draw point.

- 7 Massive fine pyrite.
- 6 Andesitic lapilli tuff containing white, sericitized and silicified scoriaceous andesite lapilli in a finer fragmental matrix with pyrite, sphalerite and chalcopyrite. Scoria fragments range from subrounded to fluoidal in form with delicate wispy tails. Framework supported and poorly sorted unit.
- 5 Plane parallel laminated pyrite and sphalerite. Beds locally slumped and broken. Thin bed of massive sphalerite containing pyrite framboids.
- 4 Ondulating laminae of grey and green ash, sphalerite and minor chert and chalcopyrite with a distinct dune-like morphology. Individual laminae are normally graded, pinch and swell along strike and are locally slumped and broken. Sphalerite laminae change abruptly into chalcopyrite laminae along strike with chalcopyrite also occurring in fractures oriented normal to bedding.
- 3 Convolute and broken beds of grey chert, ash and sulphides.
- 2 Andesite lapilli tuff with scoriaceous andesitic lapilli identical to unit 6.
- 1 In situ brecciated andesite with angular, dark green to grey amygdaloidal andesite fragments within a vein network matrix of quartz and sulphide (10% pyrite) and <5% fine white scoriaceous andesitic fragments.



Chalcopyrite filled fractures with chloritic margins.



### #1 DRAW POINT - 12-09 DRIFT

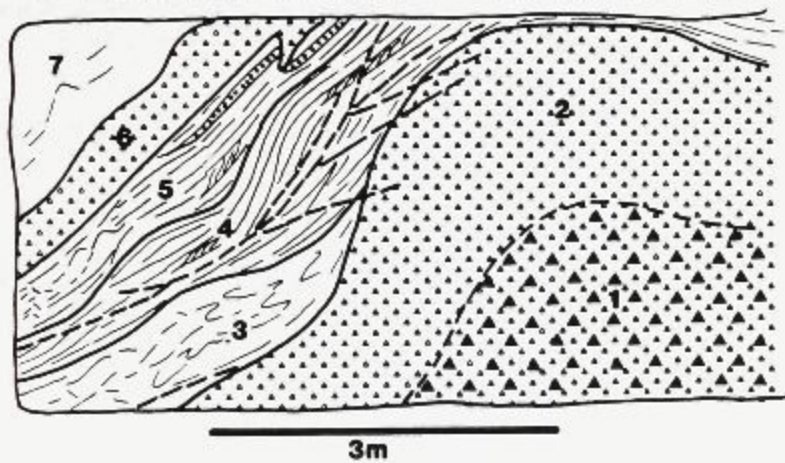


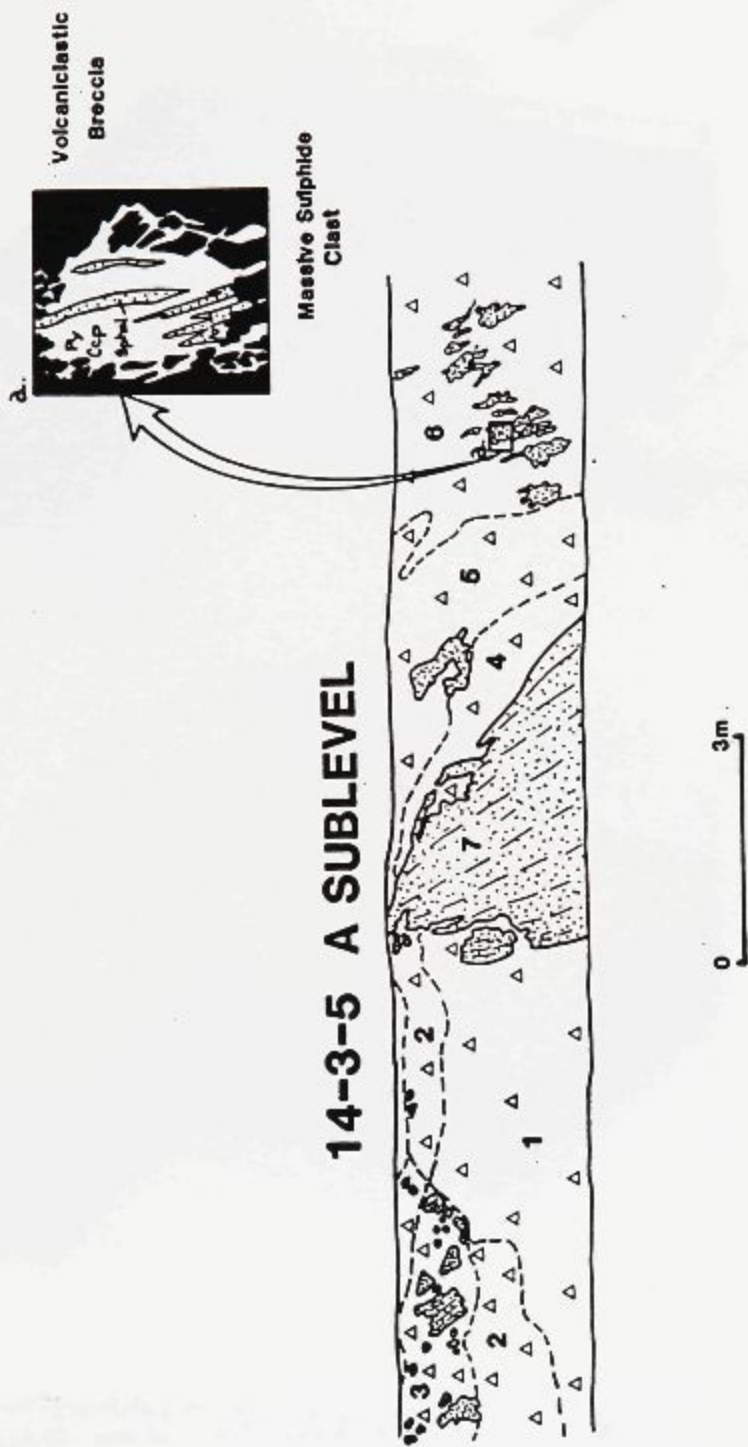


Figure C.9. Detailed geology of the 14-3-5 A sublevel where bedded volcanoclastic breccias comprise the "tongue of ore" along the northeast slope of the Corbet breccia pile.

- △ Volcanoclastic breccia
-  Angular massive sulphide fragments
-  Irregular massive sulphide fragments
- 7 Large block of massive, finely banded pyrite, chalcopyrite and sphalerite. Irregular contact with surrounding breccias and flame-like projections of massive sulphide at fragment margin suggest block was transported in a semi-consolidated state.
- 6 Poorly sorted tuff breccia with irregular fragments of massive sulphide. Inset shows detail of incorporation of volcanoclastic fragments (block) into margins of massive sulphide clast.
- 5 Lapilli tuff with altered andesite and massive sulphide lapilli is a  
4 siliceous and ash matrix.
- 3 Poorly sorted, framework supported lapilli tuff with chloritized andesite lapilli and angular blocks of massive sulphide.
- 2 Matrix supported, poorly sorted, lapilli tuff containing chloritized andesite lapilli and blocks in a grey to buff weakly laminated siliceous matrix.
- 1 Framework supported, poorly sorted lapilli tuff containing angular lithic and subrounded scoriaceous fragments of andesite that are strongly silicified and sericitized in a pale green to white siliceous and sulphide-rich (>10%) matrix. Poorly graded with an increase in matrix (to 30%) toward the top.

# 14-3-5 A SUBLEVEL



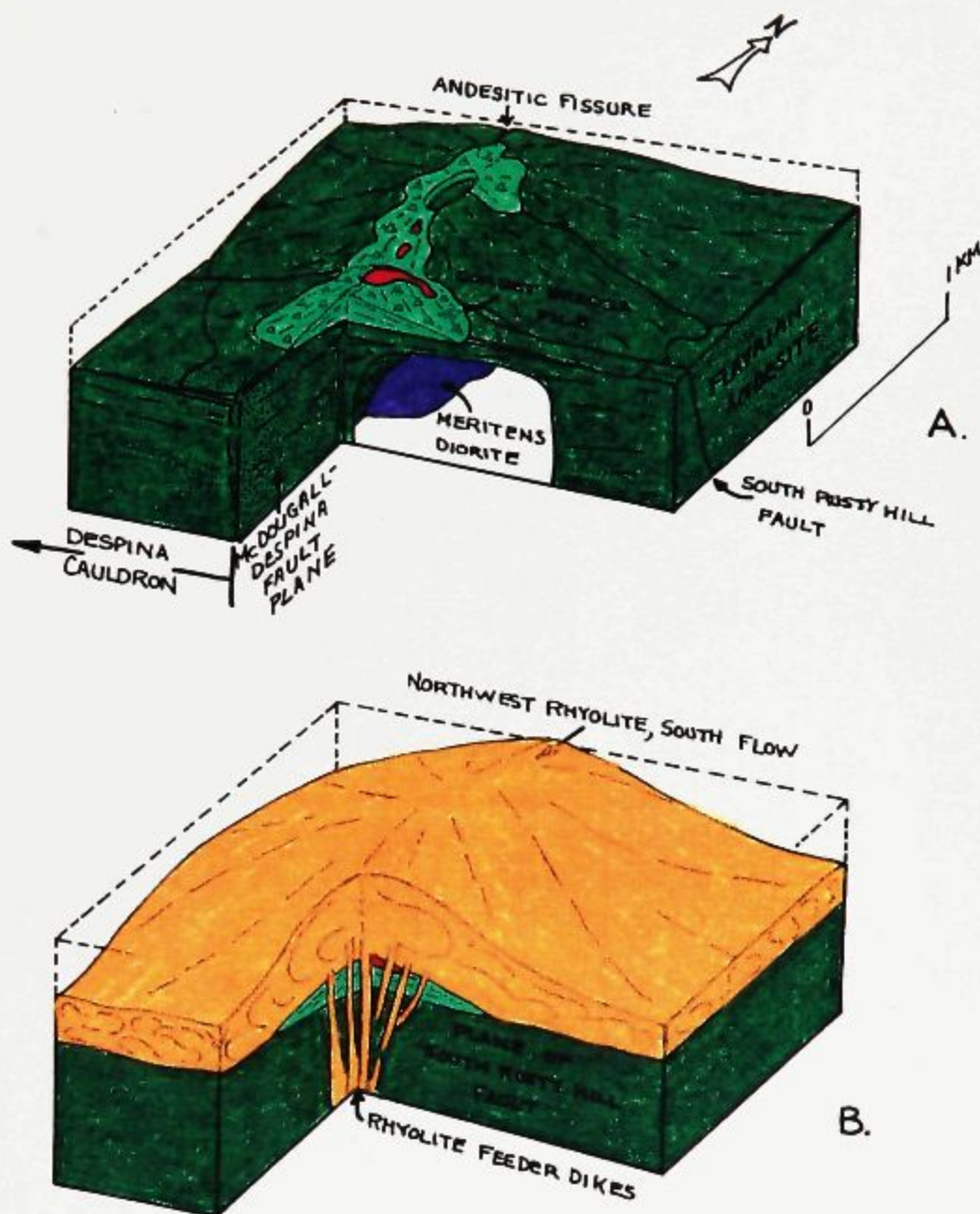


Figure C.10. Cartoon illustrating an interpreted volcanological reconstruction of the Corbet volcanic edifice and massive sulphide deposit. A. Depicts the shield-like Corbet edifice, localized breccia piles and massive sulphide deposits along the McDougall-Despina Fault. B. Illustrates the extrusion of the south flow of the Northwest formation from feeder dikes along and parallel to the McDougall-Despina Fault and from dikes parallel to the South Rusty Hill Fault.

## PLATE C.1

**A.** Aphanitic and aphyric weakly quartz amygdaloidal, andesitic fragment (A) and chloritized shards (S) within a typical lapilli tuff.

**B.** Amygdaloidal andesite fragment (A), chloritized shards and altered andesitic lapilli in a matrix of finer fragments, chlorite and quartz.

**C.** Altered (sericitized) microlitic andesitic fragment (A) and angular, plate-like chloritized shards in a finer breccia and quartz matrix.

**D.** Matrix to transported sulphide breccia of the #3 lens. Note the rounded appearance of the chloritized shards (S) as compared to identical shards in **E**, **F**, and **G**.

**E.** Delicately shaped chloritized shards with ragged margins and tails. Note the xenolith of altered andesite (X) within the larger shard.

**F.** Plate-like, angular chloritized shards and minor altered andesitic fragments in a finer breccia matrix.

**G.** Amygdaloidal shards containing numerous fine oxides.

**H.** Amygdaloidal and massive shards constitute the dominant fragment type within this lapillistone tuff.

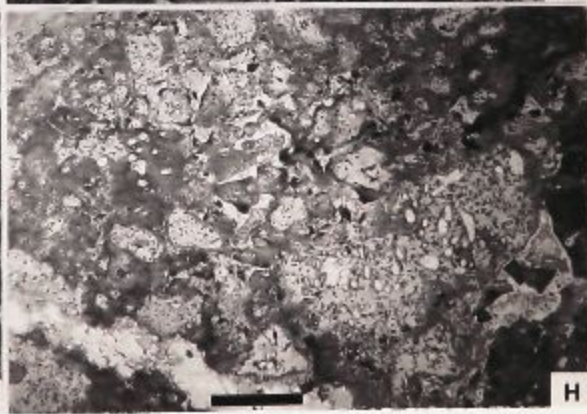
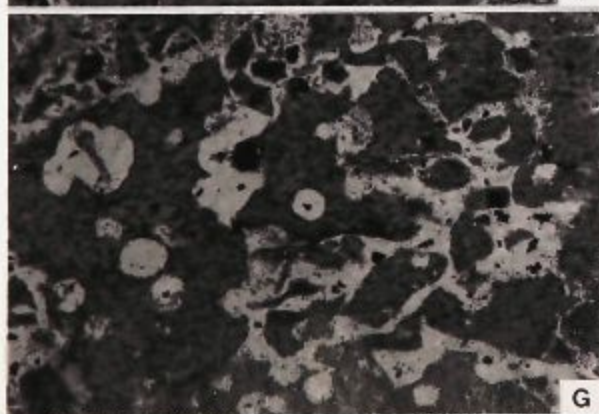
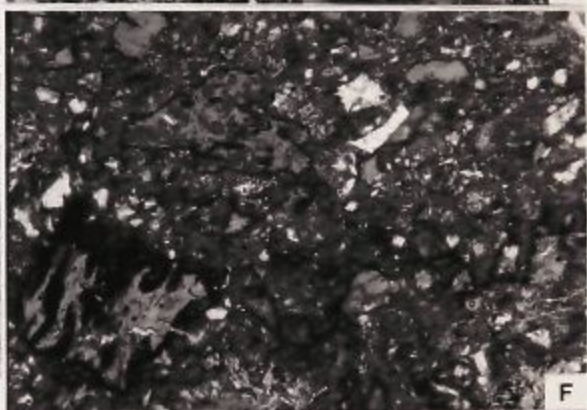
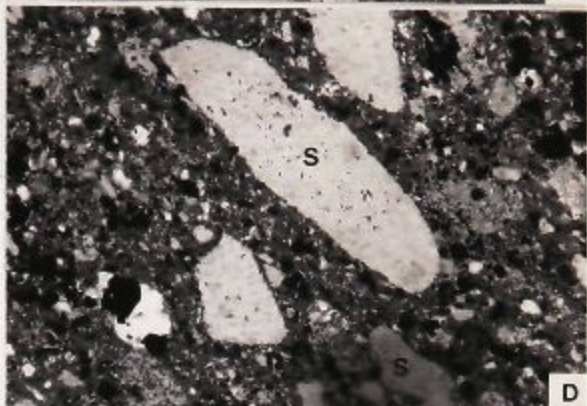
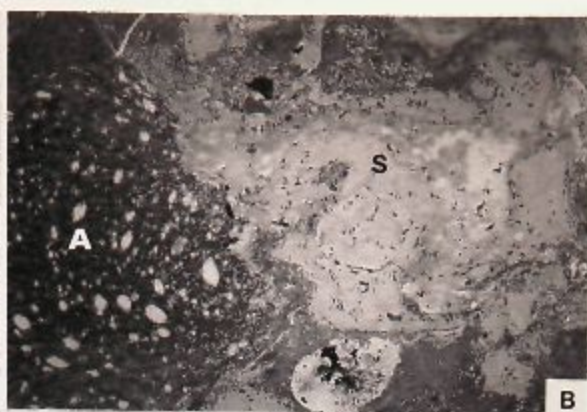
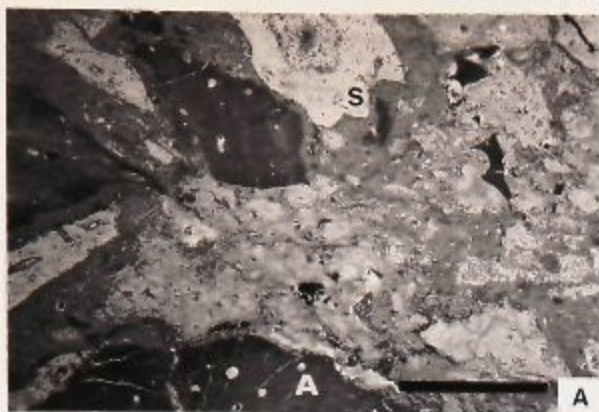




## PLATE C.2

A. Amygdaloidal andesitic fragment (A) and similar fragments to right that are partially enclosed with more weakly amygdaloidal andesite (composite lapilli). Matrix contains angular chloritized shards and andesitic fragments.

B. Strongly amygdaloidal, "scoriaceous" andesitic fragments. The tightly packed nature of these fragments, their irregular fluidal form and flattened amygdules suggest they were deposited hot.

C. Broken composite lapilli. Amygdaloidal andesitic fragments (A) partially surrounded by weakly amygdaloidal andesite. Chloritized shards (S) dominate the matrix.

D. Plane bedded tuff showing normal grading and numerous faults that offset bedding. Tuff consists of broken quartz and feldspar crystals, fine opaque minerals, quartz and chlorite.

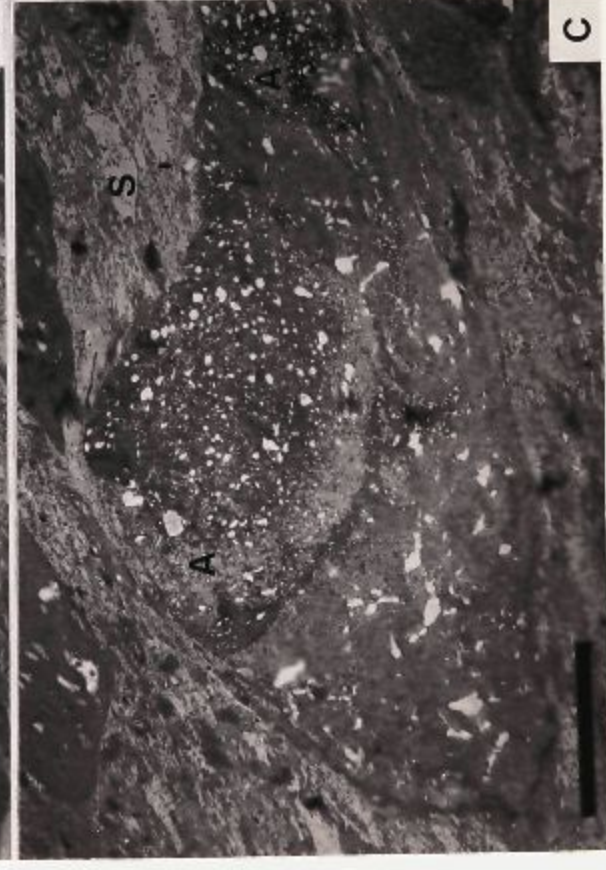
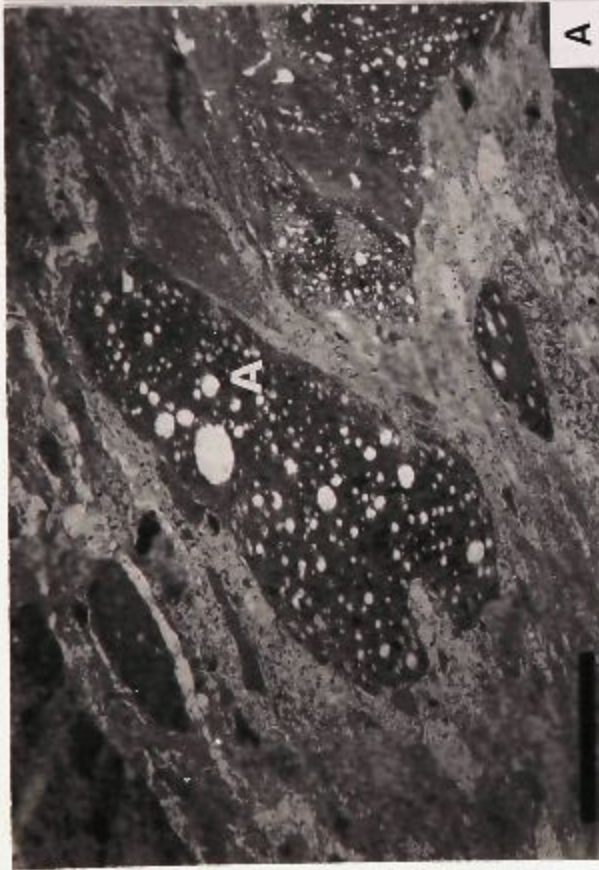
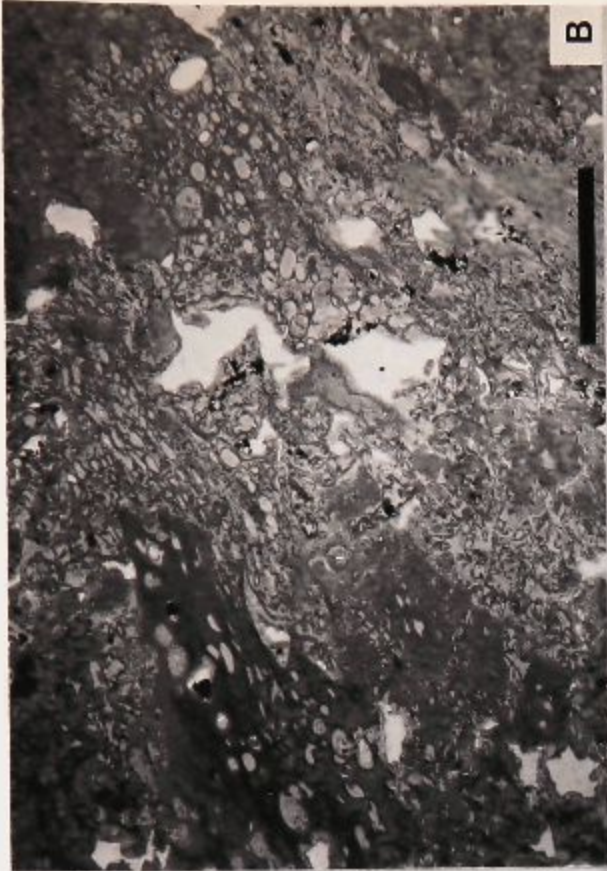




Plate C.3. Lapilli tuff characterized by numerous altered, angular fragments of andesite in a finer-grained ash-sized matrix.



Plate C.4. Numerous sericitized andesitic "scoria" fragments and minor lithic clasts in a fine tuff matrix.

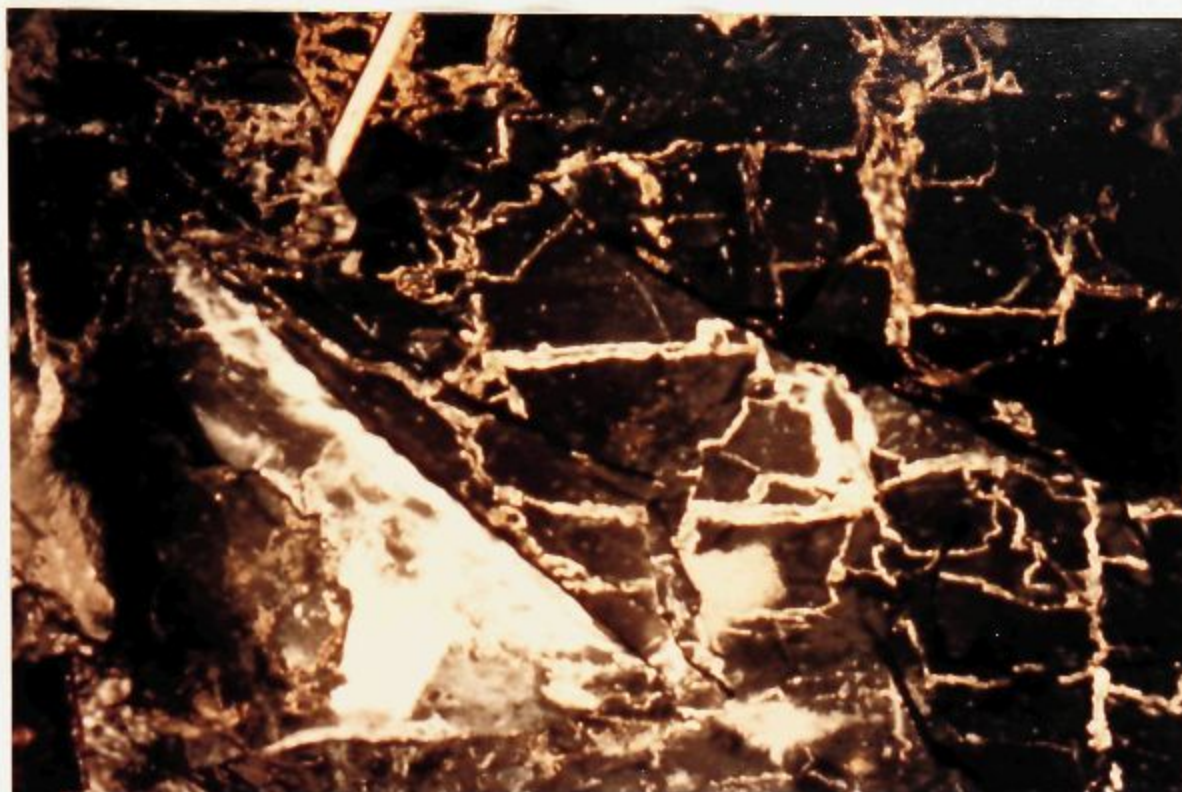


Plate C.5. In situ brecciated massive andesite flow. Veins separating angular fragments are filled by pyrite, sphalerite and quartz.

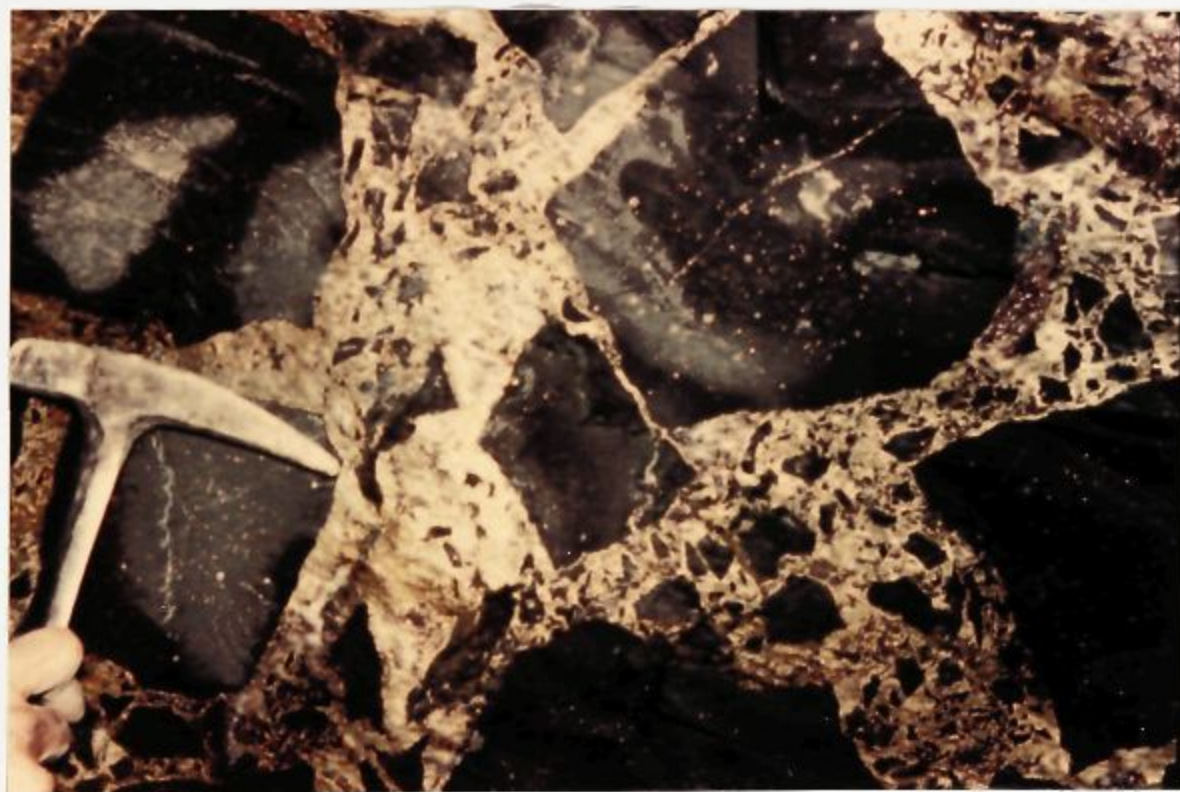


Plate C.7. Close-up of the breccia in C.6.

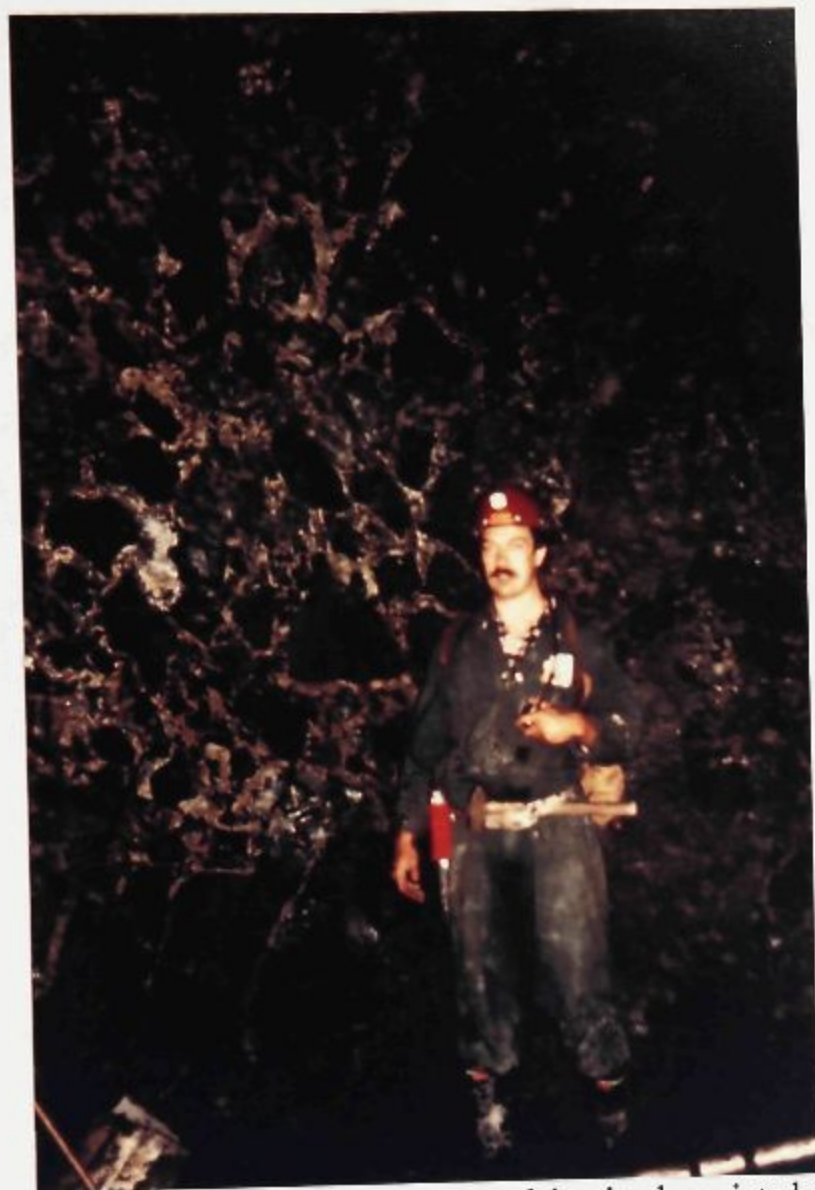


Plate C.6. In situ brecciated pillows. Intact and in situ brecciated pillows at the base of the photo grade upward into a breccia composed of angular blocky fragments separated by sulphide.

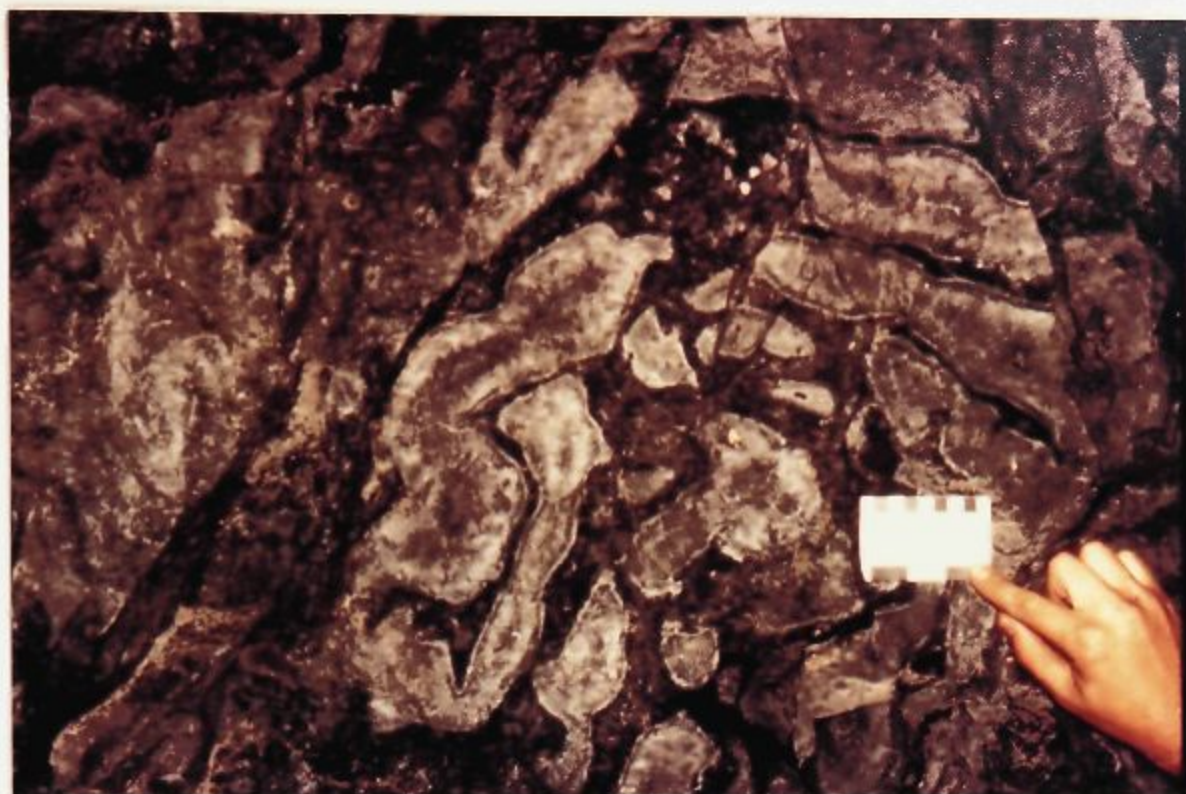


Plate C.8. Amoeboid, highly amygdaloidal, silicified fragments that occur as "mounds" within volcaniclastic breccias. The fragments are separated by strongly chloritized hyaloclastite.



Plate C.9. Transported sulphide, #3 lens. Blocks of massive sulphide and andesite are mixed within a finer breccia of the same.

APPENDIX D.

MINE SEQUENCE STRATIGRAPHY OF  
THE POWELL AND HUNTER BLOCKS,  
ALDERMAC AREA, CYCLE IV FORMATIONS  
AND HORNE MINE STRATIGRAPHY

D.1 THE MINE SEQUENCE OF THE POWELL AND HUNTER BLOCKS AND  
ALDERMAC AREA

To facilitate stratigraphic correlation and interpretation, formations which comprise the Mine Sequence in the Powell and Hunter Blocks and at Aldermac are briefly described (Tables 2.3 and 2.4). Exposures of the Mine Sequence in both Blocks were examined during reconnaissance traverses and field trips. The descriptions provided below are from de Rosen-Spence (1976) and Lichtblau and Dimroth (1980) for the Powell Block and de Rosen-Spence (1976), Mattinen (1975) and Simmons (1972) for the Hunter Block, and Hunter and Gibson (1986) for the Aldermac area.

### **D.1.1 POWELL BLOCK**

Four formations comprise the Mine Sequence of the Powell Block and are described below from oldest to youngest (Tables 2.3 and 2.4). Stratigraphic sections through the Powell Block are contained in Figure 9.2, and the location of these sections is illustrated on the generalized geologic map of Figure 9.30.

#### **Brownlee Rhyolite Formation (VI-IX BR)**

The Brownlee Rhyolite formation (Figure D.1) is a single aphyric, spherulitic rhyolitic flow that is conformably overlain by the Powell Andesite formation and is underlain by the Here Diorite and Powell Pluton. The unit is exposed over a strike length of 2km and has a minimum thickness of 500m.

#### **Joliet Rhyolite Formation (VI-IX J)**

The Joliet Rhyolite formation consists of aphyric, spherulitic rhyolitic flows, flow breccia and pyroclastic rocks, the latter best developed at the top of the formation. The formation has a maximum thickness of 900m and a strike length of 2.5km (Figure D.2); the Western Quemont feeder dike and Eastern QFP feeder dike and Horne Creek Fault define the west and east contacts of the formation, respectively. The Joliet formation is conformably overlain by the Quemont formation. The main massive sulphide lens of the Quemont orebody is situated



at this contact and a smaller lens of massive sulphide occurs 60m below the contact within pyroclastic breccias of the Joliet formation. The Powell Pluton marks the base of the formation.

Rhyolitic flows and breccias of the Joliet formation are interpreted as proximal deposits that directly overlie their vent area. Intrusion of the Quemont feeder dikes and Powell Pluton may have obscured recognition of distinct vents for the Joliet formation.

#### **Quemont Rhyolite Formation (X-XIIQ)**

The Quemont Rhyolite formation consists of rhyolitic flows and pyroclastic breccias. The formation is exposed over a strike length of 4.0km and has a maximum thickness of 900m (Figure D.3). The Western Quemont feeder dike and Horne Creek Fault define the west and east limits of the Quemont Rhyolite formation. De Rosen-Spence (1976) subdivided the Quemont Rhyolite formation into 7 members (Figure D.3). Members 1, 3, and 6 consist of poorly sorted, phreatomagmatic, heterolithologic lapilli tuff and tuff breccia. Members 2 and 5 are aphyric rhyolitic flows and members 4 and 7 are QFP rhyolitic flows.

The Quemont Rhyolite formation conformably overlies the Joliet formation. Members 1-3 are separated from the Powell Andesite formation by the Western Quemont feeder dike which occupies a synvolcanic fault (de Rosen-Spence, 1976; Lichtblau and Dimroth, 1980) whereas member 4 is conformably overlain by the

Powell Andesite formation in the west and by member 5 east of the Eastern QFP feeder dike. East of the Eastern QFP dike members 4 through 7 are conformably overlain by the Here Creek Rhyolite and Delbridge Rhyolite formations.

The Western QFP feeder dike and two identical and parallel dikes to the east are interpreted as feeders to members 4 through 7 (de Rosen-Spence, 1976; Lichtblau and Dimroth, 1980). Extrusion of rhyolitic flows and Ultra-volcanian phreatomagmatic pyroclastic eruptions were contemporaneous with subsidence and eastward tilting of underlying strata along faults now occupied by the feeder dikes channelling the Quemont flows and breccia deposits eastwards. The Quemont lava dome complex acted as a southeast barrier to contemporaneous or slightly younger andesitic flows of the Powell Andesite formation. Andesitic flows eventually overrode the margin of the Quemont dome complex (member 4) but were confined and ponded by rhyolitic flows (member 5) of the Quemont Rhyolite formation.

### **Powell Andesite Formation (XI P)**

The Powell Andesite formation comprises a 900m thick succession of principally aphyric andesitic flows, which in the west contain a 300m thick succession of bedded andesitic tuffs, the Powell Tuffs, and a QFP rhyolitic flow, the Powell Rhyolite (Lichtblau and Dimroth, 1980). The Powell formation has a strike length of 4km between the Beauchastel Fault in the west and Quemont

Rhyolite formation and Western QFP feeder dike to the east (Figure D.4).

The Powell Andesite formation conformably overlies the Brownlee Rhyolite formation and is in part intruded by the underlying Powell Pluton. The Powell Andesite formation is separated from the Joliet Rhyolite formation and lowermost members (1-3) of the Quemont Rhyolite formation by the Western QFP feeder dike but conformably overlies a portion of the Quemont Rhyolite formation (member 4). The Here Creek Rhyolite formation (XIV) unconformably overlies the Powell Andesite formation (Chapter 9); the contact is locally marked by a thin tuff and lapilli tuff deposit (Lichtblau, 1983).

The Powell Andesite formation thins to the east and the principal vents for this formation lie near the Beauchastel Fault and in the Flavrian Block. The Powell Rhyolite and andesitic tuffs occupy a localized depression (de Rosen-Spence, 1976; Lichtblau and Dimroth, 1980); the former may be a satellite body to the Quemont Rhyolite formation to the east.

#### D.1.2 HUNTER BLOCK

Five formations comprise the Mine Sequence of the Hunter Block and are briefly described in Tables D.1 and 2.3. A single stratigraphic section through the Hunter Block is contained in Figure 9.2, with the location of the section illustrated on the generalized geologic map of Figure 9.29. Stratigraphic subdivision of the Hunter Block is tentative due to low outcrop density and few drill holes; estimates

of formation thicknesses are from de Rosen-Spence (1976).

The formations were interpreted (Simmons, 1972, Mattinen, 1974 and de Rosen-Spence, 1976) to have erupted from a volcanic centre located within the Hunter Block, 3.5km north of the Hunter Creek Fault. This volcanic centre is defined by an increase in thickness of these units.

### D.1.3 ALDERMAC AREA

Mine Sequence strata in the Aldermac area are the southwest continuation of those in the Despina sector of the Flavrian Block (Figure 9.31). The Aldermac area is complexly block-faulted with blocks having opposing dips and facing directions that crudely define an southeast-trending syncline (Figure 9.31) interpreted to be a primary volcanic depression or graben by Hunter and Moore (1983). The north side of the syncline is interpreted to have been uplifted and tilted southward, during intrusion of the Aldermac syenite (Hunter, 1979).

Four conformable units are recognized in the Mine Sequence of the Aldermac area. A stratigraphic column based on surface exposures, drilling and mine workings is illustrated in Figure 9.31. Description of stratigraphic units are summarized in Table D.2.

## D.2 CYCLE IV FORMATIONS

To facilitate interpretations and volcanic reconstruction, formations overlying the Mine Sequence are briefly described in Tables D.3 and 2.4, and their

distribution illustrated in Figures 9.29 and 9.30. Unlike rhyolitic and andesitic formations of the Mine Sequence these later formations are not confined to either the Flavrian, Powell or Hunter Blocks.

Post Mine Sequence (Cycle 4) formations represent a conformable succession that overlies the Mine Sequence. The one exception is the Here Creek Rhyolite formation which, in the Flavrian Block, unconformably overlies the Amulet Andesite formation. This unconformity is defined by east - west striking shallow south dipping flows of the Here Creek Rhyolite formation lying on north-south striking and east dipping flows of the Amulet Andesite formation. This angular unconformity suggests that eruption of the Here Creek formation from feeder dikes within the McDougall-Despina Fault was accompanied by subsidence along the same faults and a general east-tilting of strata in the Flavrian Block relative to that in the Powell Block.

### D.3 HORNE MINE STRATIGRAPHY

A description of the Horne Mine strata, south of the Horne Fault is summarized in Table D.4.

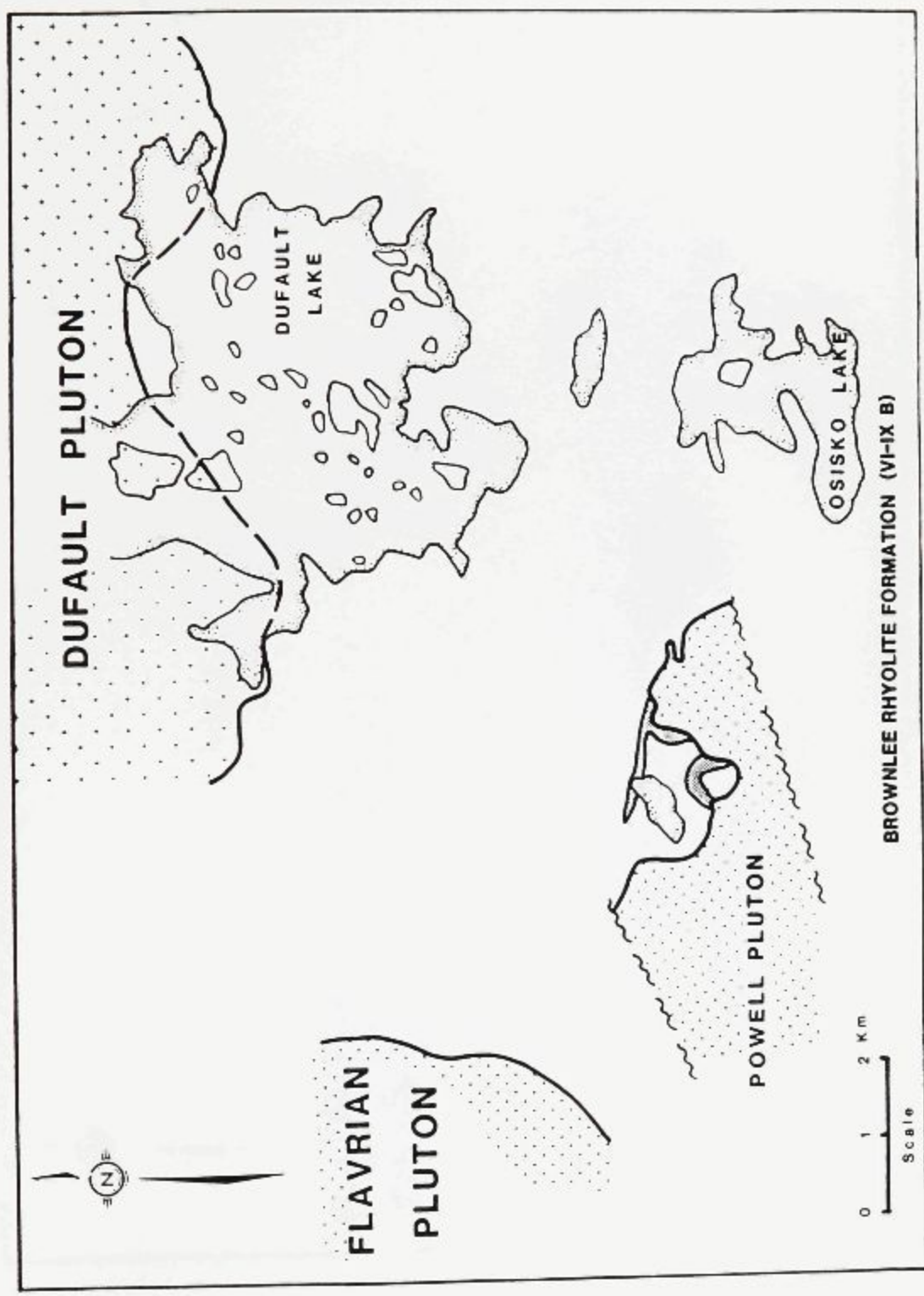


Figure D.1. Surface distribution of the Brownlee Rhyolite formation.

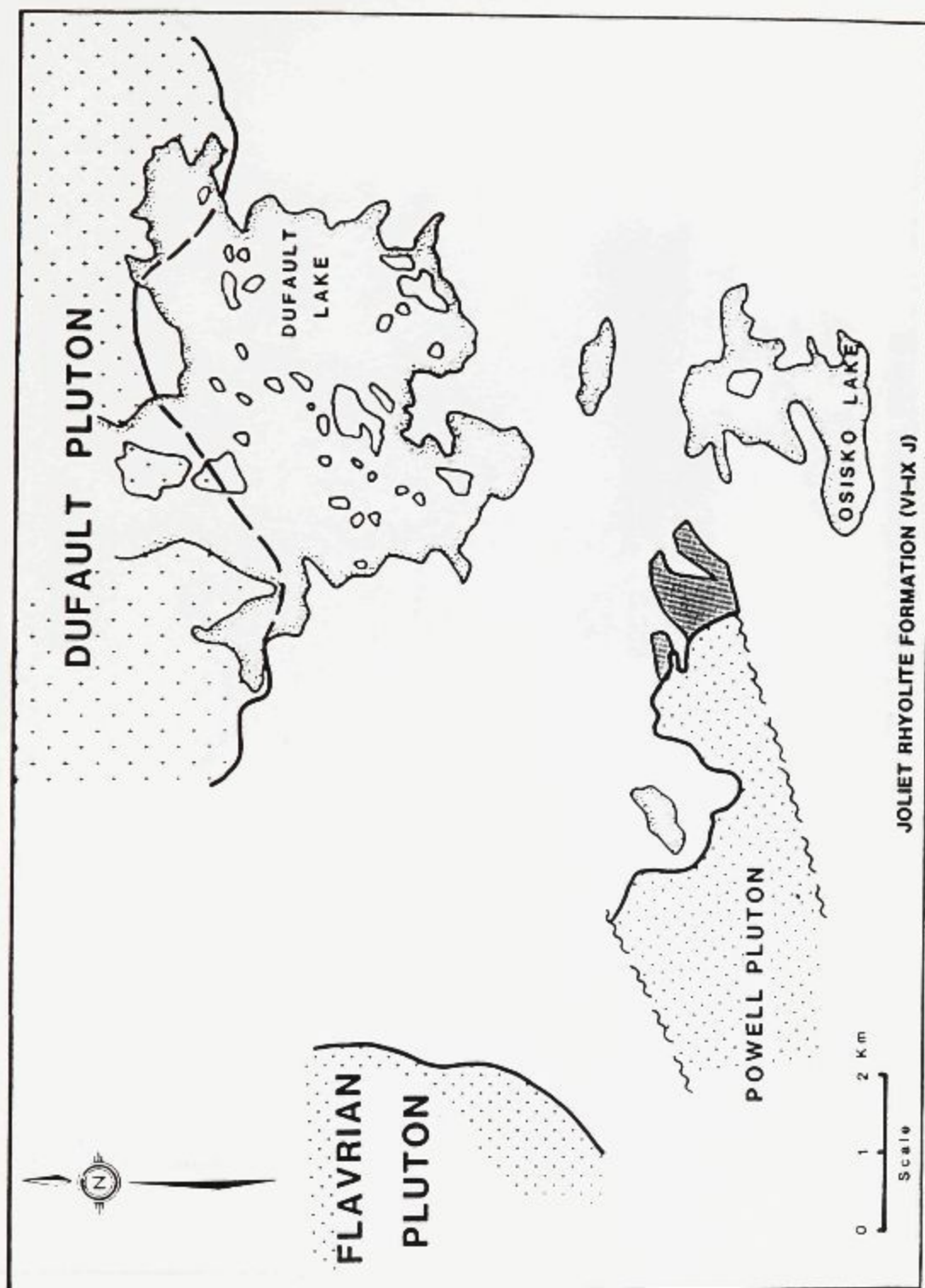


Figure D.2. Surface distribution of the Joliet Rhyolite formation.

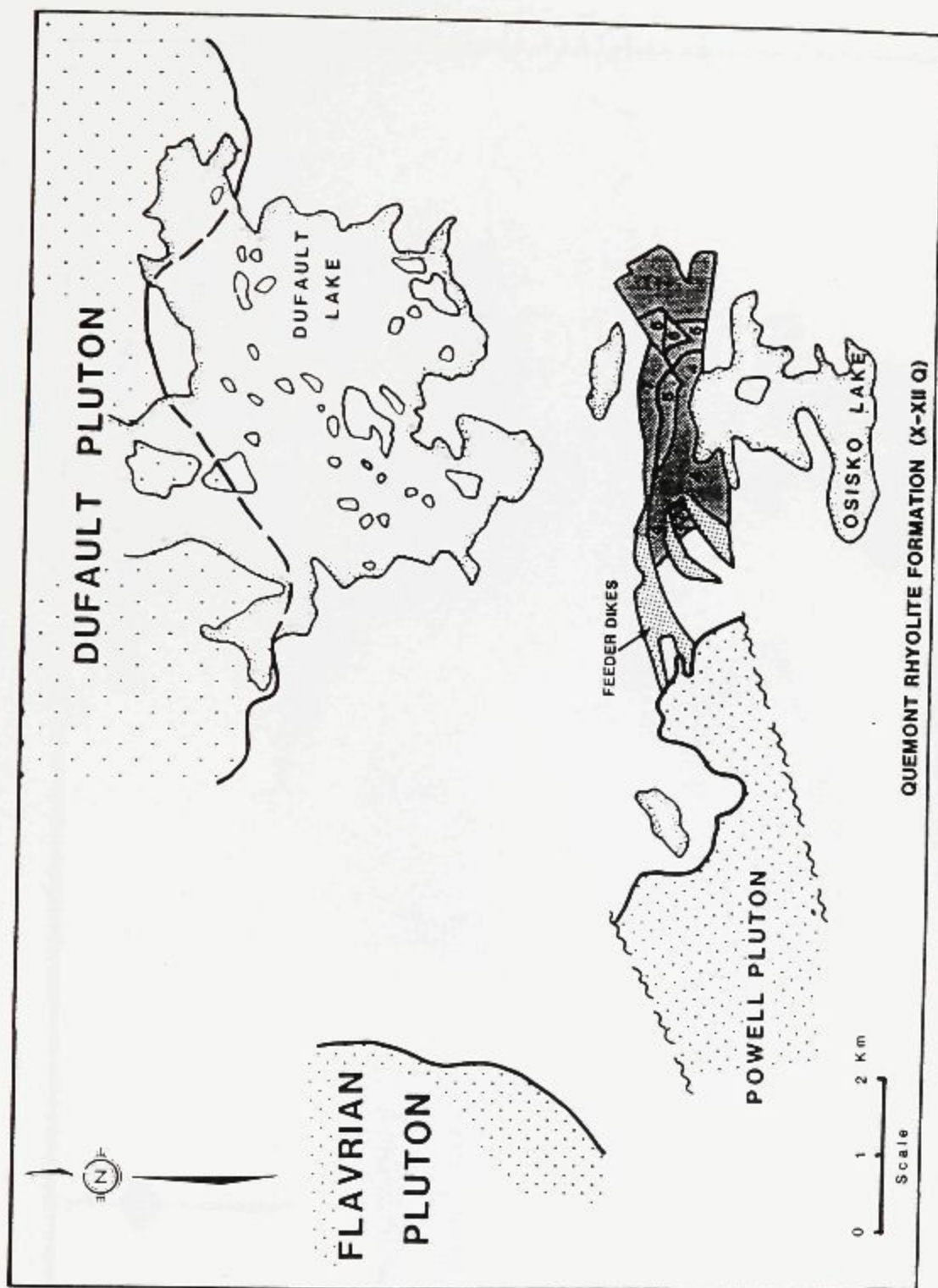


Figure D.3. Surface distribution of the Quemont Rhyolite formation (numbers refer to members described in text).



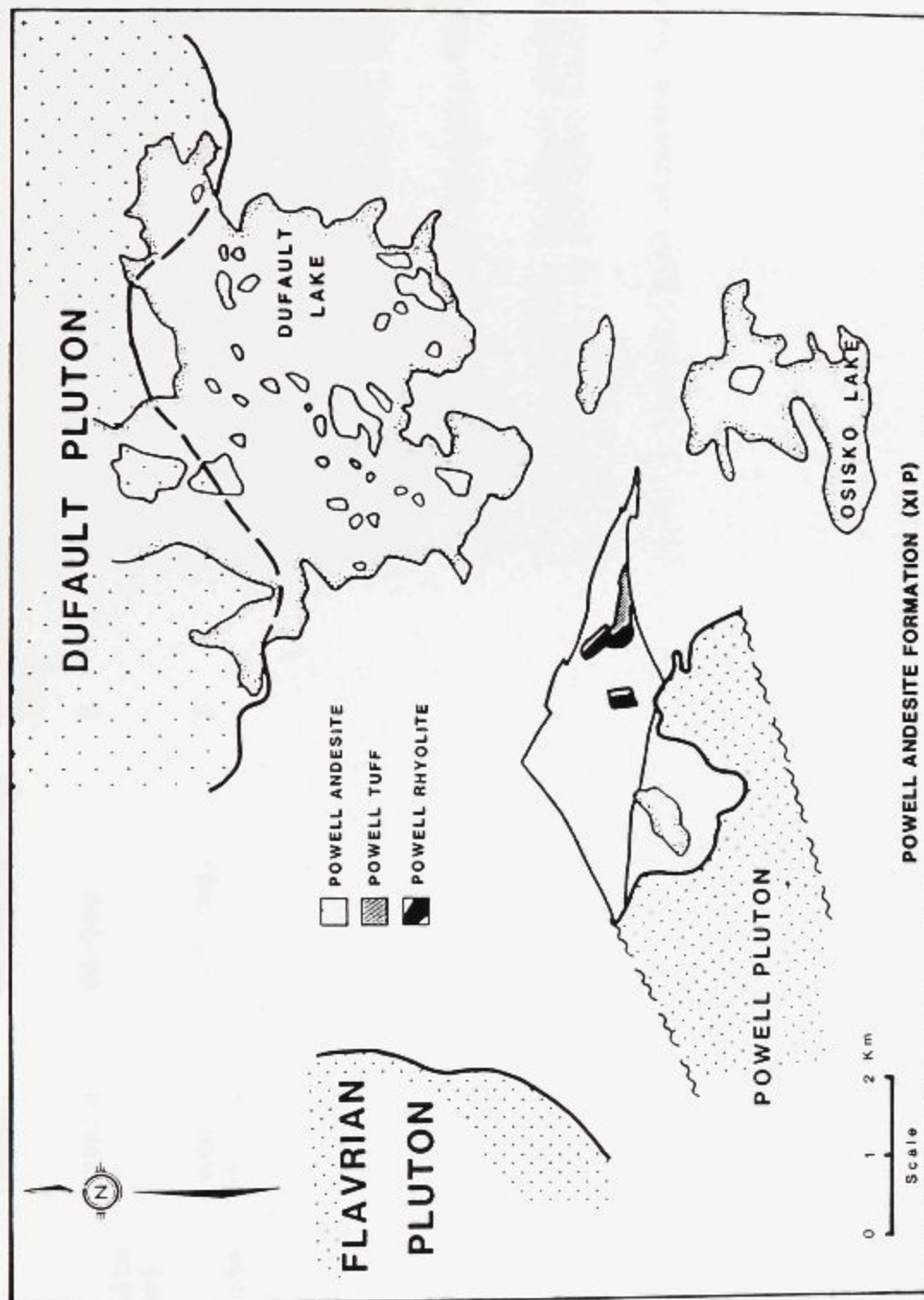


Figure D.4. Surface distribution of the Powell Andesite formation.

TABLE D.1. MINE SEQUENCE FORMATIONS IN THE HUNTER BLOCK

Formation	Number	Thickness (m)	Length (Km)	Lithology
Upper North Duprat Andesite (Lower member)	UNDA XI	60-200	5	Aphyric andesite flows.
Upper North Duprat Rhyolite	UNDR VIII-X	1-2 (km)	5	Aphyric and weakly feldspar porphyritic rhyolite flows with minor inter-flow silicified andesite. Spence (1976) divided the unit into two flows which have similar textures, mineralogy and compositions to the number 1 and 4 rhyolite flows of the Waite Rhyolite formation in the New Vauze Sector Flavrian Block.
Lower North Duprat Andesite	LNDA VII	200-500	3	Massive and pillowed andesite flows, locally silicified.
Lower North Duprat Rhyolite	LNDR VI	0.7-1 (km)	3	Aphyric and weakly feldspar porphyritic rhyolite flows. A QFP flow occurs at the top of the unit.
Hunter Andesite	H V	700	4	Massive and pillowed andesite flows.

TABLE D.2. MINE SEQUENCE STRATA OF THE ALDERMAC AREA

Formation	Number	Thickness (m)	Length (km)	Lithology
Amulet Andesite	XIA	>500		Massive and pillowed, aphyric to Andesite feldspar porphyritic andesite flows with minor flow breccia and intercalated tuff. Unit extends eastward, around the south end of the Flavrian pluton and into the Despina sector.
Macanda Rhyolite	X	300	<0.5	QFP rhyolite lave dome; well developed carapace breccia.
Middle Andesite	IX2		2	Massive and pillowed andesite flows and breccia. Andesite breccias adjacent to the Macanda QFP Rhyolite contain QFP rhyolite fragments and may in part be contemporaneous with the emplacement of the Macanda Rhyolite lava dome. Flows are intruded by a quartz-crystal, pumaceous tuff dike.
Silicified Andesite	VIII		4	Thick, massive, silicified andesite flows that are identical to those of the Amulet upper member. Overlain by a thin bedded tuff.
Aldermac Rhyolite	VIII	>500	<1	QFP rhyolite debris flows, talus breccias and ash flow tufts Rhyolite constitute a lower unit that is overlain by an upper unit of massive QFP and aphyric rhyolite flows and breccia. Three massive sulphide lenses occur at or near the top of the lower unit at the Aldermac mine.
Lower Andesite	VII			Intersected only in drill holes the unit consists of epidote, altered, amygdaloidal massive and weakly feldspar porphyritic andesite flows overlain by a thin, bedded tuff unit.

TABLE D.3. POST MINE SEQUENCE (CYCLE 4) FORMATIONS (modified from Spence, 1976; Boldy, 1968)

Formation Name	Formation Number	Maximum Thickness (m)	Strike Length (Km)	Characteristics
Mesipi Andesite	XXM	800	5.5	Consists of an upper part of aphyric, amygdaloidal andesite flows (magnetite crusts on pillows) and a lower part composed of aphyric and feldspar porphyritic, andesite flows, tuff and rhyolite lapilli tuff.
Dalembert Andesite Upper Member	XXDL			Aphyric, amygdaloidal andesite flows. A thin, laminated tuff separates the upper and lower members
Mesipi Rhyolite	XIXM	270	2.5	Aphyric, rhyolite flow
Don Rhyolite	XVIID	600	4	Consists of 7 aphyric and quartz-feldspar porphyritic rhyolite flows. A 60m wide neck of QFP rhyolite south of Dufault Lake is interpreted to be a feeder to the #5 flow.
Dalembert Andesite Lower Member	XVIDL	400	6.5	Aphyric, amygdaloidal andesite flows.
South Bay Andesite	XVISB	180	6.5	Aphyric to weakly feldspar porphyritic andesite flows. Minor heterolithic andesite lapilli tuff and monolithic rhyolite lapilli tuff. Basal andesite tuff with sulphides.
Deldona Andesite	XVIDD	300	3.7	Aphyric massive andesite flows and tufts. Tufts correlated with those in XVISB.
Delbridge Rhyolite	XVDB	600	5	Quartz-feldspar porphyritic rhyolite flows/domes and feeder dikes. Well developed carapace/flank breccias. Minor andesitic tuff.

TABLE D.3. POST MINE SEQUENCE (CYCLE 4) FORMATIONS (continued)

Formation Name	Formation Number	Maximum Thickness (m)	Strike Length (Km)	Characteristics
Norque Rhyolite	XVNIQ	60	3.5	Quartz crystal, rhyolitic, lapilli tuff and flow.
Fish-Roe Rhyolite	XIVF	10	4	Coarsely spherulitic rhyolitic/dacitic flow (?).
Héré Creek Rhyolite	XIVH	700	3.5	Consists of a basal rhyolitic lapilli tuff unit overlain by 2 aphyric rhyolite flows (lower flow massive and columnar jointed) in the Flavrian Block and an additional andesite and overlying aphyric rhyolite flow in the Powell Block. Principal vents are rhyolite dikes occupying the MacDougall-Despina fault and a neck of massive rhyolite exposed along the Beauchastel fault.
Newbec Andesite	XIIIINB	300	12	Amygdaloidal, aphyric to feldspar porphyritic andesite flows and the Newbec Rhyolite, a thin (<20 m) massive QFP rhyolite flow (sill?)
Insko Rhyolite	XIIIIN	650	1.6	Consists of 3 flows, a basal feldspar porphyritic dacitic flow overlain by two quartz-feldspar porphyritic flows

TABLE D.4. FORMATIONS SOUTH OF THE HORNE FAULT AND WEST OF OSISKO LAKE, POWELL BLOCK  
(modified from Wilson, 1941; Spence, 1976)

Unit	Thickness (m)	Lithology
Horne Rhyolite	600 m (fault bounded except to east)	<p>The upper part (150 m) consists of massive, weakly quartz porphyritic rhyolite and minor lapilli tuff containing both aphyric and quartz porphyritic fragments.</p> <p>The lower part consists of an upper succession, up to 300m thick, of well bedded rhyolitic tuff and tuff breccia interlayered with laminated rhyolitic ash which constitutes units up to 10 m thick. Fragments of aphyritic rhyolite range to 1.5 m in size but on average are &lt;5 cm. The breccias are interpreted as subaqueous ash flow deposits and constitute the principal host for the No. 5 and Main (Lower H) Horne orebody.</p>
Osisko Andesite	uncertain, may be repeated or faulted out, probably >1000 m thick	<p>The pyroclastic breccias (above) overly a lower succession of massive and brecciated aphyric rhyolite flows and a thin (&lt;80 m thick), well bedded unit of rhyolitic lapilli tuff that may be the folded equivalent (west limb?) of the upper, ore-hosting pyroclastic breccias.</p> <p>Aphyric, weakly amygdaloidal andesitic and basaltic flows. Upper flows west of Osisko Lake with magnetite crusts on pillows may be a different unit (fault slice) and have been interpreted (Spence, 1976) as the stratigraphic equivalent of similar magnetite bearing pillowed flows of the Mesipi Andesite formation (XXM).</p>

## APPENDIX E. VOLCANIC AND SUBSIDENCE HISTORY

The volcanic and subsidence history of each formation within the Mine Sequence of the Noranda Cauldron is outlined in detail below and summarized in Table 11.1 , and Figure 11.4.

### CAULDRON CYCLE #1

#### Stage I Tumescence

Tumescence of the cauldron and surrounding area above a rising, shallow level magma chamber is indicated by the generation of radial and ring fault systems and central or apical graben (Old Waite Dike Swarm) in the domed cauldron area. The intrusive Meritens phase was emplaced within 500m of surface along the McDougall-Despina ring fault during extrusion of the Flavrian formation.

#### Stage II Cauldron Collapse and Eruptions

Stage II overlapped with Stage I and is represented by formations V F to VIII. Although volcanism and subsidence occurred simultaneously, initial cauldron subsidence is interpreted to have followed magma withdrawal during eruption of the Flavrian formation (V F).

### **Flavrian Formation (VF)**

1. Andesitic flows issued from fissures localized along major faults and a central graben area (Old Waite Dike Swarm) producing a low relief lava plain covering the cauldron floor.
2. Phreatomagmatic and Strombolian eruptions during the waning stages of volcanism were localized along feeding fissures such as the McDougall-Despina Fault.
3. along the north margin of the cauldron the Ansil QFP dome was extruded contemporaneously with andesitic flows which nearly buried it.
4. Submarine hot spring activity within a volcanic vent along the McDougall-Despina Fault formed massive sulphide lenses at the Corbet deposit contemporaneous with Phreatomagmatic and Strombolian eruptions.

### **Northwest (VI N), Lower North Duprat Rhyolite (VI LND), Brownlee and Joliet Rhyolite Formations (VI B/J)**

1. The North and South rhyolitic flows of the Northwest formation spread laterally away from northeast and northwest trending fissures located along cauldron margins to partially cover the cauldron floor.
2. Rhyolitic flows of the Brownlee/Joliet formations issued from a fissure along the south margin of the cauldron.



3. The Lower Duprat rhyolitic flow erupted from a "flank" vent located 10km north of the cauldron.
4. Rhyolitic flows built up broad shields or plateaus with slopes ranging from 10<sup>0</sup>-20<sup>0</sup>.
5. Minor subsidence accompanied eruption of rhyolitic flows with localized hot spring activity and deposition of waterlain tuff (Lewis tuff).

#### **Cranston Member (VI NC)**

1. Eruption of the Cranston QFP dome from a northeast trending fissure along the north margin of the cauldron followed and was contemporaneous with extrusion of andesite from a fissure located along the Cranston Fault.
2. Debris-flow deposits shed from the steep slopes (+30<sup>0</sup>) of the Cranston dome and possibly by phreatomagmatic eruptions produced a blanket-like breccia apron extending south to Ansil Hill.
3. Subsidence along the cauldron's north margin caused the ponding of the Cranston rhyolite.
4. On the cauldron's south margin the Brownlee Rhyolite was down faulted from the Joliet Rhyolite. Following down-faulting phreatomagmatic explosions on the cauldron margin deposited a heterolithologic breccia on the south-east tilted Joliet Rhyolite.

5. Submarine hotspring activity accompanied volcanism, a small massive sulphide lens (precursor to the Quemont deposit) formed along the ancestral Horne Creek Fault.

**Rusty Ridge Formation (VII R), Lower North Duprat Andesite (VII LND)**

1. Voluminous eruptions of andesitic flows issued from fissures principally within the Old Waite Dike Swarm but also along the McDougall-Despina Fault, Cranston Fault and at Ansil Hill, covering and inundating the irregular topography of underlying rhyolitic flows.

2. Andesitic flows erupted from "flank" vents north of the cauldron (VII LND).

3. Phreatomagmatic explosions accompanied localized, contemporaneous rhyolite volcanism producing small deposits of heterolithologic breccia near the base and top to the Rusty Ridge formation south of Ansil Hill.

4. Subsidence, principally in the Old Waite vent area, accompanied volcanism resulting in the development of a low, broad, lava plain covering the floor of the cauldron. Absence of the Rusty Ridge formation in the Powell Block suggest it was barred by subsidence along the ancestral Beauchastel Fault.

5. Submarine hotspring activity accompanied volcanism forming the massive sulphide lens at the Ansil deposit and the Quemont deposit on the cauldron's south margin.

## **Amulet Formation (VIII A), Lower and Upper Members**

### **Lower member (VIII Al)**

1. Near-surface phreatomagmatic eruptions marked the ascent of rhyolitic magma within the McDougall-Despina Fault and deposited Beecham Breccia to areas south of its main vent.
2. Subsidence of the cauldron floor accompanied or immediately followed phreatomagmatic explosions.
3. Three rhyolitic flows, erupted from vents located within and along the cauldron margin, spread across the cauldron floor. The south and north advance of the flows was blocked by subsidence along the Bancroft and ancestral Hunter Creek Fault.
4. Submarine hotspring activity accompanied volcanism with localized deposition of waterlain tuff.

### **Upper member (VIII Au)**

1. Thick, massive, flood-type andesitic flows were rapidly erupted from 4 main vents spread across the cauldron floor but were barred to the north and south by subsidence along the Cranston and ancestral Beauchastel Faults.
2. The Bedford rhyolitic flow, erupted from vents within and adjacent to the McDougall-Despina Fault, covered Beecham Breccia south of the Bancroft Fault and directly overrode contemporaneous andesitic flows north of the fault. The F-

rhyolitic flow, was emplaced near the top of the Upper member in the F-shaft sector.

3. Andesitic flows of the Upper member buried the irregular topography of the rhyolitic lower member producing a relatively flat lava plain that covered the cauldron floor between the Cranston and Beauchastel Faults.

4. Submarine hot spring activity accompanied volcanism and along the south margin continued to form the Quemont deposit.

### **Stage III Sedimentation**

1. A cauldron-wide hiatus in volcanic activity and subsidence allowed deposition of the C Contact Tuff which covered the cauldron floor north of the Beauchastel Fault.

2. Submarine hot spring activity accompanied sedimentation and was most vigorous in the Amulet-Millenbach sector where the C Contact tuff, a pyritic sulphide facies iron-formation, contains small, zinc-rich VMS lenses. Hot spring activity continued in the Quemont deposit area at the cauldron's south margin.

### **CAULDRON CYCLE #2**

#### **Stage IV Tumescence (overlaps with stages III and V)**

1. Renewed volcanic activity and subsidence was preceded by a period of tumescence that reactivated pre-existing faults and generated new ones.

2. Asymmetric disposition of rhyolitic flows about their vents suggests that during uplift the cauldron floor was tilted to the east and south east in the Norbec sector and Powell Block during extrusion of the Waite and Quemont Rhyolite formations.

### Stage V Cauldron Eruptions and Collapse

#### Waite/Millenbach Andesite formation (IX W/M)

1. Andesitic flows, were erupted from fissures within the Old Waite Dike Swarm and New Vauze sector to completely cover the cauldron floor north of the Beauchastel Fault.
2. Andesitic volcanism in the north part of the cauldron (New Vauze Sector) was interrupted by extrusion of a rhyolitic flow.
3. Subsidence accompanied volcanism, both in the vent areas and cauldron margins; upper flows of the Waite Andesite formation were ponded north of the Vauze Fault.
- 4) Submarine hotspring activity accompanied volcanism. A tuff was locally deposited on the cauldron floor.

#### Waite Rhyolite (XW), Millenbach Rhyolite (XM), Upper North Duprat Rhyolite (X UND) and Quemont Rhyolite (X Q) Formations

1. Rhyolitic lava that issued from vents in the Vauze Mine area and Old Waite Dike Swarm merged to form the #1 flow of the Waite Rhyolite formation which

flowed east of its vent on the east-tilted cauldron floor.

2. Rhyolitic flows of the Upper North Duprat Rhyolite formation were erupted from a "flank" vent north of the cauldron.

3. Three rhyolitic flows and thin andesitic flows erupted from vents located on the north flank of the Waite Rhyolite #1 flow in the New Vauze sector.

4. Subsidence along the north margin of the cauldron ended with extrusion of the Waite Rhyolite flows.

5. Hotspring activity accompanied rhyolitic volcanism, with VMS deposits at Vauze, Norbec and East Waite formed during this interval.

6. The Millenbach-D68 lava dome erupted from 3 vents along a 2.0km northeast-trending fissure extending across the Despina cauldron wall to build up a steep-sided ( $20^{\circ}$  -  $70^{\circ}$ ) rhyolitic ridge. Submarine debris flows, produced by collapse of the domes steep slopes and possibly by phreatomagmatic eruptions, formed a blanket-like breccia deposit northwest of Millenbach.

7. Rhyolitic eruptions in the D-68 area were accompanied by extrusion of contemporaneous andesitic flows which were incorporated within the growing D-68 lava dome.

8. Two small satellite flows, the Turcotte and K rhyolite flows, were erupted contemporaneously with the Millenbach-D68 lava domes.

9. Hotspring activity accompanied rhyolite volcanism producing massive sulphide deposits at the base, within and on top of the Millenbach-D68 ridge.

10. Along the south margin of the cauldron, rhyolitic flows and heterolithic, phreatomagmatic explosion breccias of the Quemont formation covered the Quemont massive sulphide deposit and Joliet formation.

#### Amulet Andesite (XI A) Powell Andesite (XI P) Formations

1. Andesitic flows, erupted from fissures in the Old Waite Dike Swarm in the Amulet-Millenbach area and McDougall-Despina Fault, flooded the irregular topography of the cauldron floor. Rhyolitic shields of the Waite Rhyolite and Quemont Rhyolite formations restricted the andesitic flows to the cauldron's interior.
2. Extrusion of the lowermost flows of the Amulet/Powell Andesite formations overlapped with rhyolitic flows of the Waite and Millenbach Rhyolite formations.
3. In the Powell Block, emplacement of the Powell Rhyolite and deposition of the Powell Tuff, which extends north to Millenbach, was contemporaneous with the uppermost units of the Quemont Rhyolite formation.
4. Andesitic flows, erupted north of the Despina cauldron, were not accompanied by significant subsidence whereas continued collapse of the Despina cauldron (Despina sector) accompanied extrusion of the Amulet Andesite formation.

5. Andesitic flows within the upper part of the Amulet/Powell formations were erupted in shallower water than flows lower in the succession as the cauldron was in-filled.

6. Hotspring activity accompanied volcanism and massive sulphide deposits formed at the base (Amulet lower A, Old Waite) , within (Amulet upper A, Old Waite) and at the top (Newbec) of the Amulet Andesite formation in proximity to its feeding fissures.

#### **Stage VI Sedimentation**

1. Deposition of tuff during a brief hiatus in volcanism and subsidence.

#### **Stage VII Tumescence**

1. Tumescence preceded eruption of the 4th cycle followed by contemporaneous eruption of the Insko Rhyolite and Newbec Andesite formation.

2. Reactivation of McDougall-Despina Fault and emplacement of rhyolitic dikes was accompanied by phreatomagmatic eruptions at surface (breccia deposited) and extrusion of Here Creek Rhyolite simultaneous with final collapse of the Despina cauldron and tilting of the cauldron floor. This resulted in an angular unconformity between Amulet Andesite flows and rhyolitic flows of the Here Creek Rhyolite formation.



3. Here Creek Rhyolite flows were ponded between the Quemont and Insko Rhyolite shields.

### CAULDRON CYCLE #3

#### Stage VIII Cauldron Eruptions and Subsidence

1. Overlaps with Stage VI.
2. Continued eruption of 4th cycle rhyolitic and andesitic formations was accompanied by subsidence along the Horne Creek Fault. Minor subsidence along the Donalda Fault, following extrusion of the South Bay Andesite formation (XVI SB), ponded rhyolitic flows of the Don Rhyolite formation (XVMD) within the Delbridge Cauldron.
3. Hot spring activity accompanied volcanism with formation of massive sulphide deposits at Delbridge, and Gallen.

APPENDIX F. CHARACTERISTICS OF ANDESITIC  
AND RHYOLITIC FLOWS

TABLE F.1.1.A. ANDESITIC FLOWS OF THE FLAVRIAN FORMATION, ANSIL SECTOR

Flow Number	Thickness (m)	Strike Length (km)	Equivalent Flow	Characteristics
F1	85	2.2		Massive flow containing <1% feldspar phenocrysts and <5% amygdules. Well developed lobe/breccia facies. Contains prismatic mafic porphyroblasts and biotite.
Ansill Member	200	1.8		Quartz-feldspar porphyritic rhyolitic lava dome.
F2	35	2		Pillowed flow containing <1% feldspar phenocrysts, 8% amygdules, concentric joints and prismatic mafic porphyroblasts.
F4	95			Massive aphyric flow with 5% amygdules, laminar joints and lobe/breccia facies.
F5	>25			Massive aphyric flow containing 3% amygdules, laminar joints and lobe/breccia facies.

TABLE F.1.B. ANDESITIC FLOWS OF THE FLAVRIAN FORMATION, F-SHAFT SECTOR

Flow Number	Thickness (m)	Strike Length (km)	Equivalent Flow	Characteristics
F1	36			Massive aphyric flow containing 8% amygdules, laminar joints and weakly silicified lobe/breccia facies.
F2	24		#5 flow in Ansil Sector	Massive aphyric flow containing <5% amygdules, laminar joints and lobe/breccia facies.

TABLE F.1.C. ANDESITIC FLOWS OF THE FLAVRIAN FORMATION, WAITE DFAULT SECTOR

F1	>24			Pillowed flow containing 20% amygdules preferentially distributed along the pillow margins.
F2	70	>0.6		Massive flow containing <2% feldspar phenocrysts, 12% amygdules and a well developed silicified lobe/breccia facies.

TABLE F.2.A. ANDESITE FLOWS OF THE RUSTY RIDGE FORMATION, CRANSTON SECTOR

Flow Number	Thickness (m)	Strike Length (km)	Equivalent Flow	Characteristics
R1	130	0.6		Pillowed flow containing <5% feldspar phenocrysts and 8-10% amygdules. Well developed flow top breccia.
R2	80	0.6	#3 flow Ansil Sector	Pillowed flow containing 8-10% feldspar phenocrysts and 6% amygdules.
Dacitic Unit	100	0.6	Dacitic Unit Ansil Sector	Massive, weakly feldspar porphyritic silicified flow (<2% phenocrysts) containing 10% amygdules. Well developed lobe/flow breccia facies.
R3	90	1.1		Massive, feldspar porphyritic flow (2% phenocrysts) weakly silicified flow unit that is weakly magnetic. Well developed laminar joints.
R4	17			Weakly magnetic, feldspar porphyritic (15% phenocrysts), amygdaloidal (<5%) flow with laminar joints.
R5	15		#12 flow Ansil Sector	Massive, weakly feldspar porphyritic (2% phenocrysts), magnetic, columnar jointed flow.
R6	8			Aphanitic, aphyric amygdaloidal (8%) pillowed flow with concentric joints.

TABLE F.2.B. ANDESITE FLOWS OF THE RUSTY RIDGE FORMATION, ANSIL SECTOR

Flow Number	Thickness (m)	Strike Length (km)	Equivalent Flow	Characteristics
R1	25	0.8		Massive, feldspar porphyritic (6-8%) amygdaloidal (6%) aphanitic flow and flow-top breccia.
R2	30	1.2		Weakly feldspar porphyritic (2%), amygdaloidal (8%) pillowed flow with concentric joints and flow-top breccia.
R3a	70	1.4		Succession of feldspar porphyritic (8% phenocrysts), amygdaloidal (8-10%) pillowed flows with concentric joints.
b	130			Unit 3c is a laminar jointed, feldspar porphyritic (8%) massive flow.
c	15			
d	25			
e	35			
f	20			
Dacitic Unit	50	0.6	Dacitic Unit Cranston Sector	Aphanitic, feldspar porphyritic (3% phenocrysts), amygdaloidal (6-8%) silicified andesite flows with a well developed lobe/flow breccia facies.
R4	90	0.9		Massive, weakly amygdaloidal (3%, trace feldspar phenocrysts) flow with fine, <2 mm, mafic spots and a thick lobe/flow breccia facies.
R5	50	0.3		Aphanitic, amygdaloidal (20%) pillowed flow (trace feldspar phenocrysts).
R6	50	0.6		Aphanitic, amygdaloidal (8%), weakly feldspar porphyritic (3% feldspar phenocrysts) pillowed flow with concentric joints.

TABLE F.2.B. ANDESITE FLOWS OF THE RUSTY RIDGE FORMATION, ANSIL SECTOR

Flow Number	Thickness (m)	Strike Length (km)	Equivalent Flow	Characteristics
R7	55	2.0		Fine-grained, amygdaloidal (5%) massive flow with trace feldspar phenocrysts and local columnar joints.
R8	35	0.6		Aphanitic, amygdaloidal (8%) pillowed flow containing trace feldspar phenocrysts.
R9	30	1.3		Aphanitic, amygdaloidal (5%), feldspar porphyritic (3% phenocrysts) massive flow with laminar joints.
R10	25	<0.5		Fine-grained, feldspar porphyritic (3-5% phenocrysts), amygdaloidal (5%) massive flow.
R11	15	<0.5		Aphanitic, amygdaloidal (10%), pillowed flow containing trace feldspar phenocrysts.
R12a	18	1	#5 flow	Weakly magnetic, aphanitic, amygdaloidal (<5%) massive flows containing trace feldspar phenocrysts. Well developed flow breccia facies.
b	24		Cranston	
c	20		Sector	

TABLE F.2.C. ANDESITE FLOWS OF THE RUSTY RIDGE FORMATION, WAITE DFAULT SECTOR

Flow Number	Thickness (m)	Strike Length (km)	Equivalent Flow	Characteristics
R1	60			Aphanitic, feldspar porphyritic (2% phenocrysts), amygdaloidal (10%) weakly silicified pillowed flow with large tubes/flows of massive andesite (lava streams).
R2	80	1		Fine- to medium-grained, amygdaloidal (5%) massive flow with fine, 1-2 mm, mafic spots and trace feldspar phenocrysts. Well developed lobe/flow breccia facies.
R3	25	0.4		Aphanitic, weakly feldspar porphyritic (2% phenocrysts), amygdaloidal (20%) pillowed flow. Amygdules concentrated along pillow margins.
R4	110	1		Medium-grained, aphyric, amygdaloidal (5%) massive flow with fine, 2 mm, mafic spots and a well developed lobe/flow breccia facies.
R5	45	1.2		Fine-grained, feldspar porphyritic (<3% phenocrysts), amygdaloidal (5%) massive flow; <1% mega-amygdules.
R6	10			Aphanitic, feldspar porphyritic (3-5% phenocrysts), amygdaloidal (10%) massive flow.
R7	45	0.7		Aphanitic, feldspar porphyritic (8-10%), amygdaloidal (10%) pillowed flow. Amygdules concentrated along pillow margins.



TABLE F.2.C. ANDESITE FLOWS OF THE RUSTY RIDGE FORMATION, WAITE DFAULT SECTOR (continued)

Flow Number	Thickness (m)	Strike Length (km)	Equivalent Flow	Characteristics
R8	40	0.3		Aphanitic, amygdaloidal (<5%) massive flow containing trace feldspar phenocrysts.
R9	14	0.1		Aphanitic, feldspar porphyritic (2-3%), amygdaloidal (15-20%) pillowed flow. Amygdules concentrated at and along pillow margins.
R10	10	0.1		Aphanitic, feldspar porphyritic (3%), amygdaloidal (10%) massive flow.
R11a	50	1.4		Aphanitic to fine-grained, laminar jointed massive flows with well developed lobe/flow breccia facies.
b	40			Flows characterized by <5% amygdules in their massive interior, 10-15% amygdules at the flow top and <1% mega-amygdules.
c	30			
d	30			
e	40			
f	35			
R12	50	1.2		Aphanitic, feldspar porphyritic (10-15%) pillowed flow. Amygdules (8-10%) concentrated at and along pillow margins.
R13	55	0.3		Aphanitic, aphyric, laminar jointed massive flow; <2% mega-amygdules.
R14	15			Aphanitic, aphyric, laminar jointed massive flow; 2% mega-amygdules.
R15	35	0.4		Aphanitic, feldspar porphyritic (10-15%) pillowed flow. Amygdules (8-10%) concentrated at pillow margins.

TABLE F.2.D. ANDESITE FLOWS OF THE RUSTY RIDGE FORMATION, F-SHAFT SECTOR

Flow Number	Thickness (m)	Strike Length (Km)	Equivalent Flow	Characteristics
R1	>40	<0.6		Fine-to medium-grained, amygdaloidal (5%), columnar jointed massive flow; trace feldspar phenocrysts.
R2	90			Aphanitic, amygdaloidal (8-10%), pillowed flow; local "pipe amygdules" and trace feldspar phenocrysts. The #2 flow may be an upward facies transition of the #1 flow?
R3	70			Fine-grained, amygdaloidal (5%), feldspar porphyritic (3%) and columnar jointed massive flow.
R4	70			Aphanitic, aphyric, amygdaloidal (8%) pillowed flow; concentric joints and "pipe amygdules" at pillow margins
R5	55			Aphanitic to fine-grained, feldspar porphyritic (4%), amygdaloidal (5%) massive flow.
R6	25			Aphanitic, amygdaloidal (8%) pillowed flow; trace feldspar phenocrysts. Flow is broken/fractured along "polygonal" fractures infilled with fine quartz (silica dumping).
R7	20	0.6		Aphanitic, aphyric, amygdaloidal (<5%) massive flow.

TABLE F.2.E. ANDESITE FLOWS OF THE RUSTY RIDGE FORMATION, AMULET-MILLENBACH SECTOR

Flow Number	Thickness (m)	Strike Length (Km)	Equivalent Flow	Characteristics
R1	110		#1 flow F-Shaft Sector	Fine- to medium-grained, aphyric, Sectoramygdaloidal (5%), columnar jointed massive flow. Transitional "pillowed facies" locally
R2	55			Aphanitic to fine-grained, aphyric, amygdaloidal (5%) massive flow
R3	35		#4 flow F-Shaft Sector	Aphanitic, aphyric, amygdaloidal (20% pipe amygdules along pillow margins) pillowed flow
R4	30			Similar to flow R2
R5	20			Similar to flow R3
R6	50			Multiple flow. Basal flow unit is an aphanitic, amygdaloidal (5%) columnar jointed massive flow, the upper flow unit is an aphanitic massive flow containing up to 10% amygdules at its upper contact. The basal and upper flow units are locally separated by an amygdule zone (10%) and thin flow breccia developed at the top of the basal unit.
R7	40		#6 flow F-Shaft Sector	Aphanitic, aphyric, amygdaloidal (30%) pillowed flow; minor pillow breccia on upper surface. Polygonal fractures infilled by fine quartz (silica dumping).
R8	60			Aphanitic, aphyric, amygdaloidal (<5%) pillowed flow; well developed concentric joints. Pods or mega-pillows of massive lava may be buried lava streams.

TABLE F.3. ANDESITE FLOWS OF THE MILLENBACH ANDESITE FORMATION  
(modified from de Rosen-Spence, 1976)

Flow Number	Maximum Thickness (m)	Characteristics
M1	15	Aphanitic, weakly silicified pillowed flow; weak concentric jointing
M2	12	Aphanitic, strongly amygdaloidal pillowed flow
M3	10	Feldspar porphyritic (<1 mm) massive flow
M4	15	Massive flow with abundant feldspar phenocrysts (<2 mm)
M5	30	Weakly feldspar porphyritic pillowed flow; concentric jointing

TABLE F.4. ANDESITE FLOWS OF THE WAITE ANDESITE FORMATION, NEW VAUZE AND ANSIL SECTORS (modified from de Rosen-Spence, 1976)

Flow Number	Maximum Thickness (m)	Characteristics
W1	<20	Aphanitic, aphyric, amygdaloidal (5-8%) pillowed flow - occasional pipe amygdules.
W2	150	Aphanitic, aphyric, amygdaloidal (8%) pillowed flow(s) with weak concentric jointing and mega-pillows (tubes) of identical massive andesite.
W3	50	Aphanitic, feldspar porphyritic, amygdaloidal (3-5%) massive flow.
W4	70	Aphanitic, amygdaloidal (10%), feldspar porphyritic (<2%) massive flow.
W5	120	Waite upper member which consists of 3 laminar jointed, fine-grained to aphanitic, feldspar porphyritic (<2%-<2mm) silicified massive flows and a single, identical, concentric jointed pillowed flow in the Ansil Sector and a single, laminar jointed massive, silicified flow in the New Vauze sector. All flows contain 1% mega-amygdules, up to 28 cm in diameter, typically filled by quartz.
W6*	120	Aphanitic, feldspar porphyritic (<2%), amygdaloidal (8%), pillowed flow
W7*	60	Weakly feldspar porphyritic (2%), spherulitic, banded rhyolite flow
W8*	60	Aphanitic, amygdaloidal (5-10%), weakly feldspar porphyritic massive flows and breccia. The breccia facies consists of white, variably silicified amygdaloidal fragments (intact and broken lobes) in an andesitic hyaloclastite matrix. Similar to silicified flows of the Waite Upper member but lack mega amygdules.
W9*	40	Aphanitic, weakly feldspar porphyritic (<2%), amygdaloidal massive flow

\* restricted to New Vauze sector., Thin, laminated tuff units separate flows W4/W5 and W5/W6.

TABLE F.5. FLOWS OF THE WAITE RHYOLITE FORMATION

Flow Number	Maximum Thickness (m)	Lithology
4	90	Feldspar porphyritic, spherulitic rhyolitic flow.
3	300	Aphyric, spherulitic rhyolitic flow.
	40	Aphyric, aphanitic, massive andesitic flow.
2	200	Quartz-feldspar porphyritic rhyolitic flow.
	30	Aphyric, aphanitic massive andesitic flow.
1	500	Feldspar porphyritic, spherulitic rhyolitic flow.

A graphitic tuff unit occurs above the #4 flow and a laminated tuff separates flows #4 and #3. The latter tuff may be the stratigraphic equivalent to the Main Contact Tuff at the Norbec and Vauze Mines (modified after de Rosen-Spence, 1976).

TABLE F.6. FLOWS OF THE MILLENBACH RHYOLITE FORMATION

Flow	Maximum Thickness (m)	Lithology
K-Rhyolite	40	Feldspar porphyritic, spherulitic rhyolitic/dacitic flow
Turcotte	50	Quartz-feldspar porphyritic rhyolitic flow. Satellite flow/dome to identical flows which comprise the Millenbach-D68 lava dome.
*Upper QFP	240	Quartz-feldspar porphyritic rhyolite, contains 5% quartz phenocrysts <2 mm in size and 4% albite phenocrysts up to 2 mm.
*Lower QFP	110	Quartz-feldspar porphyritic rhyolite, contains 15% quartz phenocrysts <3 mm in size and 8% albite phenocrysts up to 3 mm. Inter-rhyolite silicified andesitic pillowed flows in the D68 area.

\* Comprise the Millenbach-D68 lava dome

# APPENDIX G.

## GEOCHEMISTRY

### AND TABLES OF CHEMICAL ANALYSES

#### G.1 INTRODUCTION

The geochemistry of the Blake River Group, and in particular the Noranda Volcanic Complex (NVC), has been described extensively in the literature by Baragar, (1968), Dimroth *et al.*, (1983), Gelinas *et al.*, (1977; 1984), Goodwin (1979) and de Rosen-Spence (1976). These workers would all agree on the subalkaline, mixed tholeiitic to calc-alkaline character of the volcanic succession but not on the origin of the magmas or the paleo-tectonic environment of the NVC.

De Rosen-Spence (1976) interpreted a) the NVC to consist of both calc-alkaline and tholeiitic basalts and andesites whereas the dacites and rhyolites are restricted to Fe-rich or tholeiitic categories, b) that both the tholeiitic and calc-alkaline andesites belong to a single, low K, calcic magmatic suite derived through differentiation of a primary olivine tholeiite magma and c) that the chemistry of the volcanic succession is compatible with either an island arc or oceanic ridge



environment. Dimroth et al., (1983) interpreted the NVC as forming above a north-dipping subduction zone with the calc-alkaline magmas derived from partial melting of subducted oceanic crust and sediments.

Gelinas et al., (1984) interpreted the NVC as a tholeiitic to calc-alkaline, rhyolite - basalt/andesite bimodal central volcano that formed in a "continental environment" where ascending mafic magmas (High-Mg basalt) fed a high-level central reservoir that was melting and assimilating sialic crust. Based on trace elements and REE, Gelinas et al., (1984) interpreted the calc-alkaline magmas of the NVC to be products of mixing between a felsic magma occupying the top of the magma reservoir and ascending mafic magma that was blocked by and essentially underplated the reservoir.

It is beyond the scope of this study to critically evaluate the models outlined above: the main emphasis during this research was to assess variations in major and some trace elements during alteration and to characterize rhyolitic and andesitic formations of the Mine Sequence. Further research will be conducted to determine if there are stratigraphic changes in the major, trace and rare earth elements within cauldron subsidence cycles and in the Mine Sequence overall. In the following discussion "andesite" refers to rocks of basalt, basaltic andesite and andesite composition.

## G.2 GEOCHEMICAL CHARACTERISTICS

1) Mine Sequence formations are subalkaline in character. All samples, regardless of degree of alteration, plot within the subalkaline field of the Ol - Ne - Qtz diagram (Figure G.1, Irvine and Baragar, 1971). Even strongly silicified andesitic flows of the Amulet upper member, although not shown in Figure G.1, plot in the subalkaline field.

2) Based on their  $\text{SiO}_2$  content Mine Sequence volcanic rocks were classified as rhyolite, dacite, andesite or basalt. Discrimination diagrams utilizing normative colour index and plagioclase composition (Figure G.2A, Irvine and Baragar, 1971) and trace elements (Figure G.2B, Winchester and Floyd, 1977) generally support this initial  $\text{SiO}_2$  classification scheme. Least altered flows from andesitic formations plot in the basalt and andesite fields on both diagrams and rhyolitic flows generally lie in the rhyolitic field but do extend into the dacitic fields. Silicified flows typically plot in the andesite and basalt fields but do extend into the dacite field on both diagrams.

3) The  $\text{SiO}_2$  content of andesitic and rhyolitic flows, excluding those that have been silicified, ranges from 50 - 64% and 66 - 78%, respectively. Figures G.3 and 4, show the variation of major oxides with respect to  $\text{SiO}_2$ ; generally both rhyolitic and andesitic formations show decreasing MgO,  $\text{Al}_2\text{O}_3$ ,  $\text{Fe}_2\text{O}_3$ ,  $\text{TiO}_2$ , MnO and CaO with increasing  $\text{SiO}_2$ .  $\text{Na}_2\text{O}$  and  $\text{P}_2\text{O}_5$  show no distinct trends with respect to  $\text{SiO}_2$  in either rhyolites or andesites; however,  $\text{K}_2\text{O}$  does show a slight

increase in rhyolites.

Except for the behaviour of  $\text{Na}_2\text{O}$ , the variation of the major oxides with respect to  $\text{SiO}_2$  are those expected in a mafic to felsic transition. The erratic, scattered behaviour of  $\text{Na}_2\text{O}$  indicates that the alkali content of the flows is not reflected by their silica content and is interpreted to be a product of Na-addition during spilitization (Chapter 12).

In silicified andesitic flows of the Amulet upper member the decrease in  $\text{MgO}$ ,  $\text{Al}_2\text{O}_3$ ,  $\text{Fe}_2\text{O}_3$ ,  $\text{TiO}_2$ ,  $\text{MnO}$ , and  $\text{P}_2\text{O}_5$  with increasing  $\text{SiO}_2$ , interpreted to be a result of Si-addition during silicification, mimics possible igneous differentiation trends in andesitic and rhyolitic formations (Figure G.5). The erratic behaviour of  $\text{Na}_2\text{O}$  and  $\text{CaO}$  is attributed to spilitization. Data from the upper member plotted on the ternary diagram of Figure G.6, ( $\text{FE} = \text{Fe}_2\text{O}_3 + \text{MgO}$ ,  $\text{SI} = \text{SiO}_2$ , and  $\text{NA} = \text{Na}_2\text{O} + \text{K}_2\text{O}$ ) form a distinct trend which essentially parallels the SI -FE sideline. It would appear that the silica/alkali ratio, possibly a product of spilitization, has remained relatively constant, with respect to components of the diagram, during progressive silicification.

4) Gelinas et al., (1984) subdivided the Blake River Group and NVC into nine chemostratigraphic units; andesitic flows of the Flavrian and Rusty Ridge formations fall within their Duprat-Montbray unit, a mixed tholeiitic to calc-alkaline succession whereas the Waite, Millenbach and Amulet Andesite formations are included within their Dufault unit, a calc-alkaline succession. As illustrated in

Figures G.7 to G.12, Mine Sequence andesitic formations and Feldspar Porphyritic and Quartz Feldspar Porphyritic rhyolitic flows plot in both the calc-alkaline and tholeiitic fields of AFM and Jensen Cation diagrams which suggests that individual lithostratigraphic formations are not readily subdivided into tholeiitic and calc-alkaline chemostratigraphic units using these diagrams. Because Si, Fe, Mg, and alkalis are relatively mobile during chloritization, silicification and spilitization (Chapter 12), classification diagrams such as the AFM and Jensen Cation plot may not be reliable. To overcome this problem Gelinis *et al.*, (1984) proposed that an effective discrimination between the calc-alkaline and tholeiitic series could be obtained by using "immobile trace elements", particularly Zr/Y and Ti/Zr ratios, which they interpreted to be  $<4$  and  $>70$  respectively, in tholeiitic andesites. Zr/Y and Ti/Zr ratios calculated for Mine Sequence andesitic flows (Tables G.6 A and B) clearly indicate their predominantly tholeiitic character. In support of this interpretation least altered andesitic and basaltic flows in Figure G.2A (Irvine and Baragar, 1971), plot in the basalt and tholeiitic andesite (icelandite) fields. The high  $\text{Fe}_2\text{O}_3$  (total Fe),  $\text{TiO}_2$  and low  $\text{Al}_2\text{O}_3$  content of the Mine Sequence andesites, along with the relatively flat REE patterns of andesitic and rhyolitic feeder dikes (Figure 8.6), is more typical of tholeiitic rather than calc-alkaline andesites. In summary, subdivision of the Mine Sequence and for that matter, the NVC, into tholeiitic and calc-alkaline units may be difficult and perhaps not justifiable. Some of the calc-alkaline and mixed tholeiitic - calc-alkaline units within the Mine

Sequence may be tholeiites that through subsequent alteration, such as spilitization, chloritization and silicification, have been chemically modified to resemble calc-alkaline andesites (de Rosen-Spence, 1976; MacGeehan and MacLean, 1980; Gibson, 1979). The strongly silicified Amulet upper member, based on Zr/Y and Ti/Zr ratios, appears to be a mixed tholeiitic to calc-alkaline succession.

5) The paleo-tectonic environment in which the NVC formed is a matter of controversy. Various authors, notably Pearce and Cann (1973) proposed that magma types, characteristic of various tectonic environments, can be distinguished on the basis of their trace element composition that was presumed to have remained immobile during alteration and metamorphism and geochemically consistent throughout time. Trace element data for Mine Sequence andesitic and basaltic flows, of Table G.6 A and B, plotted on Ti/Zr and Ti/100 - Zr - YX3 (Pearce and Cann, 1973) diagrams show considerable scatter but commonly fall in Fields 1, 3 and 5 (Figure 13 A and B) which encompass ocean floor basalts, within plate basalts and island arc volcanoes, a wide spectrum of environments. None of the andesites, however, plotted within the field of low K island arc tholeiites (a paleo-environment proposed by de Rosen-Spence, 1976), and only one sample plotted in the field occupied by calc-alkaline island arc basalts.

6) Based on 1265 chemical analyses Gelinas et al., (1984) interpreted the Blake River Group and NVC to be a bimodal basalt/andesite - rhyolite succession. Their histogram (Figure 5, Gelinas et al., 1984) of silica content illustrates the

bimodal character of the volcanic rocks with two peaks, at approximately 58% and 75 % SiO<sub>2</sub>, and a distinct "gap" between 65-70 % SiO<sub>2</sub>. Histograms of the SiO<sub>2</sub> and TiO<sub>2</sub> content of the Mine Sequence flows and feeder dikes (Figure G.14) clearly illustrate the bimodal character of this succession. Andesitic flows have a median value of 57% SiO<sub>2</sub> and 1.1% TiO<sub>2</sub> in contrast to a median value of 75% SiO<sub>2</sub> and 0.3% TiO<sub>2</sub> in rhyolitic flows. Silicified andesite flows of the Amulet upper member neatly fall within the "SiO<sub>2</sub> gap" (60 - 70% SiO<sub>2</sub>); however, the TiO<sub>2</sub> content of these flows is similar to that of non-silicified andesite.

### G.3 INTERPRETATION

The Mine Sequence is interpreted to be a subalkaline, primarily tholeiitic, basalt/andesite - rhyolite bimodal succession. The compositional bimodality of the Mine Sequence flows and feeder dikes, occurrence of contemporaneous rhyolite and andesite-basalt magma in composite dikes, and a general upward trend in the percentage of phenocrysts within the Mine Sequence and an overall greater abundance of phenocrysts in Cycle IV formations is interpreted to be a product of continuous "tapping" of an open, high level, compositionally zoned magma chamber characterized by a more felsic, "rhyolitic" top and a more mafic, "basalt-andesite" bottom (Hildreth, 1981; Thurston *et al.*, 1985). The Flavrian pluton is interpreted to be the intrusive equivalent of this compositionally zoned magma chamber (Goldie, 1978). Using major element data, trace elements and REE

Paradis *et al.*, (1988) interpreted the Flavrian trondhjemite, diorite and gabbro to be co-magmatic and the intrusive equivalent of Blake River Group rhyolitic, andesitic and basaltic flows. Paradis *et al.*, (1988) also noted that the tonalitic and hybrid phases, that they interpreted to be a product of fractional crystallization and that Goldie (1978) interpreted to be a product of magma mixing between an early gabbroic and later trondhjemitic phases, had no known extrusive equivalent. This may not be the case. The marked similarity in major oxide composition, trace elements and Zr/Y and Ti/Zr ratios between least altered andesitic flows of the Amulet upper member (<65% SiO<sub>2</sub>) and tonalitic rocks containing <65% SiO<sub>2</sub> (Tables 1 and 2, Paradis *et al.*, 1988) suggests they may be co-magmatic. Thus, andesitic flows of the Amulet upper member may be the product of complete mixing between a more mafic, perhaps differentiated magma and a more felsic magma within a compositionally zoned magma chamber.

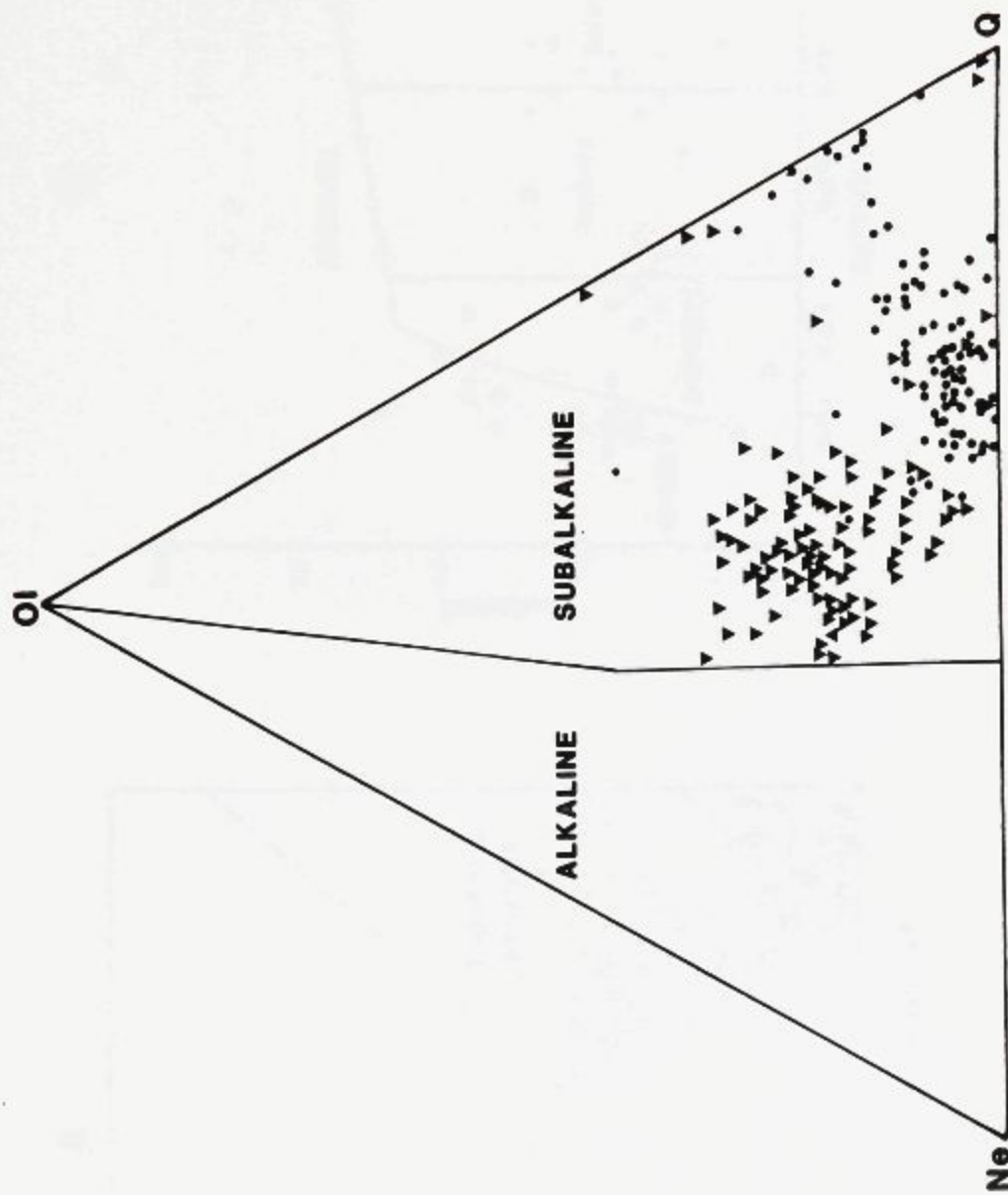


Figure G.1. Olivine (Ol)-Nepheline (Ne)-Quartz (Q) ternary diagram showing the subalkaline character of the Mine Sequence andesitic (inverted triangle) and rhyolitic (closed circles) flows (Irvine and Baragar, 1971).



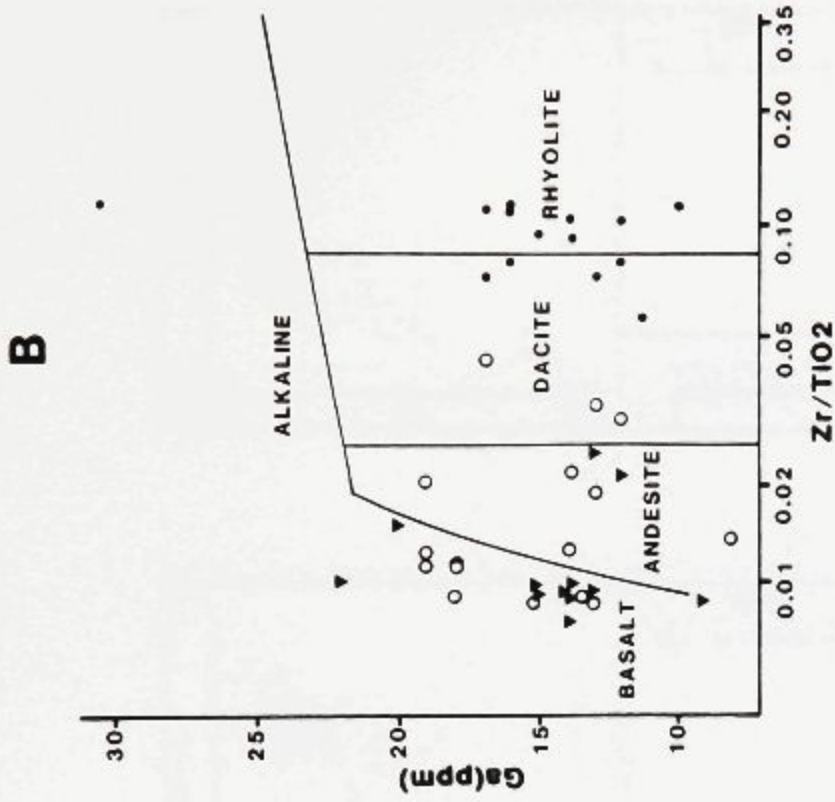
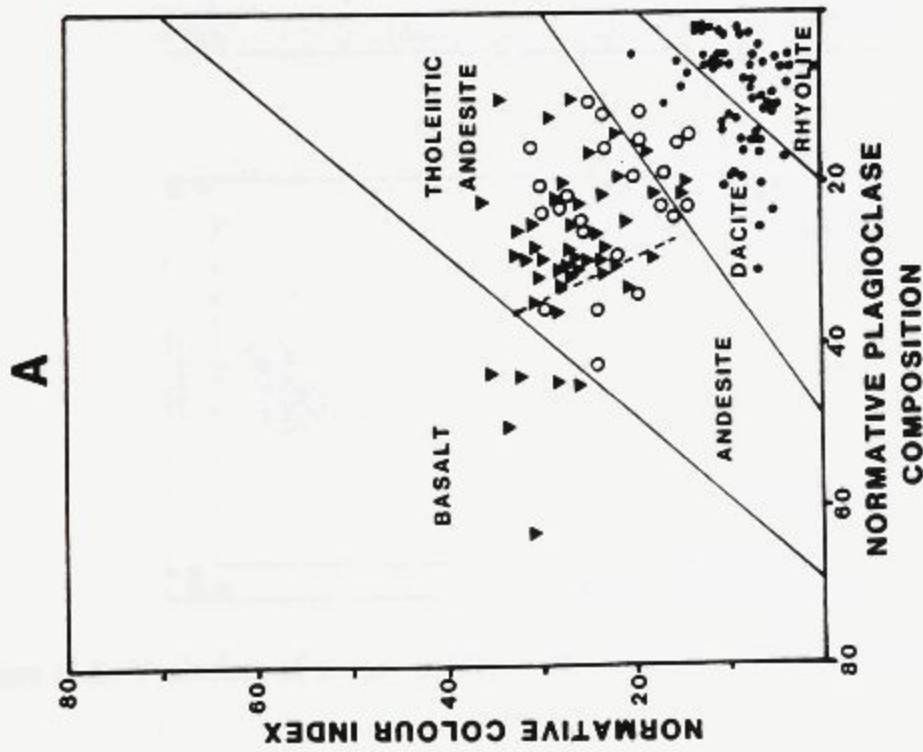


Figure G. 2. Composition of Mine Sequence volcanic rocks; A. Normative classification after Irvine and Baragar (1971) and B. Ga vs Zr/TiO<sub>2</sub> diagram after Winchester and Floyd (1977). Andesite = inverted triangles, Silicified flows of the Amulet upper member = open circles, and rhyolite = closed circles. Only least altered data plotted (Na<sub>2</sub>O > 2.5%, CaO < 8%, SiO<sub>2</sub> for andesites < 65% and totals > 97%). Data in B from Tables G.6A-C.

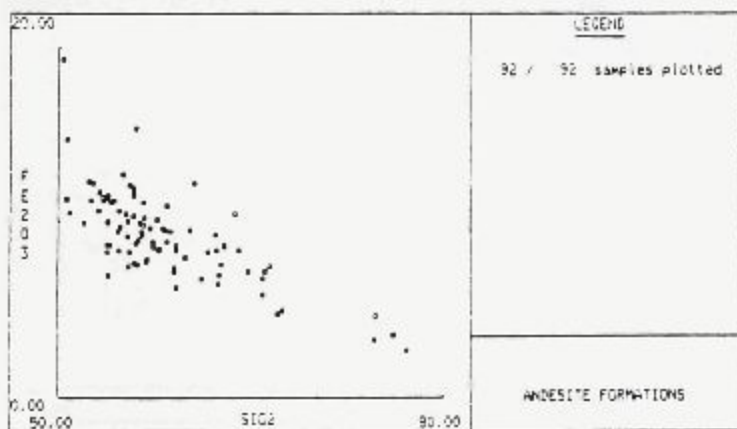
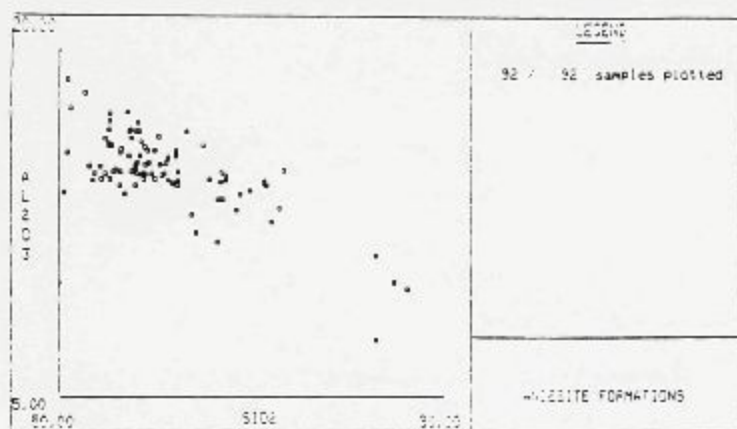
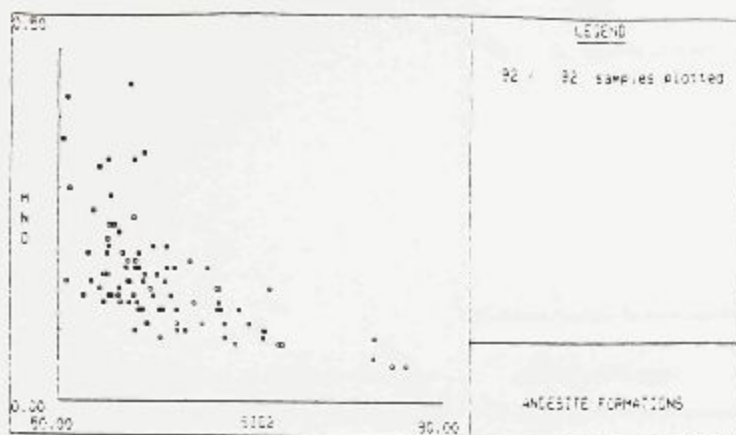


Figure G.3. Variation of major oxides with respect to SiO<sub>2</sub>, andesitic flows.

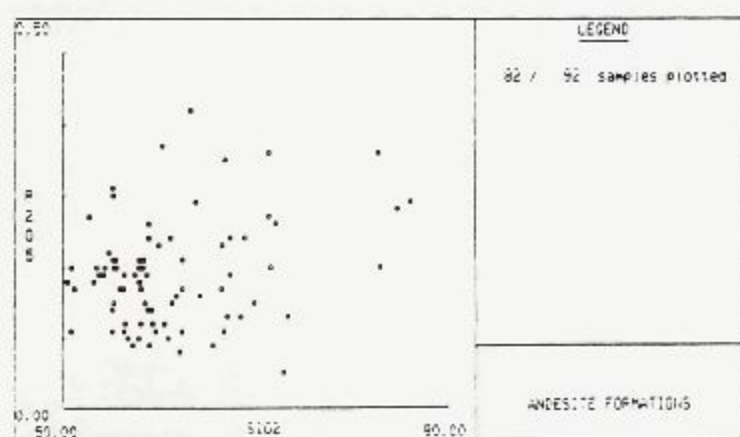
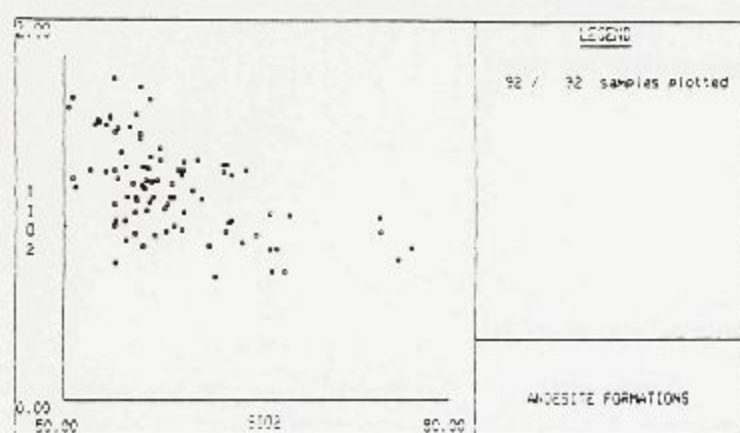
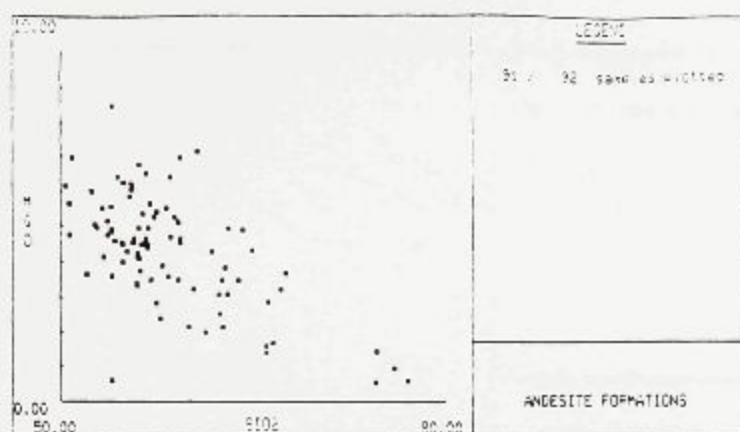


Figure G.3. Variation of major oxides with respect to SiO<sub>2</sub>, andesitic flows.

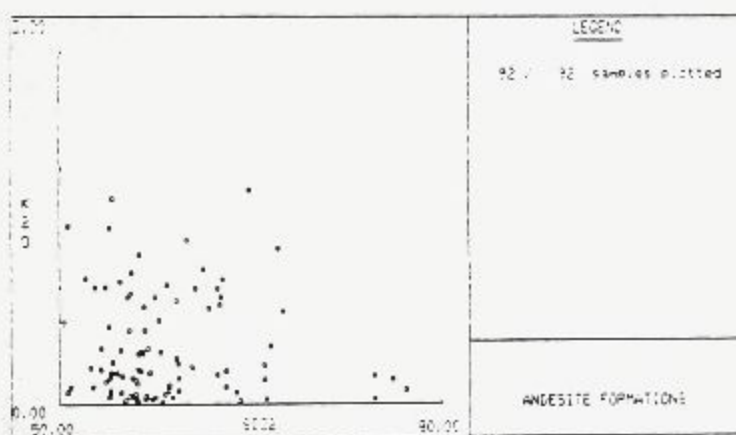
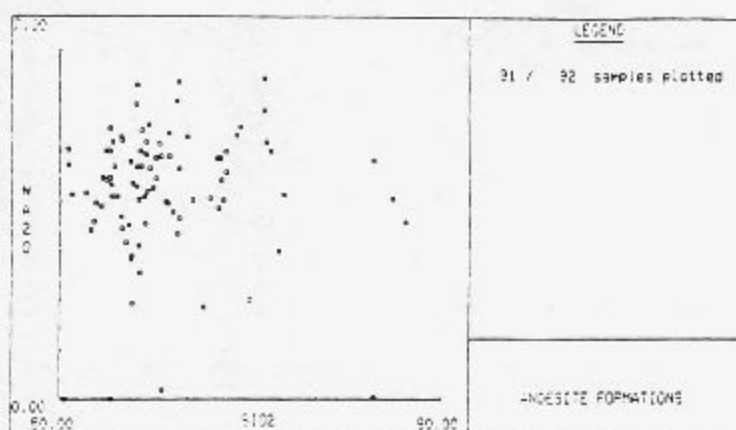
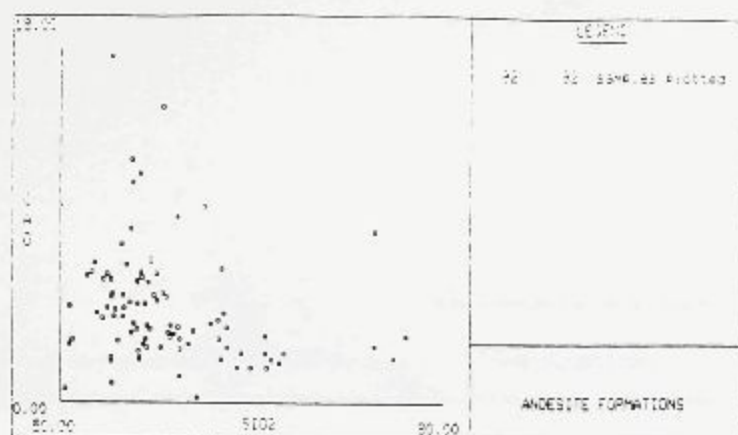


Figure G.3. Variation of major oxides with respect to SiO<sub>2</sub>, andesitic flows.

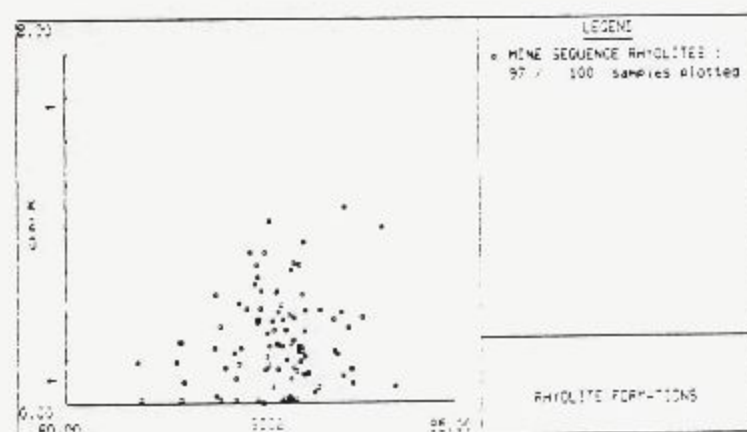
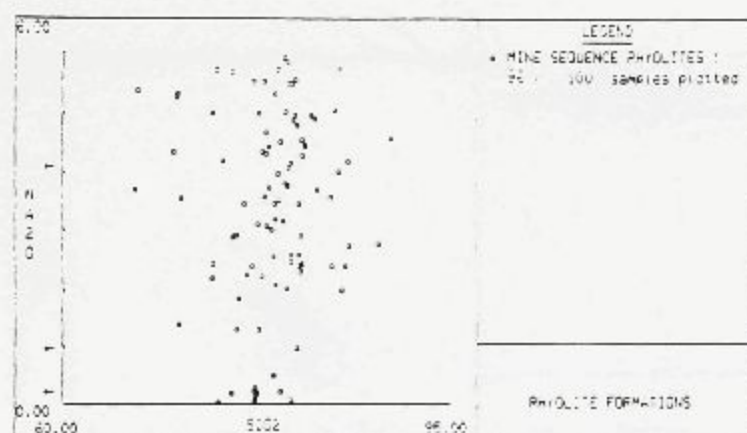
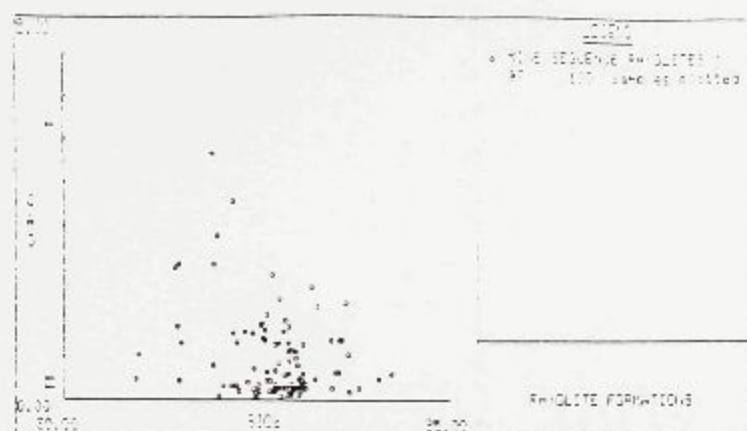


Figure G.4. Variation of major oxides with respect to SiO<sub>2</sub>, rhyolitic flows.

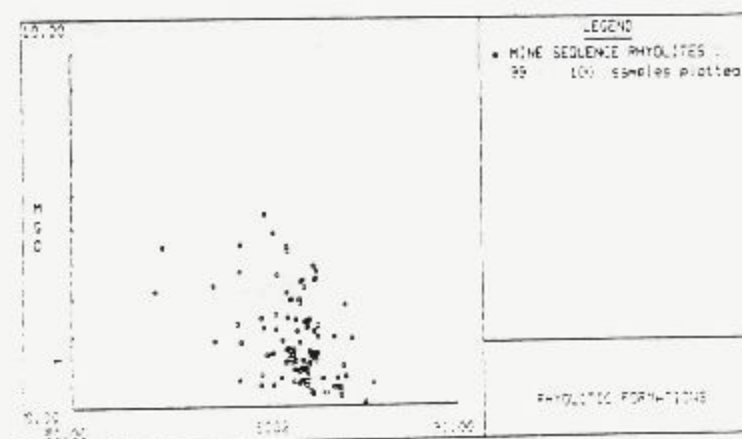
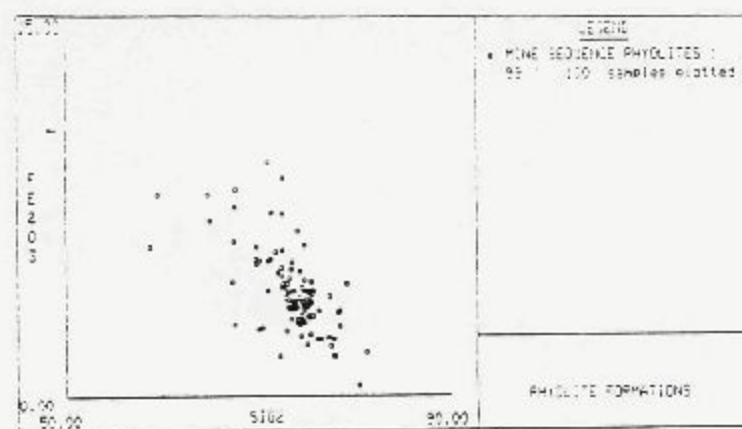
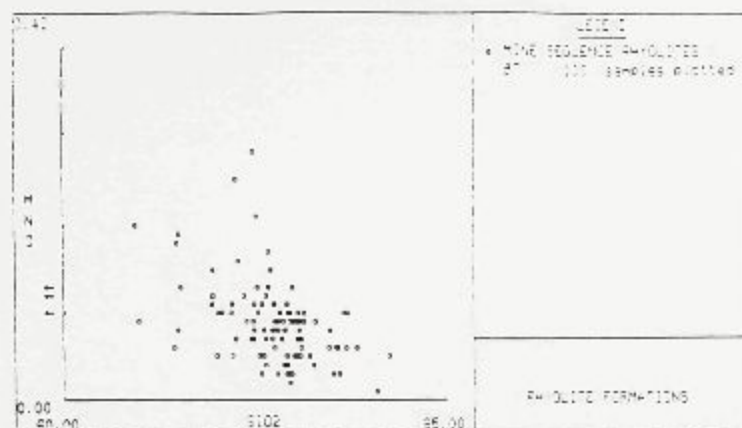


Figure G.4. Variation of major oxides with respect to SiO<sub>2</sub>, rhyolitic flows.

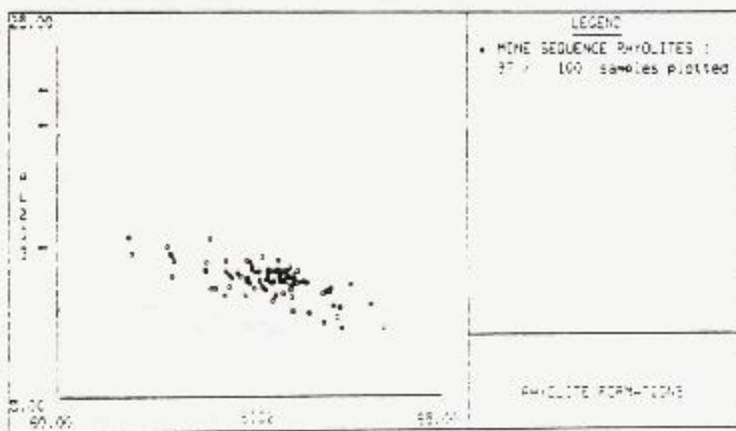
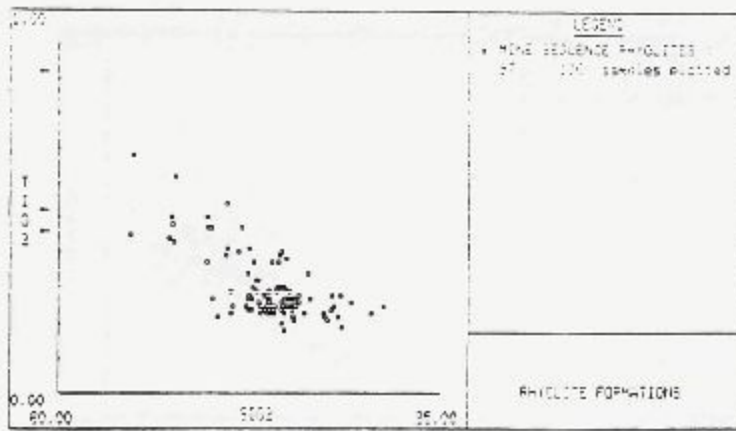
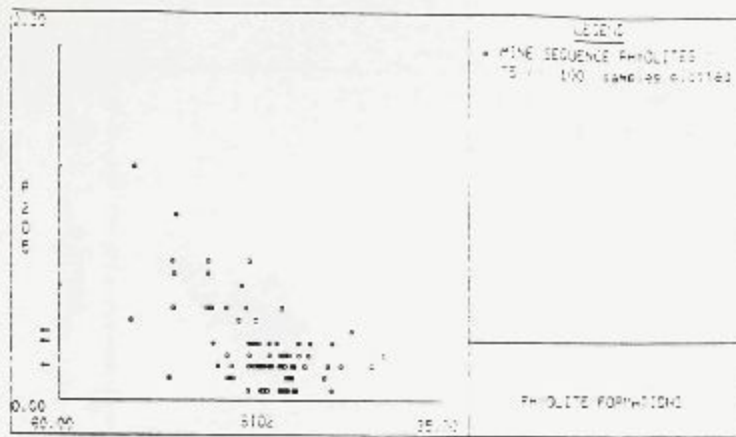


Figure G.4. Variation of major oxides with respect to SiO<sub>2</sub>, rhyolitic flows.

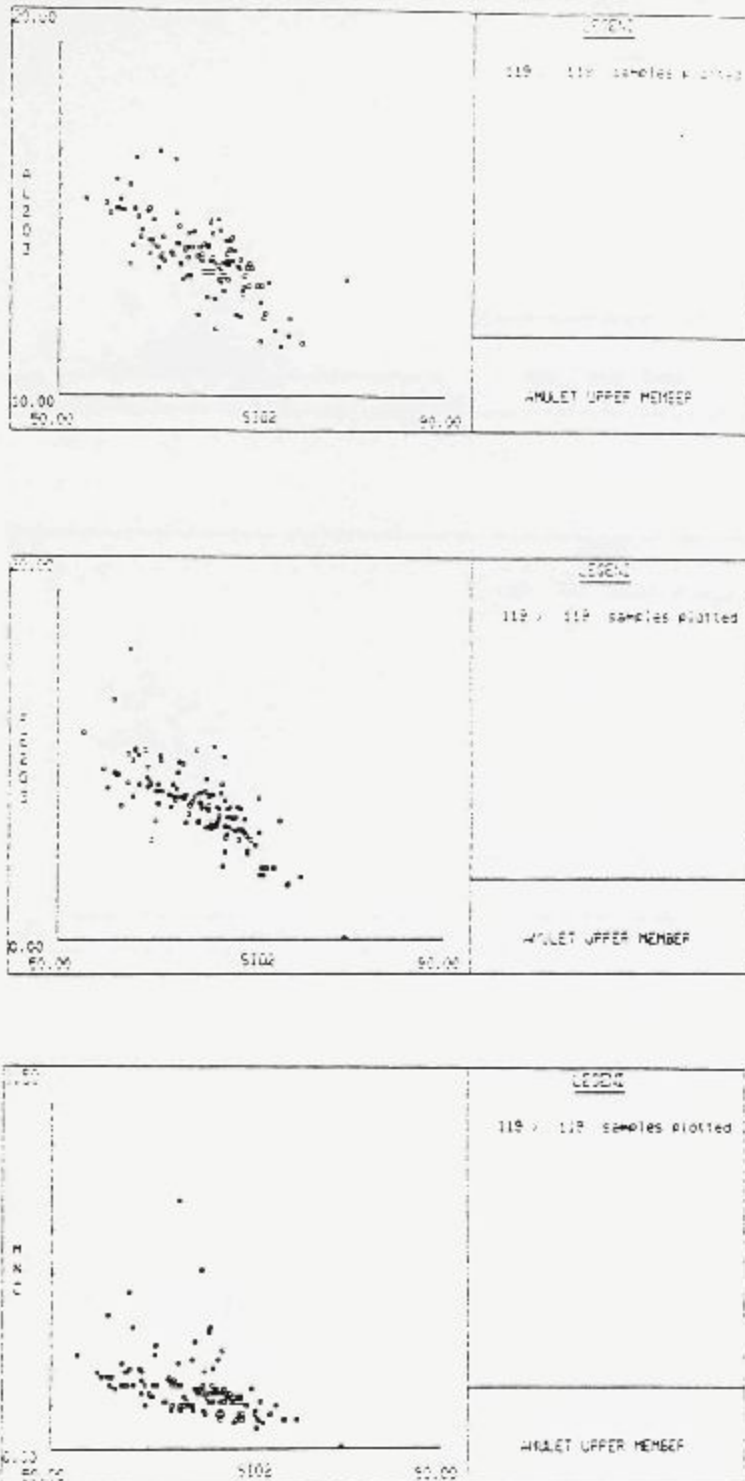


Figure G.5. Variation of major oxides with respect to SiO<sub>2</sub>, silicified flows, Amulet upper member.



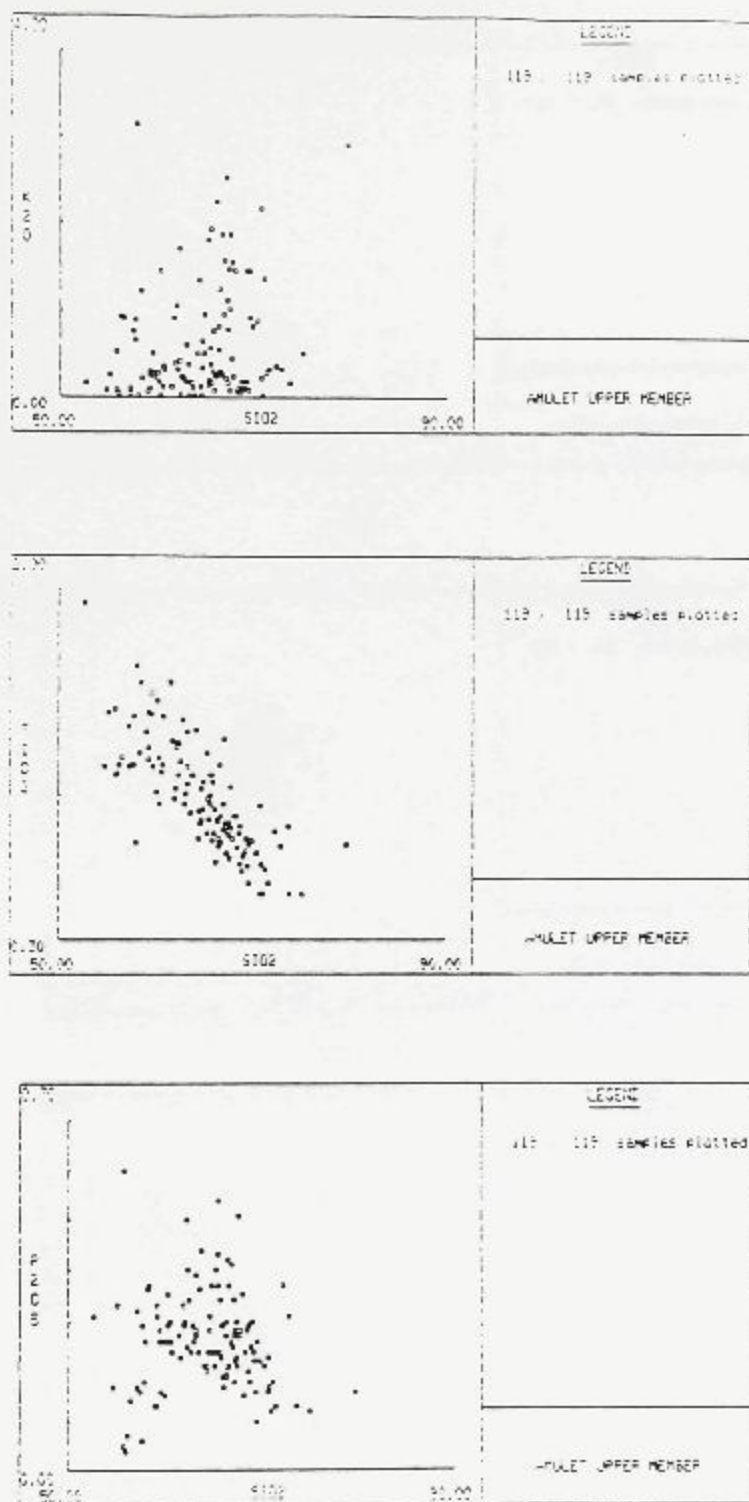


Figure G.5. Variation of major oxides with respect to SiO<sub>2</sub>, silicified flows, Amulet upper member.

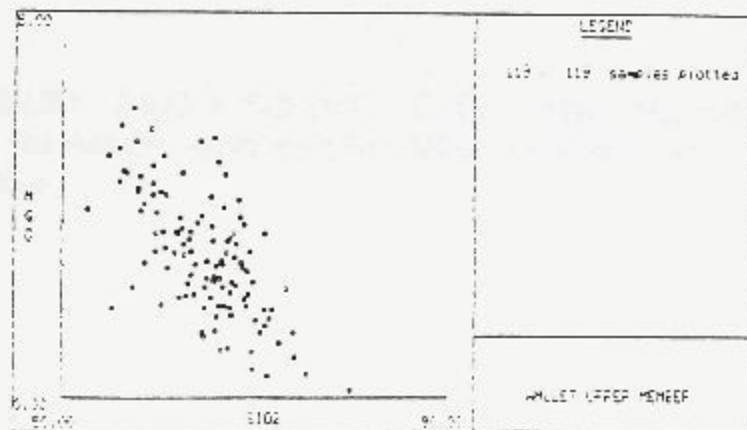
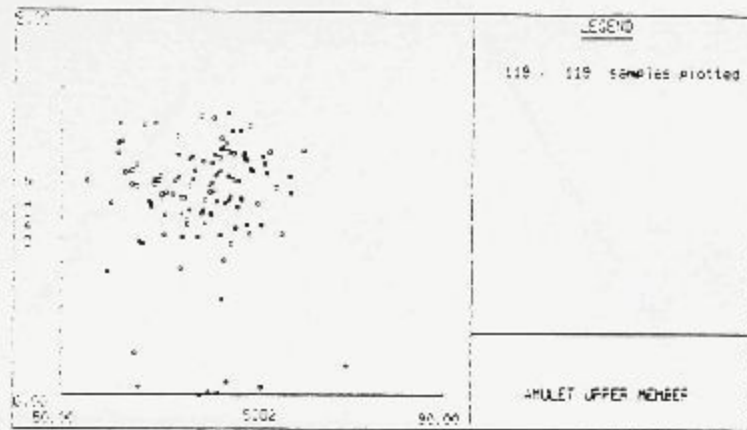
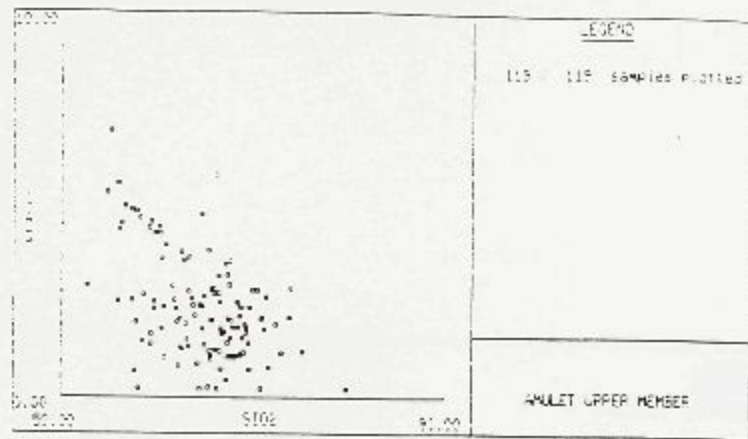


Figure G.5. Variation of major oxides with respect to SiO<sub>2</sub>, silicified flows, Amulet upper member.

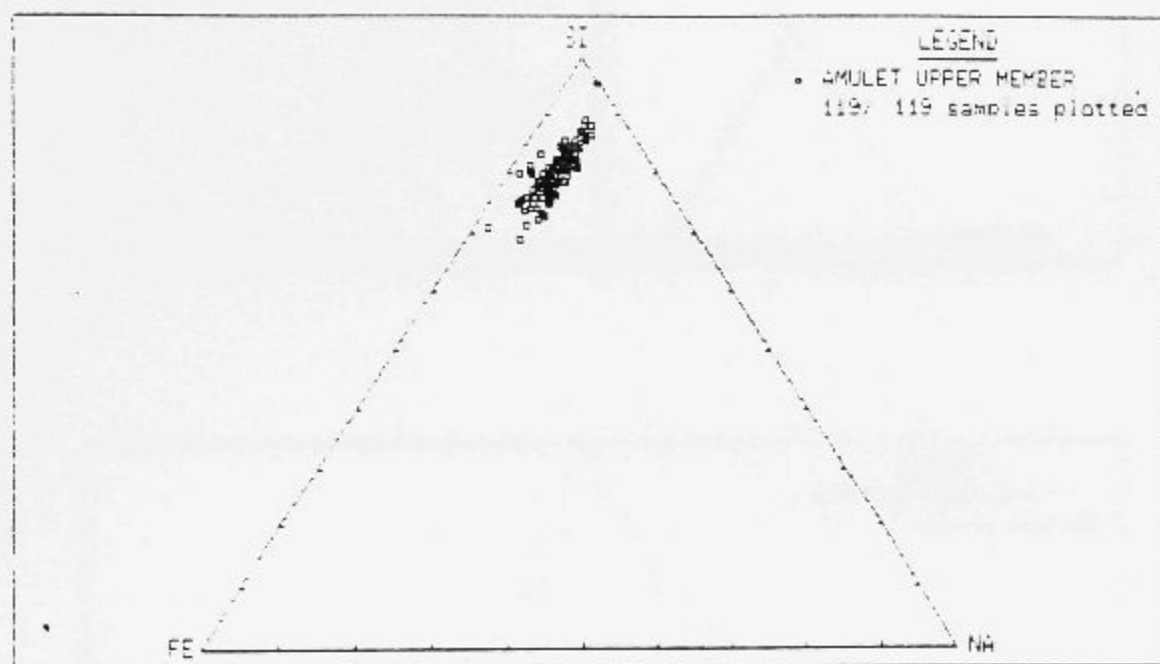


Figure G.6. A  $\text{SiO}_2(\text{SI}) - \text{Na}_2\text{O} + \text{K}_2\text{O} (\text{NA}) - \text{Fe}_2\text{O}_3 + \text{Mgo} (\text{FE})$  ternary diagram. Data from the Amulet upper member define a distinct trend parallel to the SI-FE sideline.

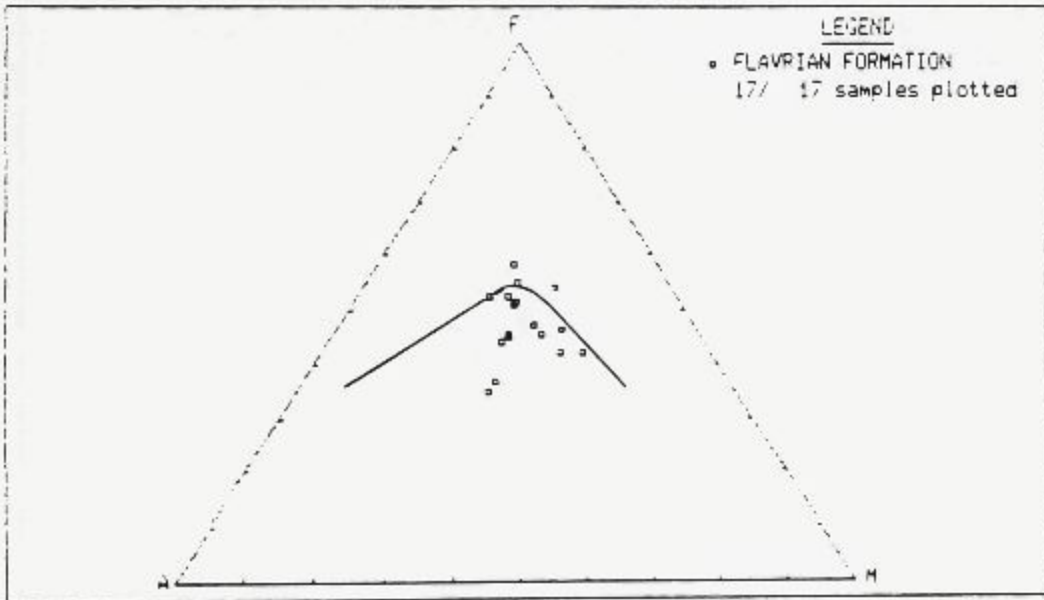
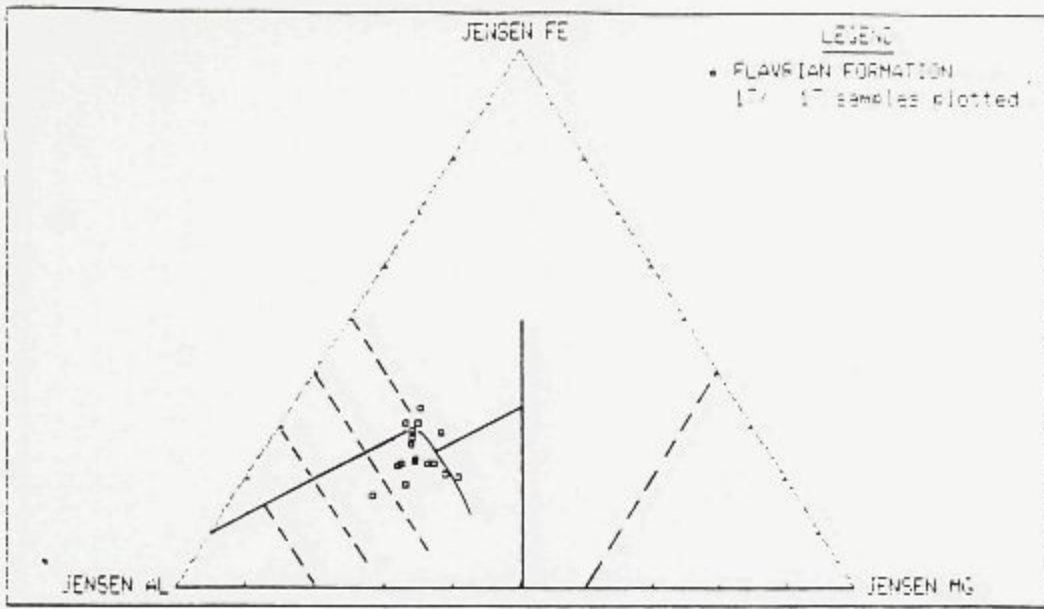


Figure G.7. An AFM diagram and Jensen Cation Plot showing the tholeiitic and calc-alkaline character of andesitic flows of the Flavrian formation.

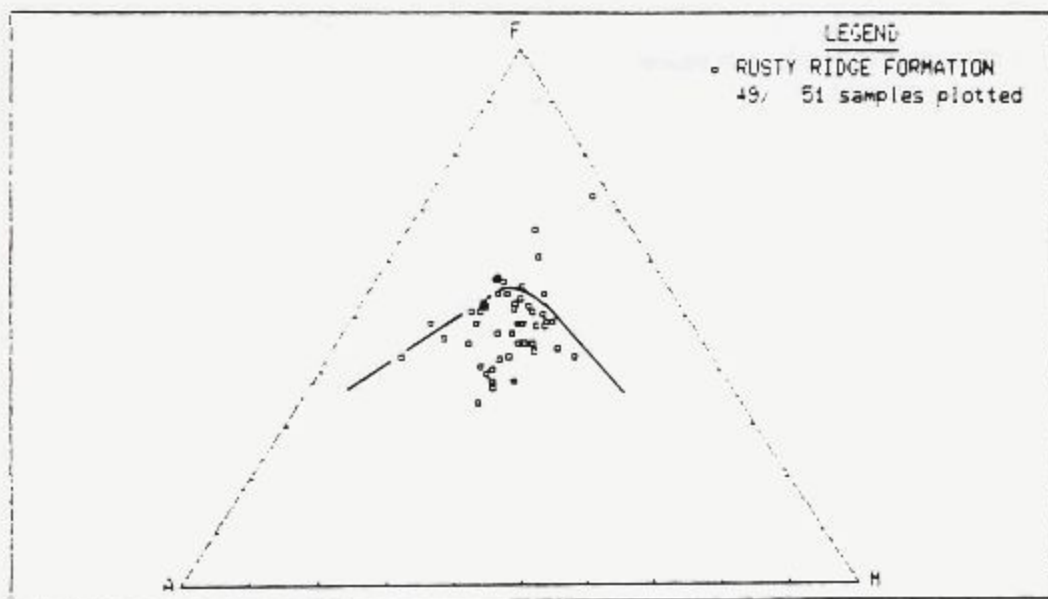
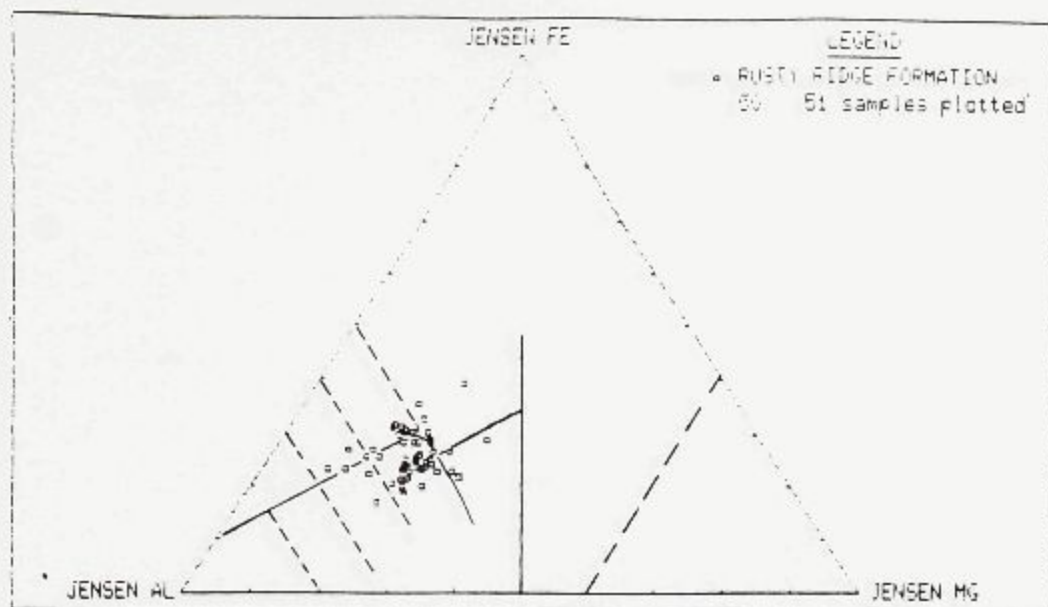


Figure G.8. An AFM diagram and Jensen Cation Plot showing the tholeiitic and calc-alkaline character of andesitic flows of the Rusty Ridge formation.

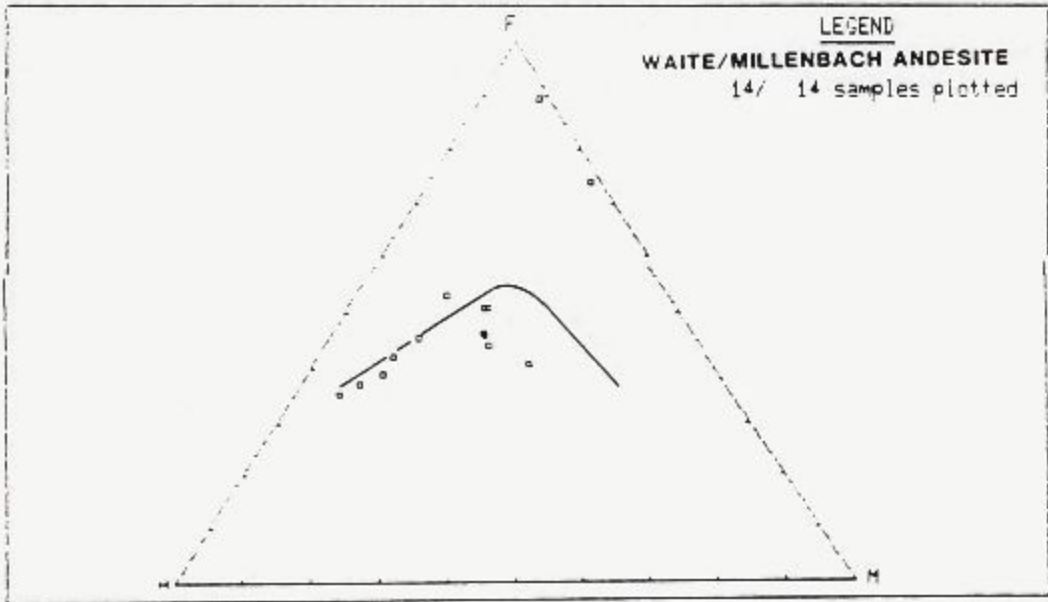
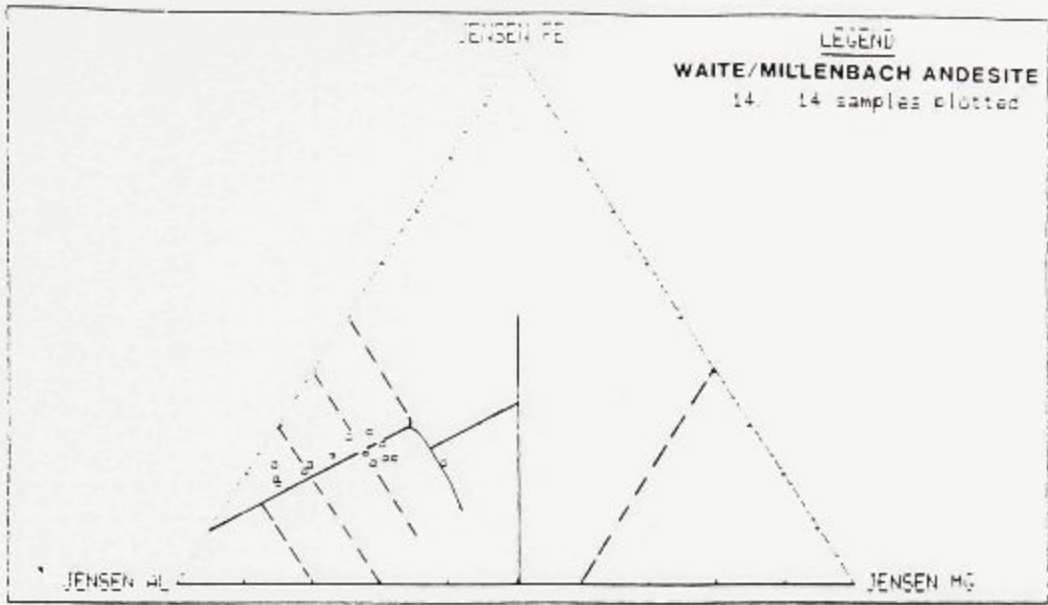


Figure G.9. An AFM diagram and Jensen Cation Plot showing the tholeiitic and calc-alkaline character of andesitic flows of the Waite/Millenbach Andesite formations.

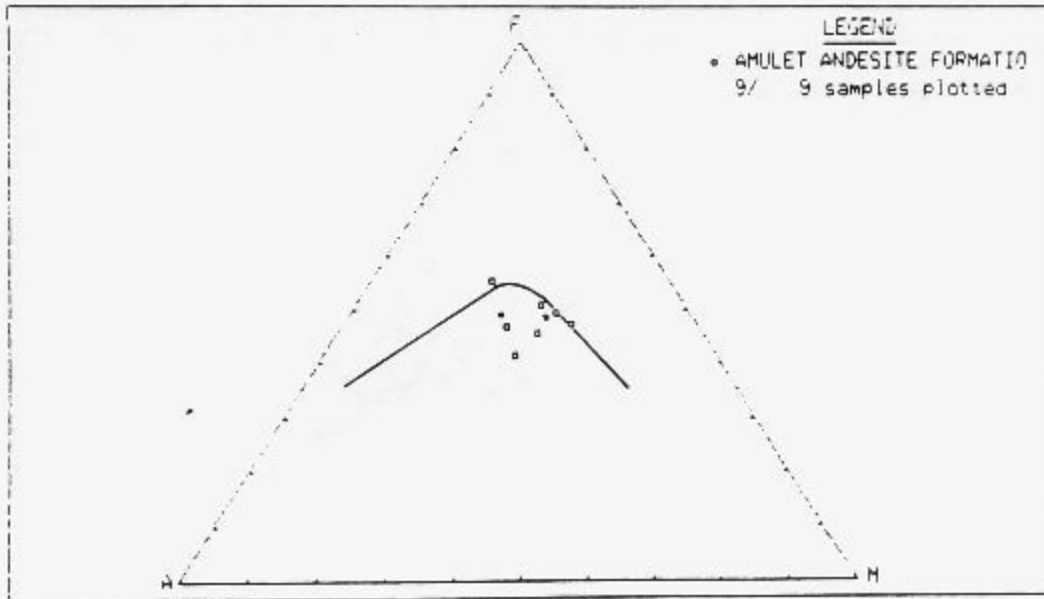
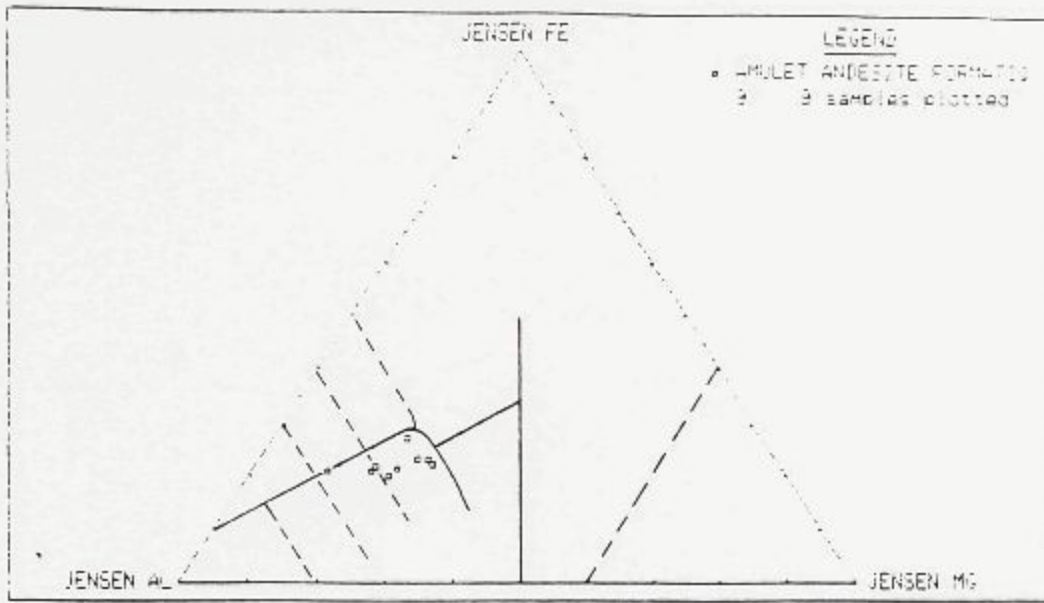


Figure G.10. An AFM diagram and Jensen Cation Plot showing the tholeiitic and calc-alkaline character of andesitic flows of the Amulet Andesite formation.

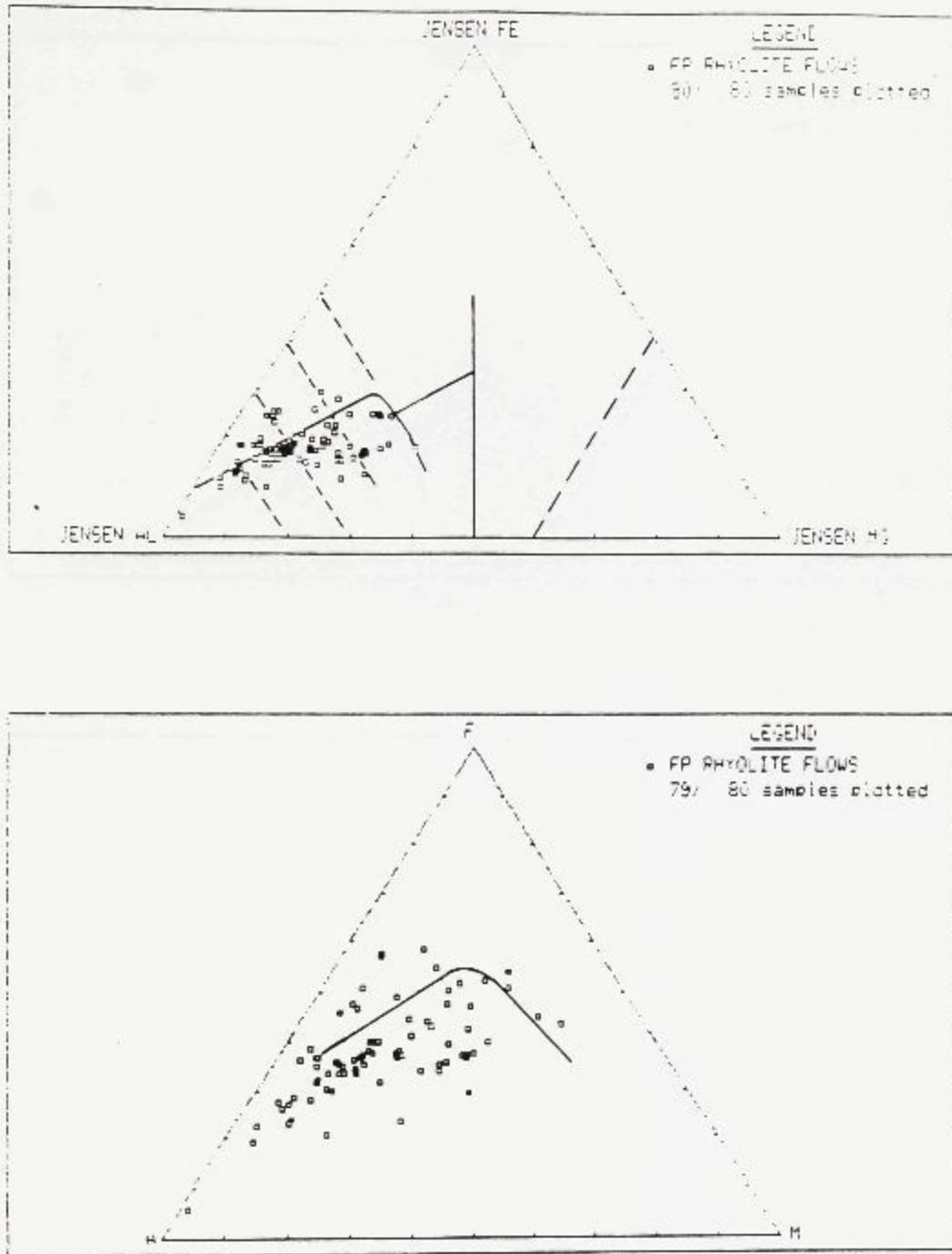


Figure G.11. An AFM diagram and Jensen Cation Plot showing the tholeiitic and calc-alkaline character of Feldspar Porphyritic Rhyolite flows.



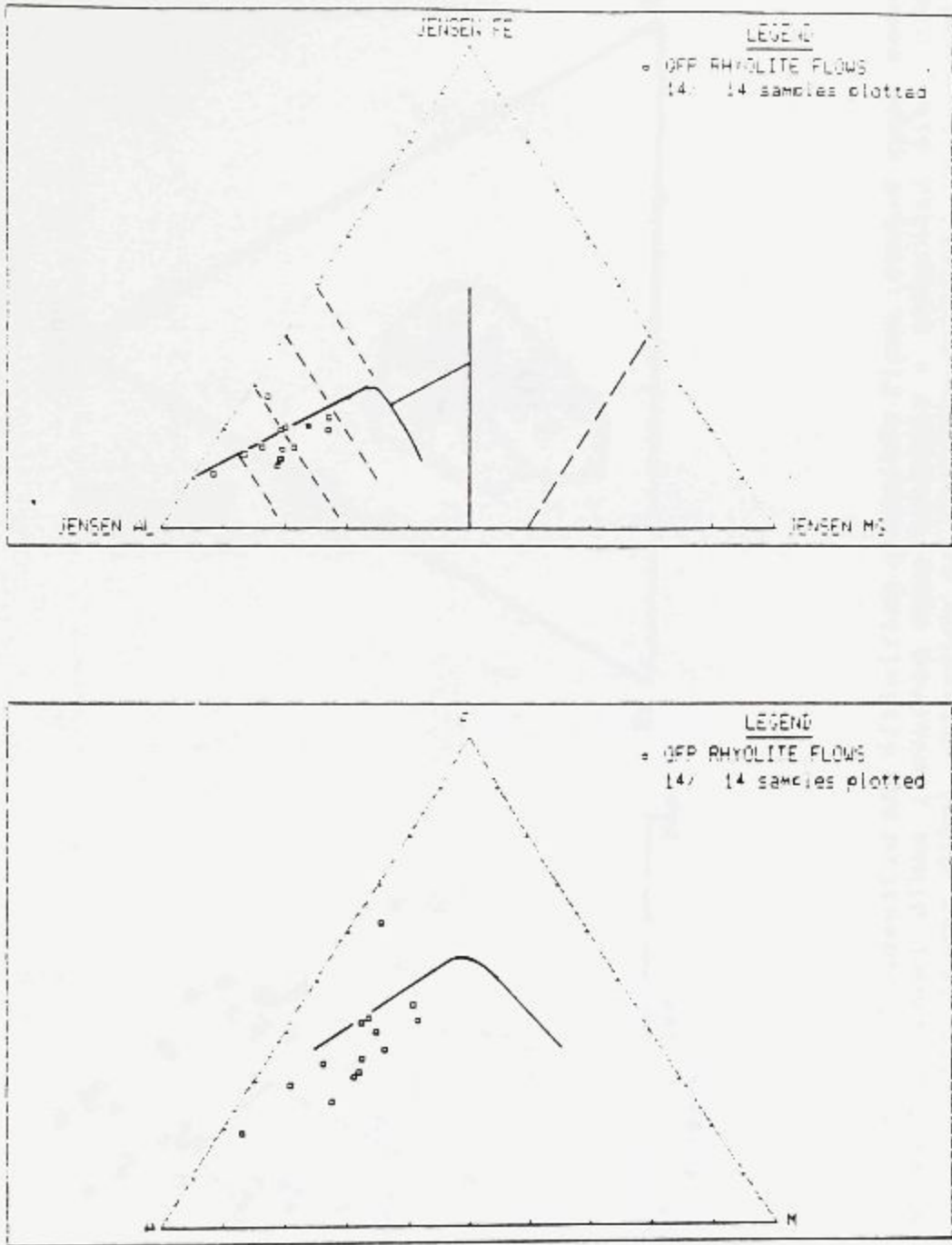


Figure G.12. An AFM diagram and Jensen Cation Plot showing the tholeiitic and calc-alkaline character of Quartz-Feldspar Porphyritic Rhyolitic flows.

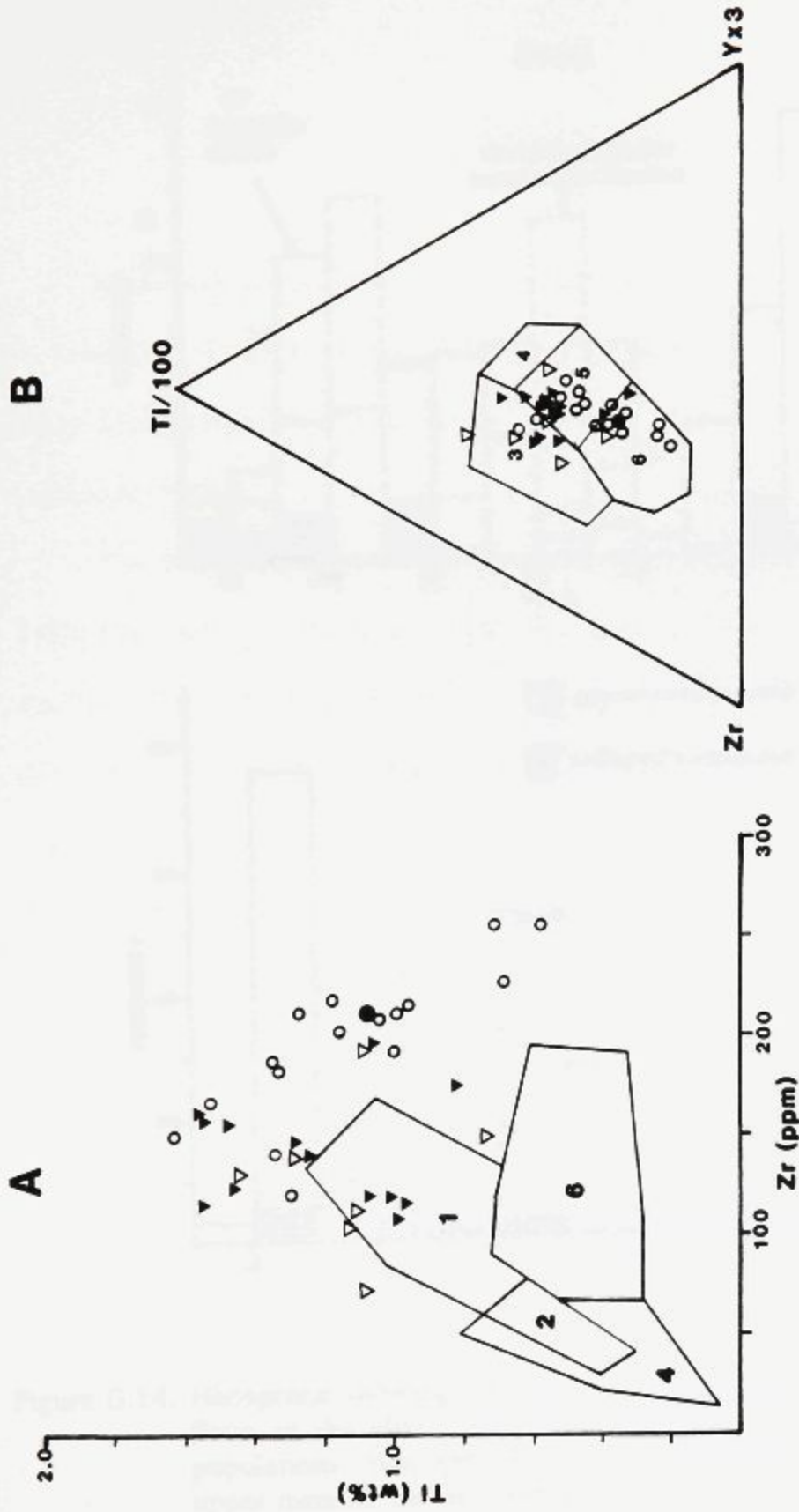


Figure G.13. Classification of andesitic and silicified andesitic flows (Amulet upper member) and andesitic feeder dikes (inverted open triangle = andesitic dike, closed circle = Amulet feeder dike) according to possible tectonic environment as suggested by A. TiO<sub>2</sub> vs Zr diagram and B. a Ti/100 - Zr - Yx<sub>3</sub> ternary diagram of Pearce and Cann (1973). Legend as in Figure G.2. and data from Table G.6A and B.

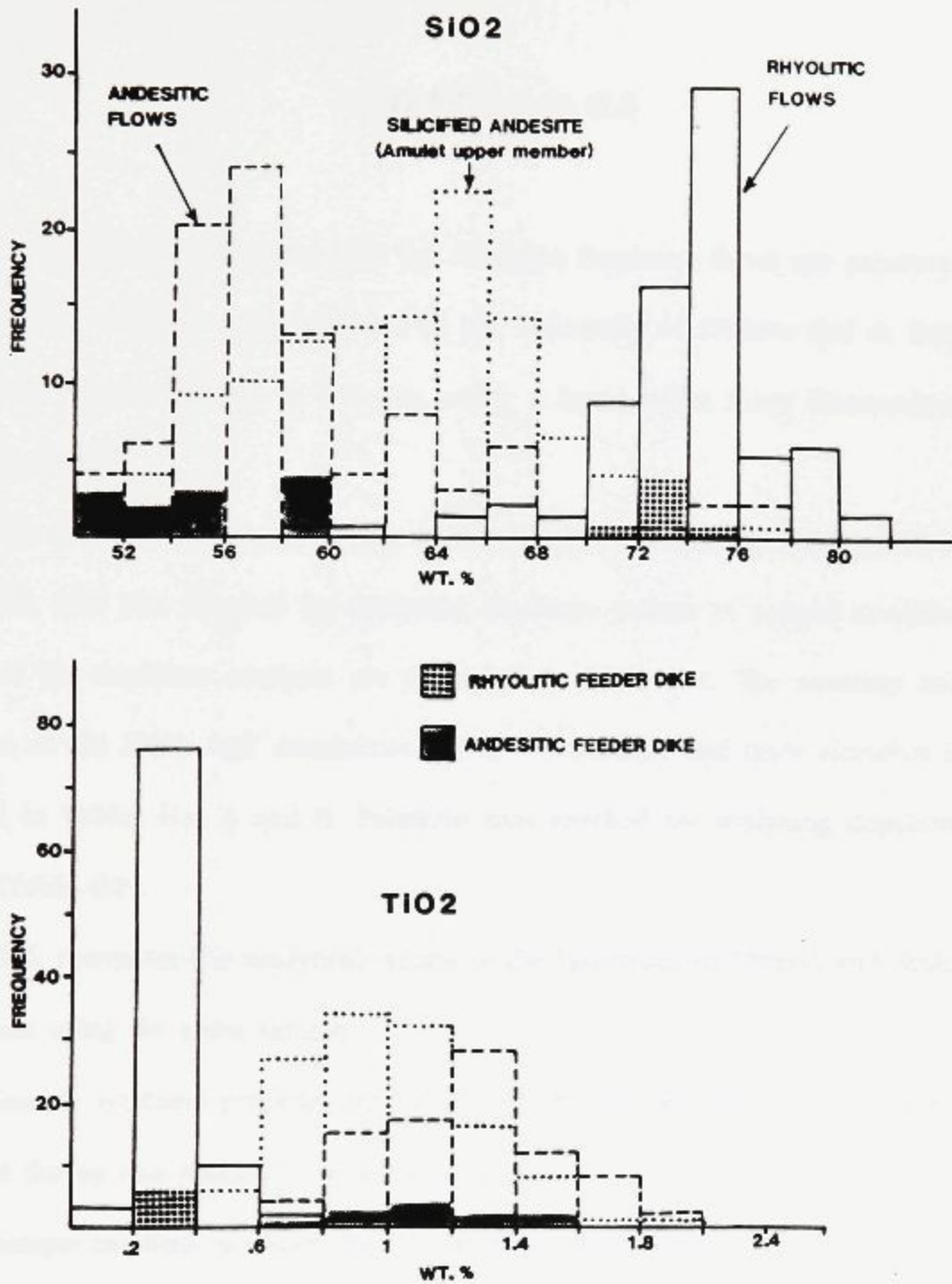


Figure G.14. Histograms showing the bimodal character of rhyolitic and andesitic flows of the Mine Sequence as suggested by their SiO<sub>2</sub> and TiO<sub>2</sub> populations. SiO<sub>2</sub> and TiO<sub>2</sub> data for silicified flows of the Amulet upper member define a separate, intermediate population.

## TABLES G.1 to G.5

Major and trace element data for the Mine Sequence flows are presented in Table G.1. Samples were analyzed at the University of Ottawa and at Xray Assay Laboratories (XRAL) in Toronto, using a fused pellet X-ray fluorescence technique (XRF).

The precision of the University of Ottawa XRF determinations is given in Table G.2, and was checked by analyzing duplicate pellets of several samples; results of the duplicate analyses are presented in Table G.3. The accuracy and precision of the XRAL ARF determinations for both major and trace elements is outlined in Tables G.4 A and B. Precision was checked by analyzing duplicate pellets (Table G3).

Table G.5, compares the analytical results of the University of Ottawa and XRAL techniques using the same sample.

Sample numbers preceded by 79, 80, 81, 82, 83, BC, BH, I or Nor were collected during this research and are located on Map 2.

Sample numbers preceded by- TS are from Smith, 1984.

- V, REA, WH, S are from de Rosen-Spence, 1976.

- 007-032 are from Ikingura, 1984.

- 21505-21571 are from Watkins, 1980.

## NORTHWEST FORMATION; NORTH FLOW; FELDSPAR PORPHYRITIC RHYOLITE

SAMP NO.->	82-167	82-169	82-171	82-175	83-166	83-67
	PA05026	PA05027	PA05028	PA05029	PA05030	PA05031
SI02	74.33	72.71	72.33	76.24	74.50	64.90
AL203	12.23	12.33	12.75	11.44	12.10	13.10
FE203	2.61	4.29	4.73	3.78	3.34	7.57
MNO	0.04	0.05	0.07	0.04	0.04	0.09
HGO	0.61	1.56	1.63	0.40	0.87	1.87
CAO	1.89	1.78	0.73	0.47	1.72	1.06
NA20	5.92	4.99	5.52	4.91	5.84	5.39
K20	0.04	0.02	0.07	0.35	0.06	0.07
TI02	0.37	0.37	0.34	0.34	0.40	0.68
P205	0.03	0.03	0.03	0.04	0.08	0.20
CR203	0.00	0.00	0.00	0.00	0.00	0.00
LOI	0.00	0.00	0.00	0.00	1.00	1.93
TOTAL	98.07	98.13	98.20	98.01	99.95	96.86
S	0.00	0.00	0.01	0.00	0.00	0.00
BA	28.00	50.00	33.00	142.00	0.00	0.00
CR	24.00	22.00	27.00	22.00	20.00	30.00
ZR	228.00	226.00	238.00	241.00	260.00	250.00
SR	62.00	75.00	32.00	26.00	120.00	40.00
RB	0.00	0.00	0.00	3.00	< 10.00	< 10.00
Y	62.00	56.00	66.00	52.00	0.00	0.00
NB	4.00	7.00	5.00	6.00	0.00	0.00
ZN	7.00	18.00	15.00	15.00	0.00	0.00
NI	0.00	0.00	1.00	0.00	0.00	0.00
83-240A						
SAMP NO.->	PA05032					
SI02	72.80					
AL203	11.10					
FE203	2.84					
MNO	0.03					
HGO	2.98					
CAO	1.79					
NA20	2.24					
K20	3.39					
TI02	0.32					
P205	0.07					
CR203	0.00					
LOI	2.00					
TOTAL	99.56					
S	0.00					
BA	0.00					
CR	10.00					
ZR	220.00					
SR	80.00					
RB	60.00					
Y	0.00					
NB	0.00					
ZN	0.00					
NI	0.00					

## NORTHWEST FORMATION; SOUTH FLOW; FELDSPAR PORPHYRITIC RHYOLITE

SAMP NO. ->	81-205	81-210	81-212	82-98	Nor 54	Nor 55
	PA05033	PA05034	PA05035	PA05036	PA05037	PA05038
SI02	74.35	70.91	73.90	74.81	64.70	67.50
AL203	12.77	12.73	12.15	12.15	14.00	11.86
FE203	4.77	4.56	3.21	4.24	8.73	8.16
MNO	0.04	0.05	0.03	0.03	0.20	0.19
MGO	2.19	1.53	1.11	1.35	3.35	4.50
CAO	0.28	1.55	1.31	0.25	0.48	0.43
NA2O	5.01	5.67	5.71	5.49	3.69	1.38
K2O	0.18	0.08	0.10	0.08	0.93	1.37
TI02	0.39	0.41	0.37	0.38	0.45	0.43
F2O5	0.04	0.02	0.00	0.02	0.07	0.11
CR203	0.00	0.00	0.00	0.00	0.00	0.00
LOI	0.00	0.00	0.00	0.00	2.96	3.44
TOTAL	100.02	97.51	97.89	98.80	99.56	99.37
S	0.00	0.00	0.00	0.01	0.00	0.00
BA	87.00	83.00	66.00	51.00	0.00	0.00
CR	23.00	29.00	26.00	21.00	0.00	0.00
ZR	307.00	227.00	299.00	301.00	442.00	372.00
SR	22.00	69.00	76.00	25.00	28.00	8.00
RB	0.00	0.00	0.00	0.00	17.00	24.00
Y	112.00	58.00	91.00	103.00	115.00	97.00
NB	8.00	4.00	11.00	11.00	0.00	0.00
ZN	22.00	8.00	5.00	9.00	0.00	0.00
NI	3.00	0.00	4.00	0.00	0.00	0.00

## NORTHWEST FORMATION; CRANSTON MEMBER; QFP RHYOLITE

SAMP NO.->	83-133	83-136	83-163
	PA05386	PA05397	FA05388
SI02	74.70	75.30	74.50
AL203	10.80	11.30	11.70
FE203	6.51	2.74	3.26
MNO	0.02	0.07	0.03
MGO	0.44	1.47	0.70
CAO	0.16	0.21	0.59
NA2O	0.08	2.32	3.79
K2O	3.16	3.64	3.00
TI02	0.18	0.21	0.20
P2O5	0.03	0.03	0.03
CR203	0.00	0.00	0.00
LOI	2.00	1.47	1.16
TOTAL	98.08	98.76	98.96
S	0.00	0.00	0.00
BA	0.00	0.00	0.00
CR	20.00	20.00	10.00
ZR	320.00	330.00	370.00
SR	< 10.00	10.00	40.00
RB	50.00	60.00	60.00
Y	0.00	0.00	0.00
NB	0.00	0.00	0.00
ZN	0.00	0.00	0.00
NI	0.00	0.00	0.00





## AMULET FORMATION; LOWER MEMBER; #1 FLOW; FELDSPAR PORPHYRITIC RHYOLITE

	83-206	83-207	83-209	83-224
SAMP NO.->	PA05051	PA05052	PA05053	PA05054
SI02	74.70	75.60	73.70	70.00
AL203	11.50	11.40	11.70	11.10
FE203	5.06	3.56	4.10	5.90
MNO	0.09	0.09	0.06	0.10
HGO	2.39	1.97	2.88	5.42
CAO	0.13	0.28	0.24	0.08
NA2O	2.46	4.43	2.07	0.03
K2O	1.41	0.69	2.03	1.71
TIO2	0.27	0.26	0.27	0.27
P2O5	0.04	0.05	0.05	0.05
CR2O3	0.00	0.00	0.00	0.00
LOI	2.00	1.54	2.85	3.54
TOTAL	100.05	99.87	99.95	98.20
S	0.00	0.00	0.00	0.00
BA	0.00	0.00	0.00	0.00
CR	10.00	100.00	10.00	10.00
ZR	340.00	320.00	350.00	370.00
SR	< 10.00	< 10.00	10.00	< 10.00
RB	20.00	20.00	30.00	30.00
Y	0.00	0.00	0.00	0.00
NB	0.00	0.00	0.00	0.00
ZN	0.00	0.00	0.00	0.00
NI	0.00	0.00	0.00	0.00

## AHULET FORMATION; LOWER MEMBER; #2 FLOW; QFF RHYOLITE FLOWS

SAMP NO.->	82-53	82-54	82-59	82-62	82-66
	PA05112	PA05113	PA05114	PA05115	PA05116
SI02	77.29	72.89	77.95	74.66	78.38
AL203	9.25	11.98	10.10	10.81	9.99
FE203	4.37	4.90	1.72	4.58	3.11
MNO	0.08	0.11	0.03	0.09	0.06
MGO	1.97	1.25	0.29	1.22	0.84
CAO	0.30	1.43	1.42	1.17	1.05
NA2O	2.42	4.32	1.99	2.59	4.19
K2O	1.16	0.78	4.44	1.92	0.77
TIO2	0.22	0.29	0.25	0.30	0.28
P2O5	0.02	0.00	0.00	0.00	0.03
CR203	0.00	0.00	0.00	0.00	0.00
LOI	0.00	0.00	0.00	0.00	0.00
TOTAL	97.08	97.95	98.19	97.34	98.70
S	0.00	0.06	0.01	0.00	0.03
BA	257.00	260.00	396.00	351.00	250.00
CR	28.00	30.00	23.00	24.00	26.00
ZR	209.00	278.00	249.00	248.00	226.00
SR	22.00	73.00	92.00	56.00	68.00
RB	22.00	6.00	64.00	46.00	13.00
Y	52.00	77.00	53.00	60.00	57.00
NB	5.00	8.00	7.00	7.00	4.00
ZN	102.00	1638.00	16.00	89.00	72.00
NI	16.00	6.00	0.00	5.00	17.00

TABLE G.1

## AMULET FORMATION; LOWER MEMBER; #3 FLOW; FELDSPAR PORPHYRITIC RHYOLITE

SAMP NO.->	81-85	81-89	81-91	81-94	81-97	81-101
	PA05067	PA05068	PA05069	PA05070	PA05071	PA05072
SI02	75.46	73.41	73.10	73.96	77.24	78.21
AL203	11.65	11.14	11.56	11.40	10.85	9.56
FE203	4.46	5.83	5.15	3.37	2.58	3.72
MNO	0.07	0.15	0.07	0.08	0.06	0.10
MGO	1.51	2.12	1.63	1.31	0.58	1.14
CAO	1.30	2.94	0.44	2.36	1.40	2.30
NA2O	4.53	3.00	4.30	3.51	3.58	2.40
K2O	1.04	1.64	1.27	1.30	1.89	1.67
TI02	0.25	0.24	0.25	0.24	0.23	0.22
P2O5	0.00	0.00	0.01	0.00	0.00	0.00
CR203	0.00	0.00	0.00	0.00	0.00	0.00
LOI	0.00	0.00	0.00	0.00	0.00	0.00
TOTAL	100.27	100.47	97.78	97.53	98.41	99.34
S	0.00	0.00	0.02	0.00	0.03	0.01
BA	135.00	426.00	273.00	251.00	481.00	412.00
CR	23.00	30.00	24.00	23.00	20.00	24.00
ZR	275.00	261.00	274.00	269.00	252.00	240.00
SR	32.00	52.00	22.00	43.00	39.00	29.00
RB	17.00	19.00	18.00	16.00	20.00	21.00
Y	56.00	69.00	55.00	64.00	56.00	49.00
NB	8.00	6.00	7.00	6.00	6.00	7.00
ZN	62.00	72.00	96.00	48.00	62.00	76.00
NI	3.00	0.00	0.00	0.00	0.00	6.00
SAMP NO.->	81-104	81-106	81-122	81-115	82-183	82-192
	PA05073	PA05074	PA05075	PA05076	PA05077	PA05078
SI02	75.43	75.39	73.64	75.21	58.65	74.86
AL203	11.96	11.77	12.06	11.25	20.45	11.55
FE203	4.16	4.96	4.17	4.51	6.49	3.87
MNO	0.06	0.05	0.11	0.07	0.10	0.13
MGO	1.32	3.78	0.68	3.52	3.23	1.53
CAO	0.62	0.43	1.30	0.14	0.28	0.30
NA2O	4.27	2.44	3.46	2.60	0.21	4.87
K2O	2.07	1.59	2.53	1.18	6.80	0.72
TI02	0.27	0.26	0.27	0.24	0.46	0.25
P2O5	0.01	0.00	0.00	0.02	0.05	0.01
CR203	0.00	0.00	0.00	0.00	0.00	0.00
LOI	0.00	0.00	0.00	0.00	0.00	0.00
TOTAL	100.17	100.67	98.22	98.74	96.72	98.09
S	0.00	0.01	0.00	0.00	0.00	0.00
BA	352.00	197.00	546.00	273.00	1237.00	162.00
CR	19.00	29.00	25.00	30.00	23.00	23.00
ZR	289.00	282.00	294.00	271.00	508.00	272.00
SR	19.00	12.00	58.00	12.00	4.00	29.00
RB	24.00	29.00	44.00	20.00	124.00	8.00
Y	61.00	57.00	64.00	56.00	103.00	59.00
NB	6.00	6.00	8.00	9.00	17.00	7.00
ZN	111.00	82.00	59.00	54.00	83.00	90.00
NI	0.00	0.00	0.00	12.00	0.00	0.00

TABLE G.1

## AMULET FORMATION; LOWER MEMBER; #3 FLOW; FELDSPAR PORPHYRITIC RHYOLITE

	81-116	81-134	81-138	81-165	81-166	81-167
SAMP NO.->	PA05055	PA05056	PA05057	PA05058	PA05059	PA05060
SI02	75.62	75.15	77.78	74.56	73.99	78.42
AL203	12.11	12.28	10.94	11.49	10.45	8.93
FE203	4.58	4.07	2.48	3.91	7.15	3.79
MNO	0.10	0.09	0.06	0.10	0.10	0.10
MGO	2.25	1.50	0.55	1.19	3.51	2.82
CAO	0.37	0.79	0.63	0.88	0.08	0.19
NA2O	4.44	4.79	4.01	5.50	0.21	2.73
K2O	0.69	0.92	2.05	0.10	1.88	0.43
TI02	0.28	0.27	0.24	0.25	0.23	0.17
F2O5	0.04	0.00	0.01	0.00	0.00	0.00
CR203	0.00	0.00	0.00	0.00	0.00	0.00
LOI	0.00	0.00	0.00	0.00	0.00	0.00
TOTAL	100.48	99.86	98.75	97.98	97.60	97.60
S	0.00	0.05	0.00	0.01	0.03	0.00
BA	222.00	236.00	541.00	76.00	518.00	133.00
CR	22.00	28.00	22.00	26.00	30.00	24.00
ZR	224.00	299.00	261.00	275.00	254.00	209.00
SR	26.00	29.00	23.00	27.00	0.00	6.00
RB	10.00	11.00	20.00	0.00	28.00	3.00
Y	41.00	60.00	56.00	52.00	42.00	47.00
NB	8.00	8.00	7.00	6.00	11.00	5.00
ZN	60.00	96.00	111.00	104.00	1980.00	99.00
NI	0.00	0.00	0.00	3.00	0.00	0.00
	81-170	81-171	81-172	82-181	82-182	82-88
SAMP NO.->	PA05061	PA05062	PA05063	PA05064	PA05065	PA05066
SI02	75.05	71.29	74.06	59.50	75.23	74.23
AL203	11.74	11.68	11.50	13.43	10.62	12.11
FE203	3.55	7.97	4.33	8.71	4.40	5.40
MNO	0.05	0.16	0.10	0.13	0.09	0.09
MGO	3.90	3.65	3.30	4.46	2.11	2.35
CAO	0.29	0.19	0.29	6.30	0.30	0.55
NA2O	0.97	1.84	4.52	4.06	2.41	3.83
K2O	3.13	1.25	0.10	0.53	2.44	0.97
TI02	0.25	0.25	0.25	0.92	0.22	0.30
F2O5	0.02	0.02	0.00	0.03	0.00	0.00
CR203	0.00	0.00	0.00	0.00	0.00	0.00
LOI	0.00	0.00	0.00	0.00	0.00	0.00
TOTAL	98.95	98.30	98.45	98.07	97.82	99.83
S	0.00	0.01	0.00	0.01	0.03	0.01
BA	525.00	359.00	66.00	111.00	720.00	140.00
CR	28.00	28.00	21.00	70.00	30.00	24.00
ZR	275.00	268.00	271.00	81.00	246.00	325.00
SR	10.00	5.00	9.00	83.00	38.00	27.00
RB	36.00	15.00	0.00	8.00	37.00	16.00
Y	65.00	71.00	58.00	23.00	56.00	62.00
NB	8.00	3.00	8.00	0.00	6.00	11.00
ZN	59.00	223.00	199.00	66.00	57.00	96.00
NI	0.00	0.00	0.00	28.00	0.00	0.00

TABLE G.1

## AMULET FORMATION; LOWER MEMBER; #3 FLOW; FELDSPAR PORPHYRITIC RHYOLITE

SAMP NO.->	82-193 PA05079	82-194 PA05080	82-198 PA05081	82-200 PA05082	82-201 PA05083
SI02	73.32	72.54	73.55	75.32	72.34
AL203	12.88	12.62	11.07	9.84	11.75
FE203	3.41	4.92	4.62	4.59	5.22
MNO	0.13	0.13	0.07	0.08	0.09
MGO	1.31	1.68	3.48	3.57	3.15
CAO	0.46	0.35	0.20	0.34	0.24
NA2O	4.41	3.09	0.49	2.92	0.21
K2O	1.84	2.12	2.47	0.65	3.12
TI02	0.28	0.27	0.23	0.21	0.24
P2O5	0.01	0.00	0.01	0.01	0.01
CR203	0.00	0.00	0.00	0.00	0.00
LOI	0.00	0.00	0.00	0.00	0.00
TOTAL	98.05	97.72	96.19	97.53	96.37
S	0.01	0.01	0.00	0.01	0.00
BA	410.00	478.00	518.00	159.00	482.00
CR	23.00	26.00	26.00	20.00	26.00
ZR	305.00	301.00	266.00	225.00	268.00
SR	49.00	29.00	6.00	23.00	11.00
RE	31.00	36.00	35.00	6.00	55.00
Y	69.00	66.00	60.00	61.00	56.00
NB	7.00	7.00	6.00	8.00	9.00
ZN	73.00	100.00	78.00	68.00	83.00
NI	1.00	0.00	0.00	0.00	0.00

## AMULET FORMATION; UPPER MEMBER; BEDFORD FLOW; FELDSPAR PORPHYRITIC RHYOLITE

SAMP NO.->	82-80 PA05090	82-144 PA05091	Nor 74 PA05092	Nor 75 PA05093	Nor 79 PA05094	Nor 80 PA05095
SiO2	73.57	70.92	72.40	72.60	79.08	72.21
AL2O3	11.61	12.10	11.70	12.20	11.37	10.75
FE2O3	4.09	5.86	6.30	4.75	4.93	1.78
MNO	0.08	0.11	0.11	0.10	0.06	0.07
MGO	2.95	0.60	2.46	2.97	1.91	1.27
CAO	0.28	4.58	0.18	0.22	0.29	1.56
NA2O	2.55	2.88	0.09	1.31	0.00	2.42
K2O	1.34	0.57	2.85	2.54	1.93	2.68
TiO2	0.25	0.54	0.28	0.30	0.26	0.25
P2O5	0.00	0.04	0.04	0.05	0.06	0.08
CR2O3	0.00	0.00	0.00	0.00	0.00	0.00
LOI	0.00	0.00	2.70	2.51	2.02	1.97
TOTAL	96.72	98.20	99.11	99.55	101.91	95.04
S	0.00	0.00	0.00	0.00	0.00	0.00
BA	293.00	94.00	0.00	0.00	0.00	0.00
CR	23.00	22.00	0.00	0.00	0.00	0.00
ZR	281.00	218.00	370.00	374.00	358.00	359.00
SR	11.00	257.00	4.00	13.00	34.00	26.00
RB	15.00	11.00	47.00	41.00	23.00	25.00
Y	58.00	49.00	55.00	65.00	55.00	55.00
NB	6.00	4.00	0.00	0.00	0.00	0.00
ZN	40.00	39.00	0.00	0.00	0.00	0.00
NI	0.00	2.00	0.00	0.00	0.00	0.00

AMULET FORMATION; UPPER MEMBER; F-SHAFT FLOW; FELDSPAR PORPHYRITIC RHYOLITE  
 =====

	83-175
SAMP NO.->	PA05096
-----	
SI02	77.80
AL203	11.10
FE203	1.72
MNO	0.06
MGO	0.42
CAO	1.42
NA2O	5.72
K2O	0.62
TI02	0.28
P2O5	0.05
CR203	0.00
LOI	0.23
-----	
TOTAL	99.42
S	0.00
BA	0.00
CR	0.00
ZR	210.00
SR	60.00
RE	10.00
Y	0.00
NB	0.00
ZN	0.00
NI	0.00

## MILLENBACH RHYOLITE FORMATION; QFP RHYOLITE FLOWS

SAMP NO.->	I-007	I-008	I-031	I-032
	PA05117	PA05118	PA05119	PA05120
SI02	70.31	74.67	73.69	75.18
AL203	11.12	11.80	11.76	11.07
FE203	3.05	3.25	3.88	3.44
MNO	0.10	0.10	0.11	0.10
MGO	1.46	1.54	1.79	1.41
CAO	0.34	0.35	0.38	0.49
NA2O	4.17	4.15	3.18	3.45
K2O	0.79	0.82	1.33	1.24
TI02	0.22	0.23	0.29	0.25
P2O5	0.03	0.01	0.03	0.03
CR203	0.00	0.00	0.00	0.00
LOI	0.00	0.00	0.00	0.00
TOTAL	91.59	96.92	96.44	96.66
S	0.09	0.11	0.04	0.04
BA	274.00	288.00	257.00	291.00
CR	17.00	26.00	29.00	34.00
ZR	186.00	190.00	183.00	173.00
SR	20.00	22.00	16.00	17.00
RE	8.00	12.00	28.00	25.00
Y	46.00	49.00	47.00	45.00
NR	10.00	7.00	8.00	6.00
ZN	1179.00	1316.00	1196.00	1393.00
NI	7.00	6.00	2.00	3.00



## MILLENBACH RHYOLITE FORMATION; K FLOW; FELDSPAR PORPHYRITIC RHYOLITE

SAMP NO.-->	80-52 PA05097	80-56 PA05098
SI02	67.64	67.19
AL203	12.76	13.57
FE203	8.91	4.99
MNO	0.13	0.06
MGO	1.79	2.31
CAO	1.34	3.09
NA2O	3.55	4.34
K2O	0.47	0.92
TI02	0.62	0.44
P2O5	0.16	0.02
CR203	0.00	0.00
LOI	0.00	0.00
TOTAL	97.37	96.93
S	0.00	0.00
BA	162.00	301.00
CR	25.00	25.00
ZR	213.00	248.00
SR	82.00	108.00
RB	5.00	14.00
Y	38.00	66.00
NB	7.00	6.00
ZN	104.00	55.00
NI	0.00	4.00



## WAITE RHYOLITE FORMATION; FELDSPAR PORPHYRITIC RHYOLITE

-----  
TS-13  
SAMP NO.-> PA05111  
-----

SI02	76.00
AL203	11.50
FE203	2.49
MNO	0.05
MGO	0.81
CAO	2.63
NA2O	4.97
K2O	0.25
TIO2	0.23
P2O5	0.03
CR2O3	0.00
LOI	0.85

-----  
TOTAL 99.81

S	0.00
BA	0.00
CR	0.00
ZR	0.00
SR	0.00
RB	0.00
Y	0.00
NB	0.00
ZN	0.00
NI	0.00
	0.00
	0.00
	0.00
	0.00
	0.00

## BEECHAM BRECCIA

SAMP NO. ->	Nor 73	Nor 77			
	PA05121	PA05122			
SI02	69.70	71.90			
AL203	12.10	11.80			
FE203	6.47	5.37			
MNO	0.15	0.09			
MGO	2.45	1.87			
CAO	0.82	0.39			
NA2O	2.43	2.26			
K2O	2.46	3.39			
TI02	0.47	0.47			
P205	0.11	0.10			
CR203	0.00	0.00			
LOI	2.08	1.54			
TOTAL	99.24	99.18			
S	0.00	0.00			
BA	0.00	0.00			
CR	0.00	0.00			
ZR	294.00	297.00			
SR	40.00	44.00			
RB	27.00	32.00			
Y	56.00	49.00			
NB	0.00	0.00			
ZN	0.00	0.00			
NI	0.00	0.00			

## FLAVRIAN FORMATION

SAMP NO.->	=====					
	82-74 PA05242	82-174 PA05243	83-170 PA05244	83-239 PA05245	21505 PA05246	21510 PA05247
SI02	59.10	55.47	52.40	67.40	54.00	54.80
AL203	15.61	16.39	14.90	14.80	16.90	15.50
FE203	7.11	10.02	12.30	4.96	10.04	8.33
MNO	0.19	0.17	0.21	0.08	0.22	0.24
MGO	5.10	6.23	6.01	3.70	8.46	4.52
CAO	3.94	3.68	6.76	2.65	1.03	4.51
NA20	5.99	4.80	3.42	4.14	4.12	5.31
K20	0.40	0.08	0.32	0.78	0.11	0.11
TI02	0.98	1.08	1.60	1.06	1.03	0.92
P205	0.08	0.09	0.18	0.13	0.15	0.11
CR203	0.00	0.00	0.00	0.00	0.00	0.00
LOI	0.00	0.00	0.93	2.31	4.38	4.46
TOTAL	98.50	98.01	99.03	102.01	100.44	98.81
S	0.00	0.01	0.00	0.00	0.00	0.00
BA	207.00	33.00	0.00	0.00	0.00	0.00
CR	101.00	107.00	30.00	20.00	0.00	0.00
ZR	100.00	100.00	80.00	150.00	0.00	0.00
SR	111.00	136.00	130.00	190.00	0.00	0.00
RB	3.00	0.00	20.00	20.00	0.00	0.00
Y	23.00	22.00	0.00	0.00	0.00	0.00
NB	0.00	4.00	0.00	0.00	0.00	0.00
ZN	40.00	32.00	0.00	0.00	0.00	0.00
NI	61.00	76.00	0.00	0.00	0.00	0.00

## FLAVRIAN FORMATION

SAMP NO.->	=====					
	21519 PA05248	21532 PA05249	21537 PA05250	21543 PA05251	21547 PA05252	21549 PA05253
SI02	56.10	53.90	53.90	55.90	56.40	55.60
AL203	15.10	16.50	15.90	15.00	16.00	14.70
FE203	8.70	9.91	11.40	11.87	9.97	12.09
MNO	0.19	0.34	0.21	0.34	0.19	0.45
MGO	6.74	5.57	4.89	4.14	5.36	4.57
CAO	2.37	2.37	2.18	3.92	3.12	4.19
NA20	4.05	4.48	5.00	5.91	5.44	4.39
K20	0.31	0.23	0.07	0.10	0.46	0.23
TI02	0.89	1.00	1.88	1.83	1.09	1.66
P205	0.12	0.14	0.31	0.21	0.15	0.19
CR203	0.00	0.00	0.00	0.00	0.00	0.00
LOI	3.92	3.08	2.92	0.85	1.77	1.69
TOTAL	98.49	97.52	98.66	100.07	99.95	99.76
S	0.00	0.00	0.00	0.00	0.00	0.00
BA	0.00	0.00	0.00	0.00	0.00	0.00
CR	0.00	0.00	0.00	0.00	0.00	0.00
ZR	0.00	0.00	0.00	0.00	0.00	0.00
SR	0.00	0.00	0.00	0.00	0.00	0.00
RB	0.00	0.00	0.00	0.00	0.00	0.00
Y	0.00	0.00	0.00	0.00	0.00	0.00
NB	0.00	0.00	0.00	0.00	0.00	0.00
ZN	0.00	0.00	0.00	0.00	0.00	0.00
NI	0.00	0.00	0.00	0.00	0.00	0.00

## FLAVRIAN FORMATION

SAMP NO.->	21553	21554	21555	21570	21571
	PA05254	PA05255	PA05256	PA05257	PA05258
SI02	58.50	56.70	61.60	50.90	50.70
AL203	15.30	14.60	14.40	17.40	15.50
FE203	10.92	11.08	8.26	10.53	14.76
MNO	0.22	0.35	0.19	0.30	0.43
MGO	4.73	4.41	4.32	6.97	4.76
CAO	4.04	2.94	4.12	3.36	5.09
NA2O	4.92	4.96	4.07	4.14	5.05
K2O	0.13	0.05	0.81	0.15	0.11
TI02	1.00	1.75	0.71	1.23	1.76
F2O5	0.15	0.24	0.09	0.17	0.20
CR2O3	0.00	0.00	0.00	0.00	0.00
LOI	0.23	1.85	1.62	3.85	2.00
TOTAL	100.14	98.93	100.19	99.00	100.36
S	0.00	0.00	0.00	0.00	0.00
BA	0.00	0.00	0.00	0.00	0.00
CR	0.00	0.00	0.00	0.00	0.00
ZR	0.00	0.00	0.00	0.00	0.00
SR	0.00	0.00	0.00	0.00	0.00
RB	0.00	0.00	0.00	0.00	0.00
Y	0.00	0.00	0.00	0.00	0.00
NB	0.00	0.00	0.00	0.00	0.00
ZN	0.00	0.00	0.00	0.00	0.00
NI	0.00	0.00	0.00	0.00	0.00

TABLE G.1

## RUSTY RIDGE FORMATION

SAMP	81-113	81-183	81-184	81-185	81-186	81-191
SiO <sub>2</sub>	56.67	67.92	60.00	49.32	71.99	58.70
Al <sub>2</sub> O <sub>3</sub>	15.49	13.46	14.71	16.43	11.00	12.65
Fe <sub>2</sub> O <sub>3</sub>	11.66	4.22	9.31	10.93	4.13	11.13
MnO	0.26	0.08	0.13	0.17	0.07	0.21
MgO	4.62	2.35	5.35	7.21	3.62	6.92
CaO	6.46	2.63	2.63	8.39	2.16	4.99
Na <sub>2</sub> O	4.62	6.04	5.55	4.05	4.10	4.72
K <sub>2</sub> O	0.23	0.60	0.35	0.15	0.04	0.05
TiO <sub>2</sub>	1.44	1.24	1.32	1.06	0.79	1.24
P <sub>2</sub> O <sub>5</sub>	0.09	0.33	0.35	0.03	0.09	0.15
CR203						
LO.I.						
TOTAL	101.64	98.93	99.76	97.83	98.04	100.82
S	0.00	0.00	0.00	0.00	0.00	0.00
BA HM	171.	250.	103.	245.	51.	81.
CR	44.	35.	39.	82.	53.	69.
ZR	106.	117.	121.	104.	79.	125.
SR	241.	57.	39.	208.	74.	48.
RB	0.	4.	0.	0.	0.	0.
Y	31.	35.	40.	36.	24.	35.
NB	0.	2.	0.	3.	2.	1.
ZN	185.	38.	108.	93.	48.	107.
NI	0.	4.	0.	17.	5.	84.

TABLE G.1

## RUSTY RIDGE FORMATION; ANDESITE

SAMP NO.->	81-193	81-194	81-197	81-198	81-201	81-202
	PA05265	PA05266	PA05267	PA05268	PA05269	PA05270
SI02	56.77	58.21	54.90	62.88	63.71	57.19
AL203	14.96	14.64	15.69	14.29	13.07	14.65
FE203	10.21	9.60	9.71	8.58	10.39	9.59
MNO	0.18	0.13	0.14	0.09	0.08	0.16
MGO	4.95	5.51	6.26	4.95	3.51	5.25
CAO	6.27	5.50	4.96	4.02	1.84	5.58
NA20	4.21	4.01	5.21	4.59	5.32	4.29
K20	0.08	0.09	0.25	0.15	0.11	0.05
TI02	1.26	1.17	1.17	1.03	0.91	1.27
P205	0.09	0.10	0.12	0.19	0.13	0.11
CR203	0.00	0.00	0.00	0.00	0.00	0.00
LOI	0.00	0.00	0.00	0.00	0.00	0.00
TOTAL	98.98	98.96	98.41	100.77	99.07	98.14
S	0.00	0.00	0.00	0.04	0.02	0.01
BA	96.00	67.00	120.00	86.00	78.00	39.00
CR	55.00	63.00	67.00	67.00	70.00	55.00
ZR	123.00	122.00	121.00	105.00	90.00	133.00
SR	164.00	142.00	103.00	116.00	84.00	148.00
RB	0.00	0.00	0.00	0.00	0.00	0.00
Y	33.00	31.00	34.00	26.00	21.00	41.00
NB	3.00	6.00	0.00	4.00	3.00	3.00
ZN	142.00	70.00	91.00	80.00	62.00	98.00
NI	12.00	6.00	10.00	12.00	0.00	10.00
SAMP NO.->	81-203	81-204	82-84	82-87	82-88	82-94
	PA05271	PA05272	PA05273	PA05274	PA05275	PA05276
SI02	64.06	62.52	62.93	57.95	57.42	66.05
AL203	13.70	14.72	14.51	14.56	15.60	14.10
FE203	8.29	6.88	8.56	8.42	8.81	7.15
MNO	0.13	0.16	0.11	0.09	0.15	0.10
MGO	4.91	2.18	3.13	0.00	2.85	2.91
CAO	2.65	6.93	2.86	15.08	5.37	1.86
NA20	5.51	4.46	5.01	0.20	4.50	5.18
K20	0.03	0.90	0.29	0.02	0.07	0.05
TI02	1.33	1.36	1.30	1.13	1.46	0.74
P205	0.24	0.35	0.24	0.00	0.23	0.20
CR203	0.00	0.00	0.00	0.00	0.00	0.00
LOI	0.00	0.00	0.00	0.00	0.00	0.00
TOTAL	100.85	100.46	98.94	97.45	96.46	98.34
S	0.00	0.01	0.07	0.01	0.01	0.00
BA	72.00	170.00	101.00	0.00	30.00	78.00
CR	44.00	27.00	38.00	34.00	45.00	32.00
ZR	132.00	155.00	110.00	99.00	131.00	150.00
SR	48.00	83.00	69.00	393.00	129.00	58.00
RB	0.00	9.00	0.00	0.00	0.00	0.00
Y	37.00	42.00	32.00	27.00	37.00	45.00
NB	3.00	3.00	1.00	4.00	2.00	4.00
ZN	82.00	82.00	103.00	1.00	91.00	42.00
NI	9.00	3.00	0.00	0.00	1.00	1.00



TABLE G.1

RUSTY RIDGE FORMATION; ANDESITE						
SAMP NO. ->	82-101 PA05277	82-106 PA05278	82-111 PA05279	82-120 PA05280	82-121 PA05281	82-178 PA05282
SI02	56.06	56.65	56.92	55.89	55.92	55.11
AL203	14.60	15.75	15.61	14.74	14.87	13.72
FE203	15.28	9.81	7.74	11.54	11.93	12.68
MNO	0.20	0.17	0.11	0.26	0.26	0.21
MGO	4.11	4.51	5.65	3.34	3.43	4.30
CAO	2.31	4.06	3.92	6.31	5.12	7.10
NA2O	3.09	5.20	5.55	4.70	4.69	3.16
K2O	0.04	0.64	0.48	0.05	0.07	0.04
TI02	1.35	1.41	1.17	1.52	1.55	1.59
P2O5	0.17	0.26	0.14	0.10	0.18	0.10
CR203	0.00	0.00	0.00	0.00	0.00	0.00
LOI	0.00	0.00	0.00	0.00	0.00	0.00
TOTAL	97.21	98.46	97.29	98.45	98.02	98.01
S	0.00	0.03	0.05	0.05	0.02	0.00
BA	0.00	120.00	121.00	0.00	38.00	0.00
CR	45.00	35.00	117.00	43.00	39.00	54.00
ZR	130.00	128.00	115.00	93.00	98.00	92.00
SR	24.00	90.00	53.00	80.00	74.00	144.00
RB	0.00	8.00	9.00	0.00	0.00	0.00
Y	32.00	39.00	28.00	28.00	29.00	28.00
NB	3.00	3.00	0.00	0.00	2.00	4.00
ZN	85.00	89.00	96.00	62.00	234.00	59.00
NI	4.00	0.00	50.00	0.00	0.00	32.00
SAMP NO. ->	83-5 PA05283	83-6 PA05284	83-7 PA05285	83-17 PA05286	83-53 PA05287	83-56 PA05288
SI02	52.80	54.00	54.10	50.40	53.90	56.60
AL203	14.60	14.40	15.80	13.80	15.80	14.40
FE203	12.20	11.50	8.58	19.30	8.67	9.27
MNO	0.27	0.25	0.29	0.37	0.18	0.13
MGO	4.95	3.63	4.60	6.14	4.93	6.52
CAO	4.74	5.65	4.54	0.71	5.49	3.39
NA2O	3.98	4.36	5.20	0.01	5.47	3.53
K2O	1.00	0.28	1.75	0.69	0.66	0.83
TI02	1.62	1.56	1.28	1.70	1.33	1.14
P2O5	0.19	0.20	0.21	0.18	0.21	0.14
CR203	0.00	0.00	0.00	0.00	0.00	0.00
LOI	2.47	2.70	1.77	5.08	1.77	2.39
TOTAL	98.82	98.53	98.12	98.38	98.41	98.34
S	0.00	0.00	0.00	0.00	0.00	0.00
BA	0.00	0.00	0.00	0.00	0.00	0.00
CR	50.00	20.00	110.00	50.00	90.00	50.00
ZR	120.00	90.00	140.00	110.00	140.00	110.00
SR	60.00	50.00	40.00	< 10.00	50.00	110.00
RB	40.00	< 10.00	30.00	20.00	< 10.00	20.00
Y	0.00	0.00	0.00	0.00	0.00	0.00
NB	0.00	0.00	0.00	0.00	0.00	0.00
ZN	0.00	0.00	0.00	0.00	0.00	0.00
NI	0.00	0.00	0.00	0.00	0.00	0.00





## RUSTY RIDGE FORMATION; ANDESITE

SAMP NO.->	Nor 67	Nor 68	Nor 71
	PA05313	PA05314	PA05315
SI02	56.50	64.79	67.02
AL203	14.60	13.87	13.11
FE203	9.39	7.12	4.68
MNO	0.13	0.11	0.08
MGO	4.68	4.34	3.26
CAO	5.18	1.86	2.11
NA2O	4.10	2.02	2.97
K2O	0.44	1.81	1.31
TIO2	1.34	0.95	0.74
P2O5	0.19	0.15	0.05
CR203	0.00	0.00	0.00
LOI	4.15	4.56	3.27
TOTAL	100.70	101.58	98.60
S	0.00	0.00	0.00
BA	0.00	0.00	0.00
CR	0.00	0.00	0.00
ZR	171.00	208.00	186.00
SR	103.00	110.00	43.00
RB	4.00	146.00	17.00
Y	37.00	45.00	42.00
NB	0.00	0.00	0.00
ZN	0.00	0.00	0.00
NI	0.00	0.00	0.00

TABLE G.1

## MILLENBACH ANDESITE FORMATION

SAMP	80-34	82-13	81-18	81-27	82-40	81-22
SiO <sub>2</sub>	64.55	55.40	57.22	64.85	57.82	63.6
Al <sub>2</sub> O <sub>3</sub>	14.20	16.98	15.79	14.50	14.24	14.5
Fe <sub>2</sub> O <sub>3</sub>	5.85	8.63	10.49	8.67	8.31	7.3
MnO	0.11	0.17	0.21	0.19	0.13	0.19
MgO	5.11	4.02	7.93	3.24	3.64	2.14
CaO	4.22	6.91	3.67	2.80	7.66	3.20
Na <sub>2</sub> O	4.17	5.19	5.21	5.58	3.93	5.48
K <sub>2</sub> O	0.04	0.83	0.85	0.26	1.64	0.41
TiO <sub>2</sub>	1.04	1.30	1.12	1.07	1.00	0.98
P <sub>2</sub> O <sub>5</sub>	0.09	0.07	0.15	0.48	0.02	0.32
CR2O3						
LO. I.						
TOTAL	99.46	99.60	102.77	101.75	96.47	98.12
S	0.0	0.00	0.00	0.00	0.00	-
BA HM	127	146.	265.	49.	234.	-
CR	53.	76.	77	28.	64.	20.
ZR	134.	114..	98.	187.	86.	180.
SR	214.	153.	54.	85.	116.	70
RB	0.	13.	12.	0.	22.	50
Y	35.	28.	24.	44.	23.	-
NB	1.	5.	5.	6.	1.	-
ZN	50.	120.	562.	414.	56.	-
NI	35.	39.	47.	0.	29.	-

TABLE G.1

## MILLENBACH ANDESITE FORMATION

SAMP	BH-9	S-92	S-93	S-94	S-95	S-96
SiO <sub>2</sub>	61.4	57.18	60.35	62.28	56.10	60.40
Al <sub>2</sub> O <sub>3</sub>	12.2	15.59	15.41	14.57	16.82	15.13
Fe <sub>2</sub> O <sub>3</sub>	14.7	8.98	8.2	7.7	8.4	8.13
MnO	0.01	0.15	0.17	0.13	0.16	0.18
MgO	4.78	4.6	4.31	3.83	4.61	3.69
CaO	0.65	6.0	3.64	4.27	6.77	5.36
Na <sub>2</sub> O	0.19	5.4	4.24	4.72	4.96	4.96
K <sub>2</sub> O	0.83	0.46	1.86	1.33	0.75	0.28
TiO <sub>2</sub>	1.02	1.18	1.21	1.14	1.08	1.84
P <sub>2</sub> O <sub>5</sub>	0.13	-	-	-	-	-
CR2O3						
LO.I.						
TOTAL	96.07	99.54	99.39	99.97	99.65	99.97
S	0.01					
BA HM	360.					
CR	26.					
ZR	103					
SR	1.					
RB	13.					
Y	24.					
NB	-					
ZN	160.					
NI	-					

TABLE G.1

## WAITE ANDESITE FORMATION

SAMP NO.->	=====					
	83-28 FA05330	83-85 FA05331	83-88 FA05332	83-210 FA05333	83-211 FA05334	83-212 FA05335
SI02	57.00	74.50	57.90	57.70	54.00	77.10
AL203	15.10	11.10	15.00	16.20	17.20	9.65
FE203	7.79	3.32	8.37	10.10	6.89	2.70
MNO	0.11	0.06	0.13	0.18	0.15	0.05
MGO	3.51	0.57	3.89	2.42	0.63	0.59
CAO	7.33	3.03	5.71	2.86	17.70	3.57
NA2O	4.67	4.85	4.91	5.15	< 0.01	3.57
K2O	0.27	0.25	0.46	0.71	0.13	0.13
TI02	0.95	1.05	0.97	1.10	0.79	0.88
P2O5	0.12	0.36	0.12	0.37	0.30	0.29
CR2O3	0.00	0.00	0.00	0.00	0.00	0.00
LOI	1.31	0.70	1.77	2.00	2.39	0.85
TOTAL	98.16	99.79	99.23	98.79	100.19	99.38
S	0.00	0.00	0.00	0.00	0.00	0.00
BA	0.00	0.00	0.00	0.00	0.00	0.00
CR	40.00	20.00	40.00	20.00	< 10.00	10.00
ZR	80.00	140.00	100.00	220.00	130.00	180.00
SR	170.00	150.00	70.00	110.00	220.00	100.00
RB	10.00	20.00	< 10.00	20.00	< 10.00	10.00
Y	0.00	0.00	0.00	0.00	0.00	0.00
NB	0.00	0.00	0.00	0.00	0.00	0.00
ZN	0.00	0.00	0.00	0.00	0.00	0.00
NI	0.00	0.00	0.00	0.00	0.00	0.00

## WAITE ANDESITE FORMATION

SAMP NO.->	=====	
	83-242 FA05342	83-233 FA05343
SI02	59.90	58.50
AL203	16.40	14.30
FE203	7.93	8.78
MNO	0.10	0.19
MGO	2.16	6.40
CAO	3.05	3.42
NA2O	5.31	5.38
K2O	1.38	0.17
TI02	1.21	1.17
P2O5	0.42	0.15
CR2O3	0.00	0.00
LOI	1.77	0.23
TOTAL	99.63	98.69
S	0.00	0.00
BA	0.00	0.00
CR	30.00	40.00
ZR	210.00	110.00
SR	50.00	40.00
RB	30.00	30.00
Y	0.00	0.00
NB	0.00	0.00
ZN	0.00	0.00
NI	0.00	0.00

TABLE G.1

## WAITE ANDESITE FORMATION

SAMP	83-214	83-217	83-218	83-221	83-222	83-241
SiO <sub>2</sub>	62.7	52.0	74.6	58.3	65.9	76.0
Al <sub>2</sub> O <sub>3</sub>	13.5	18.1	7.50	15.1	14.3	9.95
Fe <sub>2</sub> O <sub>3</sub>	7.55	9.90	4.67	9.54	5.86	3.60
MnO	0.13	0.15	0.09	0.17	0.10	0.50
MgO	3.88	3.66	1.44	3.62	1.41	0.95
CaO	4.68	6.60	8.77	3.72	3.57	2.33
Na <sub>2</sub> O	4.03	4.18	0.05	3.96	5.81	4.07
K <sub>2</sub> O	1.06	1.07	0.05	1.01	0.21	0.22
TiO <sub>2</sub>	1.02	1.33	0.97	1.25	1.07	0.81
P <sub>2</sub> O <sub>5</sub>	0.13	0.27	0.20	0.24	0.36	0.28
CR2O3						
LO.I.	1.70	2.23	0.77	2.08	1.08	0.93
TOTAL	100.4	99.5	99.1	99.0	99.7	99.2
S						
BA HM						
CR	50	20	10	20	20	20
ZR	100	150	110	150	170	130
SR	80	190	150	130	110	70
RB	<10	30	<10	30	10	10
Y						
NB						
ZN						
NI						



## ANDESITE BETWEEN RHYOLITE FLOWS OF THE MILLENBACH RHYOLITE FORMATION

I-018	
SAMP NO.->	PA05344
SI02	62.45
AL203	14.22
FE203	6.42
MNO	0.14
MGO	3.49
CAO	2.31
NA2O	4.86
K2O	0.85
TI02	0.97
P2O5	0.11
CR203	0.00
LOI	0.00
TOTAL	95.82
S	0.05
BA	404.00
CR	116.00
ZR	137.00
SR	47.00
RB	8.00
Y	29.00
NB	9.00
ZN	165.00
NI	16.00

TABLE G.1

## AMULET ANDESITE FORMATION

SAMP NO.->	v501	V503	ReA3	WH2	WH3	WH4
	PA05345	PA05346	PA05347	PA05348	PA05349	PA05350
SI02	55.30	53.62	55.49	56.16	59.07	55.56
AL203	17.21	16.12	15.37	16.80	15.35	16.52
FE203	10.40	11.25	9.17	7.53	7.28	7.44
MNO	0.19	0.18	0.20	0.14	0.19	0.14
MGO	5.87	4.77	4.08	3.77	3.53	4.54
CAO	5.21	6.67	8.86	11.64	9.47	12.37
NA2O	3.51	5.02	2.80	2.52	3.32	2.88
K2O	0.91	1.00	0.63	0.44	0.87	0.93
TI02	1.25	1.64	0.96	1.23	1.30	1.17
P2O5	0.00	0.00	0.00	0.00	0.00	0.00
CR203	0.00	0.00	0.00	0.00	0.00	0.00
LOI	2.93	1.58	1.22	1.64	1.40	1.40
TOTAL	102.78	101.85	100.78	101.87	101.78	102.95
S	0.00	0.00	0.00	0.00	0.00	0.00
BA	0.00	0.00	0.00	0.00	0.00	0.00
CR	0.00	0.00	0.00	0.00	0.00	0.00
ZR	0.00	0.00	0.00	0.00	0.00	0.00
SR	0.00	0.00	0.00	0.00	0.00	0.00
RB	0.00	0.00	0.00	0.00	0.00	0.00
Y	0.00	0.00	0.00	0.00	0.00	0.00
NB	0.00	0.00	0.00	0.00	0.00	0.00
ZN	0.00	0.00	0.00	0.00	0.00	0.00
NI	0.00	0.00	0.00	0.00	0.00	0.00

## AMULET ANDESITE FORMATION

SAMP NO.->	WH6	WH9	WH24
	PA05351	PA05352	PA05353
SI02	61.21	57.40	55.59
AL203	15.83	14.40	16.09
FE203	6.75	8.50	8.18
MNO	0.11	0.22	0.17
MGO	2.03	5.42	4.65
CAO	10.05	6.64	11.17
NA2O	1.87	4.88	1.94
K2O	1.14	0.90	1.11
TI02	0.89	1.39	1.15
P2O5	0.00	0.00	0.00
CR203	0.00	0.00	0.00
LOI	1.50	1.64	0.80
TOTAL	101.38	101.39	100.85
S	0.00	0.00	0.00
BA	0.00	0.00	0.00
CR	0.00	0.00	0.00
ZR	0.00	0.00	0.00
SR	0.00	0.00	0.00
RB	0.00	0.00	0.00
Y	0.00	0.00	0.00
NB	0.00	0.00	0.00
ZN	0.00	0.00	0.00
NI	0.00	0.00	0.00

TABLE G.1

## AMULET UPPER MEMBER

SAMP	79-30	79-31	79-34	80-63	82-73	82-78
SiO <sub>2</sub>	70.90	72.40	69.94	67.45	72.53	74.49
Al <sub>2</sub> O <sub>3</sub>	10.68	11.59	13.97	13.03	11.38	11.53
Fe <sub>2</sub> O <sub>3</sub>	10.17	7.87	2.92	3.15	9.47	4.13
MnO	0.10	0.08	0.05	0.08	0.21	0.11
MgO	4.88	4.31	2.21	3.77	1.37	2.26
CaO	0.32	0.18	3.79	3.16	0.08	1.11
Na <sub>2</sub> O	0.20	0.28	5.72	5.33	0.18	3.77
K <sub>2</sub> O	1.11	1.80	0.09	0.10	1.89	0.56
TiO <sub>2</sub>	0.39	0.41	0.47	0.48	0.24	0.24
P <sub>2</sub> O <sub>5</sub>	0.08	0.12	0.08	0.08	0.0	0.0
CR203						
LO.I.						
TOTAL	98.90	99.15	99.32	96.69	97.60	98.33
S	0.00	0.0	0.0	0.0	0.11	0.01
BA HM	268.	508.	82.	73.	475.	420.
CR	30.	30.	25.	30.	27.	25.
ZR	209.	225.	279.	248.	244.	267.
SR	1.	3.	157.	103.	0.	38.
RB	15.	29.	0.	0.	26.	4.
Y	57.	72.	68.	59.	47.	68.
NB	4.	4.	7.	4.	5.	5.
ZN	54.	57.	0.	45.	189.	38.
NI	0.	0.	0.	5.	12.	0.

TABLE G.1

## AMULET FORMATION; UPPER MEMBER; SILICIFIED FLOWS

SAMP NO. ->	79-4	79-26	80-6	80-18	80-22	80-23
	FA05123	FA05124	FA05125	FA05126	FA05127	FA05128
SI02	60.42	56.11	64.12	70.68	63.81	70.81
AL203	13.89	15.36	13.98	12.65	14.66	13.13
FE203	8.88	9.43	8.27	8.14	7.90	3.75
MNO	0.15	0.15	0.10	0.08	0.11	0.05
MGO	3.75	6.21	5.85	3.73	3.95	1.66
CAO	3.99	4.87	0.97	0.24	2.34	2.31
NA2O	4.56	6.17	3.61	0.15	5.07	5.39
K2O	0.02	0.04	0.50	2.17	0.03	0.03
TI02	0.96	1.11	1.32	0.52	1.10	0.67
P2O5	0.35	0.04	0.21	0.16	0.44	0.17
CR203	0.00	0.00	0.00	0.00	0.00	0.00
LOI	0.00	0.00	0.00	0.00	0.00	0.00
TOTAL	96.97	99.49	98.93	98.52	99.41	97.97
S	0.00	0.00	0.00	0.00	0.00	0.00
BA	12.00	42.00	176.00	844.00	56.00	53.00
CR	34.00	77.00	54.00	26.00	31.00	25.00
ZR	168.00	95.00	130.00	213.00	172.00	206.00
SR	101.00	122.00	56.00	4.00	108.00	138.00
RB	0.00	0.00	3.00	30.00	0.00	0.00
Y	42.00	25.00	48.00	27.00	43.00	38.00
NB	4.00	0.00	0.00	9.00	3.00	4.00
ZN	68.00	62.00	23.00	21.00	34.00	12.00
NI	0.00	37.00	18.00	0.00	0.00	31.00
SAMP NO. ->	80-27	80-29	80-35	80-66	80-67	80-69
	FA05129	FA05130	FA05131	FA05132	FA05133	FA05134
SI02	68.15	59.31	57.35	64.49	63.15	68.64
AL203	12.33	15.34	16.07	13.90	14.61	13.85
FE203	6.23	8.68	8.99	6.86	6.74	5.68
MNO	0.13	0.13	0.15	0.09	0.15	0.06
MGO	4.09	4.90	6.60	1.42	2.81	2.25
CAO	2.75	5.10	2.82	5.31	4.05	2.60
NA2O	4.27	4.33	4.75	4.13	5.33	4.44
K2O	0.06	0.11	0.04	0.02	0.03	0.18
TI02	0.90	1.18	1.14	0.86	1.06	0.85
P2O5	0.15	0.13	0.17	0.24	0.39	0.29
CR203	0.00	0.00	0.00	0.00	0.00	0.00
LOI	0.00	0.00	0.00	0.00	0.00	0.00
TOTAL	99.06	99.21	98.08	97.32	98.32	98.84
S	0.00	0.00	0.00	0.00	0.00	0.00
BA	78.00	56.00	91.00	26.00	77.00	135.00
CR	46.00	42.00	60.00	29.00	25.00	25.00
ZR	146.00	118.00	137.00	174.00	176.00	192.00
SR	120.00	186.00	206.00	209.00	178.00	167.00
RB	0.00	0.00	0.00	0.00	0.00	0.00
Y	29.00	28.00	24.00	27.00	49.00	34.00
NB	5.00	2.00	3.00	7.00	3.00	7.00
ZN	46.00	24.00	61.00	21.00	37.00	20.00
NI	34.00	9.00	39.00	0.00	0.00	0.00





TABLE G.1

## AMULET FORMATION; UPPER MEMBER; SILICIFIED FLOWS

SAMP NO.->	81-123	81-124	81-129	81-131	81-133	81-141
	PA05159	PA05160	PA05161	PA05162	PA05163	PA05164
SI02	71.24	67.65	67.98	69.20	67.16	65.66
AL203	12.36	14.49	14.10	13.49	13.79	13.93
FE203	3.71	7.59	6.90	6.89	9.07	6.71
MNO	0.11	0.13	0.12	0.12	0.11	0.08
MGO	1.81	2.57	4.48	3.34	2.40	2.99
CAO	2.93	2.01	1.17	2.03	2.27	2.19
NA2O	5.04	4.90	3.79	3.90	4.98	4.65
K2O	0.29	1.54	1.44	1.44	1.13	0.76
TI02	0.64	0.84	0.90	0.79	0.85	0.78
P2O5	0.18	0.27	0.35	0.22	0.28	0.24
CR203	0.00	0.00	0.00	0.00	0.00	0.00
LOI	0.00	0.00	0.00	0.00	0.00	0.00
TOTAL	98.31	101.99	101.23	101.42	101.04	97.99
S	0.00	0.00	0.00	0.00	0.00	0.00
BA	0.88	184.00	238.00	364.00	294.00	106.00
CR	23.00	24.00	29.00	30.00	22.00	28.00
ZR	198.00	205.00	186.00	219.00	201.00	198.00
SR	33.00	35.00	46.00	60.00	47.00	40.00
RB	0.00	22.00	18.00	19.00	8.00	7.00
Y	44.00	44.00	44.00	51.00	46.00	35.00
NB	5.00	5.00	2.00	6.00	5.00	7.00
ZN	79.00	75.00	135.00	89.00	74.00	81.00
NI	1.00	0.00	0.00	0.00	0.00	0.00
SAMP NO.->	81-142	81-143	81-147	81-150	81-152	81-156
	PA05165	PA05166	PA05167	PA05168	PA05169	PA05170
SI02	62.30	66.02	65.53	66.44	66.30	70.30
AL203	14.82	12.78	15.02	13.29	13.65	13.11
FE203	8.19	8.32	7.74	7.64	6.54	5.43
MNO	0.09	0.27	0.09	0.19	0.15	0.14
MGO	5.13	2.08	2.64	3.04	1.08	1.50
CAO	1.40	6.46	2.21	2.75	3.49	3.11
NA2O	2.89	4.39	4.79	3.66	5.38	4.35
K2O	1.70	0.25	1.93	1.25	0.55	0.88
TI02	1.10	0.93	1.10	0.75	0.88	0.72
P2O5	0.50	0.19	0.37	0.19	0.30	0.21
CR203	0.00	0.00	0.00	0.00	0.00	0.00
LOI	0.00	0.00	0.00	0.00	0.00	0.00
TOTAL	98.12	101.69	101.42	99.20	98.32	99.75
S	0.00	0.02	0.00	0.00	0.03	0.02
BA	157.00	83.00	167.00	101.00	112.00	121.00
CR	32.00	29.00	26.00	25.00	28.00	26.00
ZR	166.00	153.00	185.00	195.00	187.00	186.00
SR	39.00	82.00	29.00	28.00	71.00	52.00
RB	30.00	0.00	34.00	17.00	1.00	13.00
Y	45.00	44.00	50.00	46.00	41.00	44.00
NB	4.00	3.00	4.00	5.00	5.00	5.00
ZN	103.00	105.00	58.00	81.00	65.00	69.00
NI	3.00	1.00	0.00	0.00	11.00	0.00

TABLE G.1

## AMULET FORMATION; UPPER MEMBER; SILICIFIED FLOWS

SAMP NO.->	81-157	81-159	82-2	82-3	82-36	82-46
	PA05171	PA05172	PA05173	PA05174	PA05175	PA05176
SI02	59.12	72.16	69.50	69.38	61.99	66.57
AL203	15.27	11.85	13.10	13.61	15.20	13.23
FE203	10.88	4.09	4.88	5.92	8.24	7.50
MNO	0.19	0.08	0.08	0.07	0.16	0.14
MGO	6.14	1.26	0.65	1.03	2.28	5.10
CAO	4.89	2.09	2.63	1.54	2.14	0.83
NA20	4.41	4.72	5.12	6.13	5.46	2.18
K20	0.06	0.37	0.93	0.08	1.06	1.87
TI02	1.31	0.82	0.57	0.66	1.03	0.90
P205	0.13	0.37	0.10	0.16	0.29	0.37
CR203	0.00	0.00	0.00	0.00	0.00	0.00
LOI	0.00	0.00	0.00	0.00	0.00	0.00
TOTAL	102.40	97.81	97.56	98.58	97.85	98.69
S	0.00	0.00	0.00	0.01	0.01	0.06
BA	50.00	68.00	185.00	43.00	499.00	273.00
CR	62.00	26.00	28.00	21.00	24.00	23.00
ZR	124.00	167.00	200.00	215.00	216.00	168.00
SR	146.00	61.00	53.00	65.00	66.00	42.00
RB	0.00	4.00	20.00	0.00	11.00	24.00
Y	36.00	39.00	41.00	47.00	46.00	46.00
NB	4.00	4.00	6.00	6.00	7.00	4.00
ZN	178.00	46.00	65.00	54.00	123.00	534.00
NI	23.00	2.00	13.00	0.00	5.00	4.00
SAMP NO.->	82-49	82-69	82-65	82-79	82-81	82-117
	PA05177	PA05178	PA05179	PA05180	PA05181	PA05182
SI02	69.51	64.84	64.55	64.76	57.82	68.83
AL203	13.74	14.32	13.79	13.50	15.33	12.91
FE203	5.17	7.49	8.43	7.82	10.32	7.48
MNO	0.08	0.14	0.14	0.13	0.18	0.07
MGO	2.64	2.73	2.51	3.11	4.75	2.07
CAO	0.83	2.90	2.60	1.53	2.18	1.73
NA20	3.68	4.43	4.21	3.94	4.71	5.40
K20	1.45	0.50	0.65	0.97	0.67	0.10
TI02	0.76	1.07	0.88	0.93	1.39	0.63
P205	0.26	0.37	0.28	0.24	0.29	0.18
CR203	0.00	0.00	0.00	0.00	0.00	0.00
LOI	0.00	0.00	0.00	0.00	0.00	0.00
TOTAL	98.12	98.79	98.04	96.93	97.64	99.40
S	0.02	0.00	0.02	0.01	0.03	0.01
BA	358.00	108.00	183.00	263.00	104.00	45.00
CR	29.00	24.00	28.00	30.00	39.00	24.00
ZR	204.00	173.00	183.00	179.00	128.00	197.00
SR	67.00	113.00	103.00	51.00	52.00	57.00
RB	20.00	7.00	11.00	7.00	6.00	0.00
Y	48.00	38.00	39.00	44.00	34.00	41.00
NB	6.00	7.00	6.00	5.00	4.00	5.00
ZN	118.00	80.00	308.00	87.00	104.00	75.00
NI	0.00	0.00	7.00	0.00	4.00	0.00



TABLE G.1

## AMULET FORMATION; UPPER MEMBER; SILICIFIED FLOWS

SAMP NO.->	82-136	82-150	82-162	82-197	82-250	82-251
	PA05183	PA05184	PA05185	PA05186	PA05187	PA05188
SI02	61.51	70.72	61.72	60.74	65.44	56.33
AL203	14.07	11.57	13.97	14.53	13.53	15.63
FE203	8.29	6.13	7.62	10.28	7.54	9.52
MNO	0.11	0.09	0.11	0.24	0.15	0.17
MGO	3.27	2.00	3.76	4.62	3.58	5.17
CAO	3.23	2.24	2.80	1.11	1.12	5.05
NA2O	4.58	3.89	4.85	4.10	4.11	5.78
K2O	0.12	0.22	0.93	0.36	0.56	0.95
TI02	1.55	0.95	1.27	1.15	0.88	1.15
P2O5	0.27	0.23	0.23	0.26	0.24	0.07
CR203	0.00	0.00	0.00	0.00	0.00	0.00
LOI	0.00	0.00	0.00	0.00	0.00	0.00
TOTAL	97.00	98.04	97.26	97.39	97.15	99.82
S	0.01	0.01	0.02	0.02	0.01	0.01
BA	13.00	41.00	260.00	99.00	159.00	158.00
CR	30.00	25.00	35.00	28.00	29.00	77.00
ZR	132.00	165.00	114.00	183.00	184.00	100.00
SR	89.00	60.00	75.00	35.00	36.00	91.00
RB	1.00	0.00	8.00	4.00	7.00	14.00
Y	31.00	38.00	34.00	49.00	39.00	26.00
NB	6.00	5.00	0.00	4.00	6.00	0.00
ZN	90.00	62.00	82.00	186.00	113.00	126.00
NI	0.00	0.00	0.00	0.00	0.00	40.00
SAMP NO.->	82-252	82-253	81-1	81-50	81-68	BC-28
	PA05189	PA05190	PA05191	PA05192	PA05193	PA05194
SI02	55.89	57.75	66.40	65.20	59.30	72.84
AL203	15.37	15.38	13.30	14.20	14.40	11.39
FE203	9.61	8.22	6.74	6.44	9.94	6.78
MNO	0.17	0.15	0.11	0.14	0.18	0.10
MGO	4.93	4.67	2.54	2.30	4.59	2.49
CAO	6.19	5.39	1.32	4.24	1.79	1.24
NA2O	5.48	5.20	5.55	4.67	4.30	3.70
K2O	0.52	0.91	0.31	0.15	0.30	0.32
TI02	1.10	1.15	0.79	1.21	1.24	0.75
P2O5	0.05	0.06	0.20	0.24	0.31	0.31
CR203	0.00	0.00	0.00	0.00	0.00	0.00
LOI	0.00	0.00	0.00	0.00	0.00	0.00
TOTAL	99.31	98.88	97.26	98.79	96.35	99.92
S	0.02	0.02	0.00	0.00	0.00	0.00
BA	107.00	240.00	0.00	0.00	0.00	99.00
CR	74.00	76.00	20.00	20.00	20.00	22.00
ZR	96.00	101.00	250.00	180.00	200.00	140.00
SR	123.00	163.00	50.00	80.00	60.00	26.00
RB	7.00	13.00	10.00	10.00	10.00	1.00
Y	24.00	25.00	0.00	0.00	0.00	30.00
NB	0.00	2.00	0.00	0.00	0.00	1.00
ZN	114.00	93.00	0.00	0.00	0.00	106.00
NI	32.00	31.00	0.00	0.00	0.00	0.00







TABLE G.1

## AMULET FORMATION; UPPER MEMBER; SILICIFIED FLOWS

SAMP NO.->	83-191	83-192	83-193	83-194	83-203	83-204
	PA05231	PA05232	PA05233	PA05234	PA05235	PA05236
SI02	66.60	58.00	65.20	62.50	71.50	60.60
AL203	13.50	16.80	12.80	13.70	13.20	14.00
FE203	7.09	10.90	8.57	10.20	4.10	10.60
MNO	0.13	0.36	0.41	0.16	0.06	0.22
MGO	2.09	5.04	4.57	3.24	2.02	3.39
CAO	1.80	0.25	0.30	1.34	0.85	2.62
NA2O	5.62	0.17	0.10	3.59	5.52	3.66
K2O	0.26	3.15	1.81	0.24	0.33	0.13
TIO2	0.77	0.77	0.81	1.17	0.57	1.12
P2O5	0.21	0.18	0.21	0.34	0.13	0.30
CR203	0.00	0.00	0.00	0.00	0.00	0.00
LOI	1.39	4.08	3.70	2.70	1.47	2.85
TOTAL	99.46	99.70	98.48	99.18	99.75	99.49
S	0.00	0.00	0.00	0.00	0.00	0.00
BA	0.00	0.00	0.00	0.00	0.00	0.00
CR	10.00	10.00	10.00	20.00	20.00	20.00
ZR	230.00	370.00	240.00	190.00	280.00	210.00
SR	50.00	< 10.00	< 10.00	10.00	20.00	30.00
RB	10.00	70.00	40.00	30.00	10.00	10.00
Y	0.00	0.00	0.00	0.00	0.00	0.00
NB	0.00	0.00	0.00	0.00	0.00	0.00
ZN	0.00	0.00	0.00	0.00	0.00	0.00
NI	0.00	0.00	0.00	0.00	0.00	0.00
	83-208	83-253	83-254	83-256	83-258	
SAMP NO.->	PA05237	PA05238	PA05239	PA05240	PA05241	
SI02	62.30	60.10	59.70	54.80	73.60	
AL203	14.30	14.20	15.00	15.50	11.70	
FE203	8.61	6.79	5.73	9.78	3.17	
MNO	0.15	0.13	0.10	0.18	0.07	
MGO	3.85	4.70	4.21	5.54	1.47	
CAO	2.28	4.96	4.75	5.96	2.31	
NA2O	4.49	4.85	6.15	2.82	4.97	
K2O	0.43	0.29	0.24	0.08	0.16	
TIO2	1.26	1.02	1.14	1.14	0.85	
P2O5	0.25	0.15	0.16	0.17	0.13	
CR203	0.00	0.00	0.00	0.00	0.00	
LOI	2.16	1.77	1.70	3.00	1.00	
TOTAL	100.08	98.96	98.88	98.97	99.43	
S	0.00	0.00	0.00	0.00	0.00	
BA	0.00	0.00	0.00	0.00	0.00	
CR	10.00	30.00	30.00	40.00	20.00	
ZR	200.00	150.00	150.00	150.00	160.00	
SR	40.00	170.00	170.00	290.00	130.00	
RB	20.00	20.00	< 10.00	10.00	10.00	
Y	0.00	0.00	0.00	0.00	0.00	
NB	0.00	0.00	0.00	0.00	0.00	
ZN	0.00	0.00	0.00	0.00	0.00	
NI	0.00	0.00	0.00	0.00	0.00	

TABLE G.1

## DIORITE-GABBRO INTRUSIONS

SAMP	I-82-2	I-82-10	I-82-11	I-82-30
SiO <sub>2</sub>	50.12	51.27	47.22	50.01
Al <sub>2</sub> O <sub>3</sub>	12.90	14.99	15.57	14.83
Fe <sub>2</sub> O <sub>3</sub>	14.38	11.36	11.54	10.92
MnO	0.26	0.20	0.18	0.19
MgO	5.51	6.76	8.06	7.56
CaO	10.28	10.77	11.66	11.63
Na <sub>2</sub> O	2.15	2.40	1.67	1.52
K <sub>2</sub> O	0.14	0.26	0.09	0.57
TiO <sub>2</sub>	1.35	0.71	0.84	0.83
P <sub>2</sub> O <sub>5</sub>	0.0	0.0	0.0	0.0
CR203				
LO.I.				
TOTAL	97.18	98.80	96.92	98.17
S	0.03	0.02	0.02	0.03
BA PPM	33.	65.	34.	83.
CR	109.	46.	275.	285
ZR	72.	41.	24.	36.
SR	81.	117.	120.	111.
RB	0.	0.	0.	8.
Y	27.	23.	18.	20.
NB	0.	0.	0.	0.
ZN	82.	83.	87.	61
NI	40.	44.	115.	49.

TABLE G.1

## DIORITE- GABBRO INTRUSIONS

SAMP	I-82-31	I-8243	I-82-13
SiO <sub>2</sub>	51.21	58.73	46.72
Al <sub>2</sub> O <sub>3</sub>	14.21	14.96	15.87
Fe <sub>2</sub> O <sub>3</sub>	13.01	9.39	13.85
MnO	0.22	0.16	0.22
MgO	5.94	3.64	8.60
CaO	9.27	1.72	8.02
Na <sub>2</sub> O	2.05	4.25	1.43
K <sub>2</sub> O	1.12	1.55	2.24
TiO <sub>2</sub>	0.86	1.25	1.24
P <sub>2</sub> O <sub>5</sub>	0.0	0.38	0.04
CR203			
LO.I.			
TOTAL	98.01	96.17	98.40
S	0.04	0.00	0.04
BA PPM	315.	642.	431.
CR	51.	31.	262.
ZR	47.	177.	39.
SR	139.	95.	100.
RB	29.	31.	58.
Y	24.	48.	20.
NB	0.	6.	2.
ZN	75.	163.	84.
NI	38.	0.	131.

TABLE G.2. PRECISION OF THE UNIVERSITY OF OTTAWA  
XRF ANALYSES  
CONCENTRATION RANGE (Wt.%)

<u>ELEMENT</u>	<u>0.1-1.0</u>	<u>0.1-2.0</u>	<u>1.0-3.0</u>	<u>1.0-20</u>	<u>50 -100</u>
SiO <sub>2</sub>					+/- 1.0
Al <sub>2</sub> O <sub>3</sub>	+10(%)		+/-1.5	+/-1.5	
Fe <sub>2</sub> O <sub>3</sub> T	+/- 5			+/-2	
MgO	+/-25			+/- 3	
CaO	+/- 5			+/- 2	
NA <sub>2</sub> O		+/-15	+/- 3		
K <sub>2</sub> O	+/- 5			+/- 1	
TiO <sub>2</sub>	+/- 2		+/- 1		
P <sub>2</sub> O <sub>5</sub>	+/-10		+/- 1		
MnO	+/-10				
S	+/-10				

CONCENTRATION RANGE (PPM)

	10	10 - 30	>30
Ba	+/- 10%	+/- 50%	+/- 30%
Cr	+/- 10%	+/- 50%	+/- 30%
Zr	+/- 10%	+/- 50%	+/- 30%
Sr	+/- 10%	+/- 50%	+/- 30%
Rb	+/- 10%	+/- 50%	+/- 30%
Y	+/- 10%	+/- 50%	+/- 30%
Nb	+/- 10%	+/- 50%	+/- 30%
Zn	+/- 10%	+/- 50%	+/- 30%
NI	+/- 10%	+/- 50%	+/- 30%
Cu	+/- 10%	+/- 50%	+/- 30%
Pb	+/- 10%	+/- 50%	+/- 30%
V	+/- 10%	+/- 50%	+/- 30%



TABLE G.3. ANALYSES OF DUPLICATE FUSED PELLETS

	<u>81-121</u>	<u>DUPL.</u>	<u>81-123</u>	<u>DUPL.</u>	<u>83-21</u>	<u>DUPL.</u>
WH. %						
SiO <sub>2</sub>	55.92	55.76	71.24	72.27	65.8	65.4
Al <sub>2</sub> O <sub>3</sub>	14.87	14.93	12.36	12.49	13.5	13.4
Fe <sub>2</sub> O <sub>3</sub>	11.93	11.95	3.71	3.79	6.32	6.39
MgO	3.43	3.57	1.81	1.79	1.86	1.98
CaO	5.2	5.11	2.93	2.94	3.01	3.10
Na <sub>2</sub> O	4.69	4.69	5.04	5.01	5.46	5.35
K <sub>2</sub> O	0.07	0.07	0.29	0.29	0.09	0.09
TiO <sub>2</sub>	1.55	1.53	0.64	0.64	1.07	1.09
P <sub>2</sub> O <sub>5</sub>	0.18	0.18	0.18	0.15	0.23	0.23
MnO	0.26	0.26	0.11	0.11	0.13	0.16
S	0.02	0.01	0.0	0.0		-
L.O.I.					1.47	1.42
PPM						
Ba	38	14	88	105	-	-
Cr	39	44	23	25	20	25
Zr	98	95	198	202	230	215
Sr	74	75	33	32	60	74
Rb	0	0	0	0	<10	<10
Y	29	30	44	46	-	-
Nb	2	4	5	4	-	-
Zn	234	240	79	83	-	-
Ni	0	12	1	0	-	-

81-121 and 81-123 - UNIVERSITY OF OTTAWA

83-21 - XRAL

TABLE G.4A

WHOLE ROCK ANALYSIS - % MAJORS &amp; MINORS - XRF - PW 1600 - REFERENCE STANDARDS

	MRG-1	SY-2	G-2	NBS-1c*	NBS-97a	NBS-99a	BX-N	GS-N	NIM-D	NIM-N	
SiO <sub>2</sub>	38.9 (39.32)	60.0 (60.10)	68.8 (67.22)	7.24 (6.84)	43.2 (43.67)	65.3 (65.2)	7.44 (7.39)	65.9 (65.98)	38.3 (38.96)	52.7 (52.64)	SiO <sub>2</sub>
Al <sub>2</sub> O <sub>3</sub>	8.41 (8.50)	12.1 (12.12)	15.4 (15.40)	1.40 (1.30)	38.7 (38.79)	20.7 (20.5)	54.0 (54.53)	14.8 (14.71)	0.25 (0.37)	16.3 (16.50)	Al <sub>2</sub> O <sub>3</sub>
CaO	14.8 (14.77)	8.01 (7.98)	1.95 (1.96)	50.6 (50.3)	0.10 (0.11)	2.15 (2.14)	0.16 (0.17)	2.55 (2.51)	0.27 (0.28)	11.7 (11.50)	CaO
MgO	13.4 (13.49)	2.68 (2.70)	0.72 (0.75)	0.40 (0.42)	0.17 (0.15)	0.01 (0.02)	0.11 (0.11)	2.28 (2.31)	43.1 (43.51)	7.34 (7.50)	MgO
Na <sub>2</sub> O	0.71 (0.71)	4.31 (4.34)	4.10 (4.06)	0.00 (0.02)	0.04 (0.037)	6.31 (6.2)	0.04 (0.06)	3.84 (3.78)	0.06 (0.047)	2.39 (2.46)	Na <sub>2</sub> O
K <sub>2</sub> O	0.18 (0.18)	4.50 (4.48)	4.40 (4.46)	0.27 (0.28)	0.52 (0.50)	5.28 (5.2)	0.06 (0.07)	4.68 (4.64)	0.04 (0.017)	0.24 (0.25)	K <sub>2</sub> O
Fe <sub>2</sub> O <sub>3</sub>	17.7 (17.82)	6.20 (6.28)	2.70 (2.69)	0.65 (0.55)	0.45 (0.45)	0.08 (0.065)	23.3 (23.27)	3.70 (3.76)	16.5 (16.96)	8.84 (8.91)	Fe <sub>2</sub> O <sub>3</sub>
MnO	0.16 (0.17)	0.32 (0.32)	0.03 (0.03)	0.01 (0.025)	0.00 (-)	0.00 (-)	0.04 (0.05)	0.05 (0.056)	0.23 (0.22)	0.18 (0.18)	MnO
TiO <sub>2</sub>	3.65 (3.69)	0.14 (0.14)	0.50 (0.48)	0.07 (0.07)	1.88 (1.90)	0.02 (0.007)	2.35 (2.41)	0.66 (0.68)	0.03 (0.02)	0.19 (0.20)	TiO <sub>2</sub>
P <sub>2</sub> O <sub>5</sub>	0.06 (0.06)	0.42 (0.43)	0.13 (0.13)	0.04 (0.04)	0.35 (0.36)	0.02 (0.02)	0.13 (0.13)	0.27 (0.28)	0.01 (0.027)	0.02 (0.03)	P <sub>2</sub> O <sub>5</sub>
Cr <sub>2</sub> O <sub>3</sub>	0.06 (0.07)	0.00 (0.002)	0.00 (0.00)	0.00 (-)	0.03 (0.03)	0.00 (-)	0.04 (0.04)	0.01 (0.01)	0.40 (0.42)	0.01 (0.005)	Cr <sub>2</sub> O <sub>3</sub>

NOTE: ( ) are usable values as per Sydney Abbey, 1979 - (-) indicates no values available. This represents only part of the group of 50 reference materials used for calibrating the simultaneous spectrometer. Others are available on request.  
\* ( ) values are certified NBS values.

## INSTRUMENT STABILITY

(10 replicate analyses)

	Mean (%)	SD (%)	Mean (%)	SD (%)
SiO <sub>2</sub>	39.5	0.06	65.1	0.07
Al <sub>2</sub> O <sub>3</sub>	2.92	0.01	18.8	0.03
CaO	1.20	0.005	0.10	0.005
MgO	34.8	0.08	0.10	0.005
Na <sub>2</sub> O	0.13	0.01	2.56	0.03
K <sub>2</sub> O	0.02	0.005	12.9	0.02
Fe <sub>2</sub> O <sub>3</sub>	8.52	0.015	0.12	0.005
MnO	0.13	0.00	0.00	0.00
TiO <sub>2</sub>	0.12	0.005	0.03	0.00
P <sub>2</sub> O <sub>5</sub>	0.04	0.00	0.02	0.00
Cr <sub>2</sub> O <sub>3</sub>	0.33	0.001	0.00	0.00

## SAMPLE PREPARATION REPRODUCIBILITY

(42 replicate analyses)

	Mean (%)	SD (%)	Mean (%)	SD (%)	
SiO <sub>2</sub>	80.7	0.25	65.9	0.25	SiO <sub>2</sub>
Al <sub>2</sub> O <sub>3</sub>	8.21	0.06	13.0	0.06	Al <sub>2</sub> O <sub>3</sub>
CaO	0.05	0.005	0.72	0.005	CaO
MgO	1.79	0.02	6.08	0.04	MgO
Na <sub>2</sub> O	0.13	0.01	0.60	0.02	Na <sub>2</sub> O
K <sub>2</sub> O	1.89	0.01	2.51	0.01	K <sub>2</sub> O
Fe <sub>2</sub> O <sub>3</sub>	4.87	0.03	7.14	0.03	Fe <sub>2</sub> O <sub>3</sub>
MnO	0.08	0.005	0.14	0.005	MnO
TiO <sub>2</sub>	0.19	0.005	0.33	0.005	TiO <sub>2</sub>
P <sub>2</sub> O <sub>5</sub>	0.05	0.00	0.10	0.00	P <sub>2</sub> O <sub>5</sub>
Cr <sub>2</sub> O <sub>3</sub>	0.02	0.00	0.02	0.00	Cr <sub>2</sub> O <sub>3</sub>
	1.59	0.08	2.95	0.09	L.O.I.

NOTE: Mean is the arithmetic mean  
SD is standard deviation

TABLE G.4B

## WHOLE ROCK ANALYSIS - ppm TRACES - XRF - PW 1600 - REFERENCE STANDARDS

	<u>MRG-1</u>	<u>SY-2</u>	<u>SY-3</u>	<u>G-2</u>	<u>Mica Fe</u>	<u>Mica Mg</u>	<u>GS-N</u>	<u>NIM-G</u>	<u>NIM-L</u>	<u>NIM-S</u>	
Rb	<10 (8)	210 (220)	200 (208)	170 (170)	2240 (2200)	1250 (1300?)	180 (190?)	310 (320)	190 (190)	490 (530)	Rb
Sr	220 (260)	260 (275)	300 (306)	510 (480)	<10 (5)	20 (25?)	640 (570?)	<10 (10)	4500 (4600)	60 (62)	Sr
Y	10 (16?)	140 (130)	730 (740)	20 (11)	40 (25?)	10 (-)	10 (-)	160 (145)	40 (25?)	<10 (3?)	Y
Zr	100 (105)	280 (280)	340 (320)	320 (300)	900 (800?)	10 (20?)	230 (240?)	280 (300)	11400 (11200)	10 (33?)	Zr
Nb	30 (20?)	10 (23?)	120 (130)	10 (13?)	300 (270?)	130 (120?)	10 (-)	60 (53?)	1000 (960)	<10 (3.5?)	Nb
Ba	100 (50?)	420 (460)	390 (430)	1900 (1900)	190 (145)	3800 (4000?)	1350 (1400?)	100 (120?)	500 (450)	2350 (2400)	Ba

NOTE: ( ) are usable values as per Sydney Abbey, 1979 - (-) indicates no values available  
 This represents only part of the group of 50 reference materials used for calibrating  
 the simultaneous spectrometer. Others are available on request.

INSTRUMENT STABILITY

(10 replicate analyses)

	<u>Mean(ppm)</u>	<u>SD(ppm)</u>	<u>Mean(ppm)</u>	<u>SD(ppm)</u>
Rb	210	10	200	10
Sr	260	10	4400	40
Y	130	10	50	10
Zr	280	10	11500	40
Nb	10	10	980	20
Ba	420	20	520	20

SAMPLE PREPARATION REPRODUCIBILITY

(42 replicate analyses)

	<u>Mean(ppm)</u>	<u>SD(ppm)</u>	<u>Mean(ppm)</u>	<u>SD(ppm)</u>	
Rb	30	10	220	20	Rb
Sr	<10	10	340	10	Sr
Y	20	10	590	20	Y
Zr	60	10	280	10	Zr
Nb	20	10	870	20	Nb
Ba	660	10	1200	40	Ba

NOTE: Mean is the arithmetic mean  
 SD is standard deviation

TABLE G.5 COMPARATIVE ANALYSES: UNIVERSITY OF OTTAWA  
AND XRAL

	<u>81 - 22</u>		<u>82-98</u>		<u>82 -121</u>	
Wt. %	A	B	A	B	A	B
SiO <sub>2</sub>	65.54	63.6	74.81	73.5	55.92	54.9
Al <sub>2</sub> O <sub>3</sub>	14.90	14.5	12.15	12.2	14.87	14.5
Fe <sub>2</sub> O <sub>3</sub>	7.45	7.30	4.24	4.15	11.93	11.6
MgO	2.75	2.14	1.35	1.51	3.43	3.74
CaO	3.13	3.20	0.25	0.30	5.12	5.03
Na <sub>2</sub> O	5.23	5.48	5.49	5.73	4.69	4.37
K <sub>2</sub> O	0.39	0.41	0.08	0.09	0.07	0.09
TiO <sub>2</sub>	0.96	0.98	0.38	0.41	1.55	1.55
P <sub>2</sub> O <sub>5</sub>	0.43	0.32	0.02	0.07	0.18	0.20
MnO	0.18	0.19	0.03	0.03	0.26	0.26
S	0.0	-	0.01	-	0.02	-
L.I.O.	-	0.39	-	1.39	-	2.47
PPM						
Ba	91	-	51	-	38	-
Cr	23	20	21	20	39	20
Zr	167	200	301	370	98	110
Sr	68	60	25	<10	74	80
Rb	7	<10	0	<10	0	40
Y	44	-	103	-	29	-
Nb	6	-	11	-	2	-
Zn	399	-	9	-	234	-
NI	0	-	0	-	0	-

A - UNIVERSITY OF OTTAWA ANALYSIS

B - XRAL ANALYSIS

**TABLES G.6 and 7**

Trace element data for Mine Sequence flows are presented in Table G.6. Samples were analyzed at Memorial University, NFLD, using a pressed pellet XRF technique. All elements are reported in ppm except Ti, which is in weight percent. One sample was analyzed with duplicate pellets to check for homogeneity of the powder. The duplicate analyses in Table G.7, compare well and are in the range of variation of replicate analyses of the standards.

Analyses of Pb, Th, U, Rb and Nb are not accurate under 5 ppm; the remaining elements have "decreasing accuracy" under 15 ppm.

TABLE G.6A. TRACE ELEMENT ANALYSES OF THE MINE SEQUENCE ANDESITE FLOWS

Element ppm	82-74	82-174	82-87	82-94	82-98	82-101	82-117	82-121	81-113	82-186	81-191	81-194	81-197	81-203	82-88	82-40	81-22
Pb	0	5	0	3	3	0	3	1	9	1	0	6	4	4	0	3	7
TH	5	3	3	3	6	0	4	6	4	0	4	5	3	2	0	0	3
U	0	0	0	0	0	1	2	3	0	0	0	0	0	0	0	0	1
Rb	5	1	3	3	3	3	5	5	4	1	2	2	1	2	1	28	15
Sr	108	126	374	58	25	24	81	71	227	70	49	136	100	46	124	107	65
Y	25	23	33	57	130	44	34	36	38	24	41	38	40	44	49	21	52
Zr	119	115	120	175	343	153	111	115	123	94	143	139	139	151	156	107	195
Nb	8	6	9	11	25	10	6	9	8	6	8	9	10	10	10	6	13
Zn	32	26	0	32	7	74	51	219	165	35	83	65	84	75	83	42	360
Cu	0	0	0	1	4	0	176	86	5	9	0	8	0	27	0	0	3
Ni	75	92	0	0	0	10	0	2	6	6	15	8	12	10	5	35	0
La	7	5	10	3	11	11	9	13	14	1	14	13	8	12	9	5	16
Ba	245	71	17	87	52	41	53	92	240	96	75	113	193	94	59	254	139
Ti %	1.03	0.93	1.08	0.83	0.39	1.56	1.44	1.57	1.46	0.90	1.30	1.24	1.26	1.45	1.58	0.99	1.07
V	258	288	200	100	7	328	314	319	355	184	257	275	317	254	234	258	31
Ce	26	19	17	27	32	32	26	31	34	24	26	28	25	29	36	27	33
Cr	64	75	0	0	0	0	0	0	0	14	0	16	15	0	0	20	0
Ga	14	16	22	12	13	14	13	14	18	5	9	13	15	15	13	14	20
Zr/Y	4.7	5	3.6	3	2.6	3.4	3.2	3.2	3.2	3.9	3.5	3.6	3.4	3.4	3.2	5	3.7
Ti/Zr	86	80	90	47	11	101	129	136	118	95	90	89	90	96	101	92	55

(1) Flavrian Formation (3) Waite Andesite Formation  
(2) Rusty Ridge Formation (4) Amulet Andesite Formation

TABLE G.6B. TRACE ELEMENT ANALYSES OF THE AMULET UPPER MEMBER

Element ppm	80-84	81-27	81-28	81-68	81-157	82-3	82-65	82-69	82-79	82-81	82-117	82-144	82-150	82-162	82-250	82-251
Pb	1	6	7	2	1	11	0	3	6	10	6	5	5	11	4	4
Th	3	5	8	4	1	8	0	3	4	2	5	5	8	5	1	
U	4	3	1		3	0	0	0	3	0	0	1		3	0	0
Rb	3	10	8	5	13	2	12	11	15	8	2	11	5	14	10	19
Sr	228	82	49	58	78	64	98	110	51	51	55	234	58	71	39	88
Y	42	55	59	51	55	60	49	48	56	47	56	58	52	42	47	25
Zr	161	213	209	184	180	253	211	200	208	148	226	254	190	139	209	119
Nb	8	12	13	10	10	11	12	12	10	10	11	15	12	9	9	8
Zn	30	372	158	169	71	42	292	70	79	96	67	28	47	81	112	119
Cu	0	0	0	0	5	73	150	0	0	17	1	1	0	105	0	0
Ni	0	0	0	0	0	0	0	0	0	2	0	0	0	0	0	49
La	3	11	21	14	9	8	10	11	10	9	8	16	8	6	13	12
Ba	57	98	89	110	212	49	190	131	318	188	49	94	45	283	215	208
Ti %	1.56	1.21	1.52	1.38	1.36	0.73	0.97	1.18	1.07	1.63	0.70	0.60	1.02	1.37	1.01	1.30
V	217	31	54	65	73	10	39	45	56	271	8	6	50	225	40	276
Ce	28	36	43	38	31	30	34	29	33	31	22	26	29	34	25	30
Cr	0	0	0	0	0	0	0	0	0	0	0	0	0	0	0	28
Ga	16	15	19	18	18	13	14	19	14	18	13	17	8	14	19	13
Zr/Y	3.8	3.8	3.5	3.6	3.2	4.2	4.3	4.2	3.7	3.1	4	4.3	3.6	3.3	4.4	4.7
Ti/Zr	96	56	72	75	75	28	50	59	51	110	30	23	53	98	48	109





TABLE G.7. ANALYSES OF DUPLICATE PRESSED PELLETS  
MEMORIAL UNIVERSITY, NFLD.

	<u>82-254</u>	<u>82-254 (Duplicate (Pellet))</u>
PPM		
Pb	0	3
Th	3	8
U	0	6
Rb	5	6
Sr	56	58
Y	42	44
Zr	193	199
Nb	11	11
Zn	76	80
Cu	0	0
Ni	0	0
La	20	11
Ba	84	73
Ti (Wt.%)	1.07	1.06
V	29	25
Ce	36	31
Cr	0	0
Ga	15	18